UNIVERSIDAD DE SEVILLA
FACULTAD DE MEDICINA
Departamento de Medicina

UNA APROXIMACIÓN NEUROPATOLÓGICA A LA FISIOPATOLOGÍA DE LA ENFERMEDAD DE ALZHEIMER

Memoria presentada por **Alberto Serrano Pozo** para optar al grado de Doctor en Medicina

Sevilla (España), Julio de 2012

UNIVERSITY OF SEVILLE
SCHOOL OF MEDICINE
Department of Medicine

A NEUROPATHOLOGICAL APPROACH TO THE PATHOPHYSIOLOGY OF ALZHEIMER DISEASE

Dissertation presented by **Alberto Serrano Pozo** to be publicly examined for the degree of Doctor in Philosophy
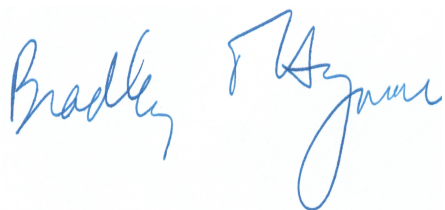(Medicine)

Seville (Spain), July 2012

UNA APROXIMACIÓN NEUROPATOLÓGICA A LA FISIOPATOLOGÍA DE LA ENFERMEDAD DE ALZHEIMER

Memoria presentada por **Alberto Serrano Pozo** para optar al grado de Doctor en Medicina

Sevilla (España), Julio 2012

Directores

Bradley T. Hyman

John B. Penney Jr.
Professor of Neurology
Harvard Medical School

Eulogio Gil Néciga

Doctor en Medicina

Enrique Calderón Sandubete

Profesor Asociado de Medicina
Universidad de Sevilla

Departamento de Medicina
FACULTAD DE MEDICINA
UNIVERSIDAD DE SEVILLA

A NEUROPATHOLOGICAL APPROACH TO THE PATHOPHYSIOLOGY OF ALZHEIMER DISEASE

Dissertation presented by **Alberto Serrano Pozo** to be publicly examined for the degree of Doctor in Philosophy (Medicine)

Seville (Spain), July 2012

Advisors

Bradley T. Hyman

John B. Penney Jr.
Professor of Neurology
Harvard Medical School

Eulogio Gil Néciga

Doctor in Medicine

Enrique Calderón Sandubete

Associate Professor of Medicine
University of Seville

**Department of Medicine
SCHOOL OF MEDICINE
UNIVERSITY OF SEVILLE**

ABBREVIATIONS

AD Alzheimer disease

Aβ Amyloid β-peptide

APP Amyloid precursor protein

ATP Adenosine tri-phosphate

BA Brodmann area

CA Cornus ammonis (hippocampal subfield)

CAA Cerebral amyloid angiopathy

CSF Cerebrospinal fluid

DAB 3, 3'-diaminobenzidine

DAPI 4',6-diamidino-2-phenylindole

DNA Deoxyribonucleic acid

GFAP Glial Fibrillary Acidic Protein

GSK3 Glycogen synthase kinase 3

IBA1 Ionized Binding Adaptor molecule 1

MCI Mild cognitive impairment

MRI Magnetic resonance imaging

NF-H Neurofilament-Heavy chain

NFTs Neurofibrillary tangles

NIA National Institute of Aging

NSAIDs Non-steroidal anti-inflammatory drugs

P.A.S. Periodic Acid-Schiff

PET Positron emission tomography

pTau Phospho-tau

PHF1 Paired helical filament 1

SDS Sodium dodecyl sulfate

ThioS Thioflavin-S

VDAC1 Voltage dependent anion channel 1

INDEX

1 INTRODUCTION TO ALZHEIMER DISEASE

1.1. Neuropathology of Alzheimer disease.

Alzheimer disease (AD) is the most common cause of dementia and the most common neurodegenerative disease. AD affects a 6% of people older than 65 and it has been estimated that its prevalence doubles every 5 years thereafter, so that nearly 50% of people over 85 suffer from AD (Hirtz et al., 2007; Alzheimer's Association 2011).

The pathological hallmarks of AD can be classified in "positive" and "negative" lesions. Positive lesions include amyloid plaques and cerebral amyloid angiopathy —its equivalent in arteries and capillaries–, neurofibrillary tangles (NFTs) and glial responses. Negative lesions consist of a progressive loss of neurons and synapses, which lead to the atrophy of cerebral cortex.

The most characteristic pathological features of AD —amyloid plaques and neurofibrillary tangles– were already described by Alois Alzheimer more than a century ago, but the knowledge

about their composition and significance is far more recent. Amyloid plaques are protein extracellular deposits mainly composed of the amyloid-β peptide, a by-product of the catabolism of amyloid precursor protein (APP) that results after its sequential cleavage by the enzymes β- and γ-secretases. Although plaques have been classified in many different morphological subtypes according to their staining properties and associated pathologic features (diffuse, primitive, classical, burn-out), presumably representing different stages in plaque evolution, this classification can be simplified in two main subtypes: diffuse and dense-core plaques. Diffuse plaques are Aβ-immunoreactive deposits that do not alter their surrounding neuropil nor induce glial responses in their vicinity, and therefore, are considered "benign". In fact, they are often seen in the cortex of elderly people without evidence of cognitive decline (Arriagada et al., 1992b). By contrast, dense-core plaques have a central compact *core* that is positive for stainings that specifically display the β-sheet pleated conformation of amyloid fibrils, such as Congo red and Thioflavin-S. In addition, since they often contain and/or are surrounded by dystrophic neurites (neuritic plaques), reactive astrocytes, and activated microglial cells, these dense-core plaques are considered toxic and more specific of AD (Mirra et al., 1991).

Neurofibrillary tangles (NFTs) are intraneuronal deposits of the microtubule-associated protein tau, which is aberrantly misfolded and abnormally hyperphosphorylated. In AD, tau aggregates forming paired helical filaments with a β-sheet pleated conformation, hence NFTs are also Thioflavin-S positive. As the disease advances, many tangle-bearing neurons die, leaving behind extracellular tangles, also called "ghost" or "tombstone" tangles.

A number of clinico-pathologic studies in the 1990s demonstrated that the amount of NFTs, neuronal loss, and particularly synaptic loss, strongly correlates with the severity of cognitive decline. By contrast, these studies revealed that amyloid burden essentially does not correlate with the degree of cognitive impairment or the duration of clinical illness (DeKosky et al., 1990; Terry et al., 1991; Arriagada et al., 1992a; Bierer et al., 1995; Gómez-Isla et al., 1996 y 1997; Ingelsson et al., 2004). Indeed, as mentioned above, amyloid plaques are relatively common in cognitively intact elderly people (Arriagada et al, 1992b). Although the pathologic diagnosis of AD has long relied on the presence of plaques and tangles in a sufficient number and distribution in the cerebral cortex of a patient with documented clinical history of dementia (Braak y Braak,

1991; Mirra et al., 1991; NIA-Reagan Consensus, 1997), as discussed below, the current view is that AD is a continuum pathological spectrum between "normal" aging and dementia and, as such, the pathological diagnostic criteria have been recently revised to consider pre-symptomatic stages of the disease (Montine et al. 2011; Hyman et al., 2011).

1.2. Pathophysiology of Alzheimer disease: the amyloid cascade hypothesis.

Despite the lack of correlation between amyloid burden and severity of cognitive deficits, the most widely accepted hypothesis gives Aβ a central role in the pathophysiology of AD. According to this hypothesis, Aβ is the trigger of a cascade of adverse events that include synaptic dysfunction, glial-mediated inflammation and oxidative stress, hyperphosphorylation and aggregation of tau in NFTs, and ultimately, neuronal loss and dementia, hence the name "**amyloid cascade hypothesis**". In its first formulation, the main contribution of this hypothesis was to place amyloid plaques and NFTs in a sequential order, attributing to Aβ an initiation effect and considering tau pathology as secondary to Aβ aggregation (Hardy and Higgins 1992, Selkoe 1992). Despite the fact that the vast majority of AD cases are sporadic, the basis of this hypothesis largely lays in genetics: the causative genes of the rare cases of familial autosomal dominant AD cases discovered so far encode the substrate (amyloid precursor protein, *APP*) and enzymes involved in Aβ generation (presenilins 1 and 2, *PSEN1* and *PSEN2*, the catalytic subunits of the γ-secretase complex). Mutations in these three genes cause a form of early-onset AD that is clinically and pathologically very similar to the sporadic late-onset form. Also, virtually all patients with Down's syndrome (trisomy 21) will develop early-onset AD in their 40s or 50s due to an excessive production of Aβ derived from their three copies of the *APP* gene (Bertram y Tanzi 2008). However, the main genetic risk factor for sporadic AD, the *ε*4 allele of the apolipoprotein E gene *APOE*, has been also associated to an increased level of Aβ, either by promoting its aggregation (Ma et al., 1994; Wisniewski et al., 1994; Castano et al., 1995) or by reducing its clearance from the brain parenchyma (Deane et al., 2008; Jiang et al., 2009; Castellano et al., 2011). In addition, other environmental factors that have been shown to

increase the risk of developing sporadic late-onset AD, such as traumatic brain injury or stroke, may also increase the production of Aβ by increasing the levels of the enzymes β- and γ-secretases (Veliquette et al., 2005; Sun et al., 2006; Tesco et al., 2007; Loane et al., 2009).

In addition, in its latest version this hypothesis elegantly sorted out the issue of the lack of correlation between plaque burden and cognitive impairment by emphasizing that AD is a "synaptic disease" and that soluble Aβ oligomers rather than Aβ fibrils within the plaques are the culprit Aβ species with toxic effects on synapses (Hardy and Selkoe, 2002). Indeed, it has been reported that the levels of soluble Aβ in the cortex do correlate with the severity of dementia (Lue et al., 1999; McLean et al., 1999; Näslund et al., 2000), and experiments in vitro and in mouse models have demonstrated that soluble Aβ oligomers cause synaptic dysfunction and loss (Lambert et al., 1998; Hsia et al., 1999; Lacor et al., 2004; Cleary et al., 2005; Lesné et al., 2006; Shankar et al., 2007; Shankar et al., 2008; Koffie et al., 2009; Li et al., 2009, Wu et al., 2010), and that they can induce neuronal tau hyperphosphorylation and aggregation (Zempel et al. 2010; Jin et al., 2011). However, a variety of oligomeric Aβ species with different physicochemical properties (tertiary conformation, molecular weight, SDS-solubility, etc.) have been described both *in vitro* and *in vivo* since this hypothesis was reformulated, and which soluble oligomeric Aβ species are present *in vivo* and whether any form of soluble Aβ is more deleterious than others are still controversial questions (reviewed in Benilova et al., 2012).
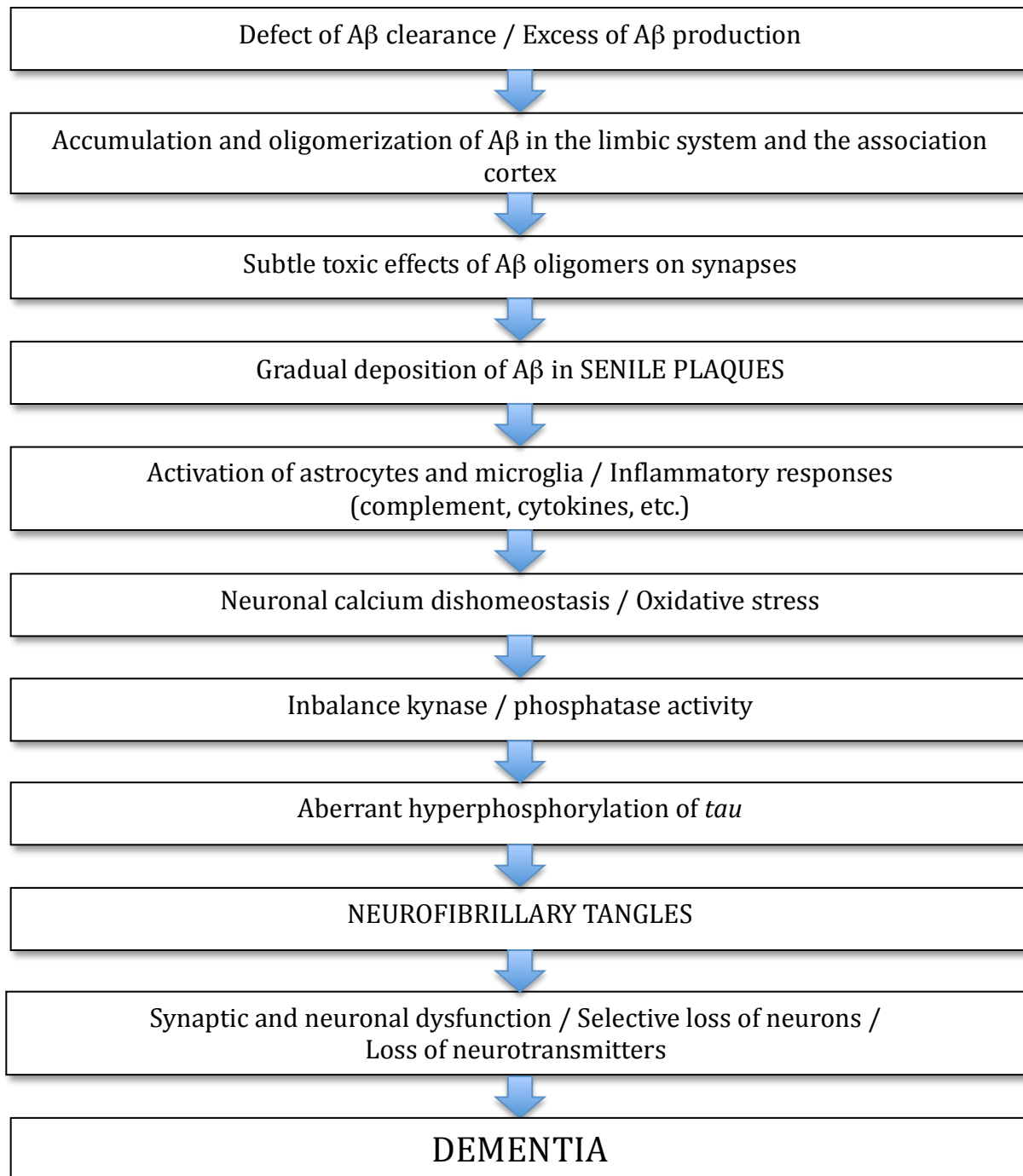
Defect of Aβ clearance / Excess of Aβ production

↓

Accumulation and oligomerization of Aβ in the limbic system and the association cortex

↓

Subtle toxic effects of Aβ oligomers on synapses

↓

Gradual deposition of Aβ in SENILE PLAQUES

↓

Activation of astrocytes and microglia / Inflammatory responses (complement, cytokines, etc.)

↓

Neuronal calcium dishomeostasis / Oxidative stress

↓

Inbalance kynase / phosphatase activity

↓

Aberrant hyperphosphorylation of *tau*

↓

NEUROFIBRILLARY TANGLES

↓

Synaptic and neuronal dysfunction / Selective loss of neurons / Loss of neurotransmitters

↓

DEMENTIA

Figure 1. Amyloid cascade hypothesis (Hardy and Selkoe, 2002).

2 *RATIONALE*

2.1. Recent criticisms to the amyloid cascade hypothesis.

Although the amyloid cascade hypothesis has been widely accepted by most scientists in the last two decades as their research framework, a number of criticisms and questions have been casted on it in the past few years, largely due to the disappointment resulting from the failure of clinical trials targeting Aβ. Given its attributed role as the initiator of the pathogenic cascade ultimately leading to AD, major efforts to develop effective therapies for AD patients were directed against Aβ, including inhibitors and modulators of the enzymes β- y γ-secretases, anti-Aβ aggregants (i.e. tramiprosate), and particularly, anti-Aβ immunization. However, so far none of the clinical trials using these approaches has significantly impacted the rate of cognitive decline of the patients enrolled (reviewed in Haas, 2012). Drugs with presumed Aβ-reducing and anti-inflammatory effects, such as non-steroidal anti-inflammatory drugs (NSAIDs) and statins, also failed in clinical trials in both MCI and mild-to-moderate AD patients, despite numerous prior epidemiological studies reporting a substantial reduction of the risk of developing AD in the general population (reviewed in McGuinness et al., 2010; Shepardson et al., 2011ab; and Jaturapatporn et al., 2012).

Although these failures could be partially explained by pharmacokinetic or pharmacodynamic issues (i.e. insufficient penetration of the drug in the brain, insufficient dose, side-effects), and specially, by the targeting of AD patients in a late stage of their disease (Selkoe, 2011), some authors have proposed a revision of the amyloid cascade hypothesis. A "dual pathway" model has been proposed in which Aβ and tau have their own parallel pathogenic cascades that would be linked by the same trigger and/or some molecular links acting more downstream. The *APOEε*4 allele and the glycogen synthase kinase 3 (GSK3) have been postulated as putative upstream molecular targets linking Aβ and tau cascades (Small and Duff, 2011). As discussed in further detail within the hypothesis section, we propose a much less drastic modification of the amyloid cascade hypothesis consisting on the differentiation of two stages: a first stage, in which Aβ ignites not only a single but multiple pathogenic cascades, including oxidative stress, glial responses, and tau hyperphosphorylation and aggregation; and a second stage, in which these processes initially triggered by and dependent on Aβ, ultimately lead to a progressive synaptic and neuronal loss in a Aβ-independent fashion (Figure 2) (Hyman, 2011).
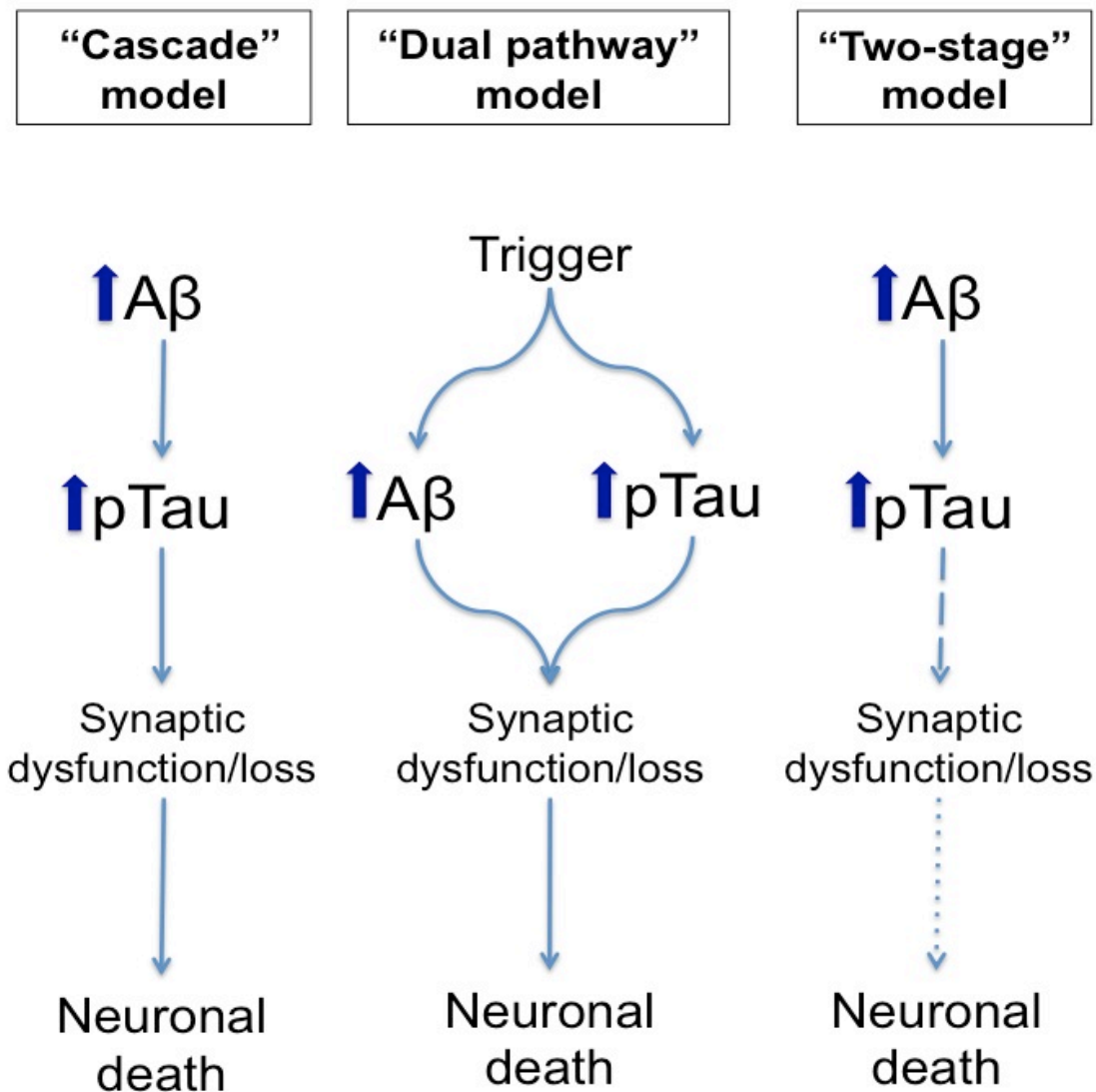
Figure 2. Proposed models for the pathophysiology of Alzheimer disease. The classical "cascade" model is a serial model in which Aβ is a trigger of a series of downstream adverse events (Hardy and Selkoe, 2002). The "dual pathway" model proposes the existence of independent pathogenic cascades for Aβ and tau that are triggered by common molecular links (i.e. *APOEɛ*4, GSK3, retromer deficiency) (Small and Duff, 2008). The "two-stage" model supports the existence of a cascade with an amyloid-dependent stage triggered by Aβ (solid arrow), and an amyloid-independent stage, in which neurotoxic processes become progressively independent of Aβ (dotted and dashed arrows) (Hyman 2011).

2.2. Role of glia in Alzheimer disease.

Besides amyloid plaques and NFTs, another very prominent (yet long neglected) positive lesion in the AD brain is the glial response mediated by reactive astrocytes and activated microglia. The classic view of glial cells as mere supporting cells offering *trophic support* to neurons is currently being revised. Microglial cells have been recently involved in the pruning of redundant and unnecessary synapses during the embryonic development and, in certain synapses, also during the postnatal period (Paolicelli et al., 2011; Schafer et al., 2012). Astrocytes modulate synaptic activity by releasing small molecules at the synaptic cleft, such as ATP, adenosine, D-serine, and possibly glutamate, a process termed *gliotransmission*. In fact, astrocytic end-feet are present in up to a 60% of excitatory synapses in the rat hippocampus, as part of the *tripartite synapse* (reviewed in Perea et al., 2009). Astrocytes are also part of the blood-brain barrier, where they regulate the *neurovascular coupling*. Both glial cell types not only produce neurotrophic factors but actively survey the environment and respond to certain signals that neurons present in their plasma membrane or secrete to the extracellular space when the brain suffers an insult or injury, either acute (i.e. infection, trauma, stroke) or chronic, such as AD and other neurodegenerative diseases. This response of glial cells is called *activation* and consist of a double change morphological and functional: on one hand, their somas become hypertrophic and their processes, normally very thinly ramified, retract and turn thicker; on the other hand, they acquire phagocytic capacity, and/or secrete potentially harmful biomolecules such as pro-inflammatory cytokines and reactive oxygen species.

The role of glial cells in AD is controversial, perhaps because their effects are dual, initially beneficial but ultimately deleterious (Wyss-Coray, 2006). In the cerebral cortex of AD patients both reactive astrocytes and activated microglia tend to cluster within and around dense-core amyloid plaques, suggesting that Aβ triggers the recruitment and activation of glia and initiates an inflammatory cascade (Itagaki et al., 1989; Pike et al., 1995; Vehmas et al., 2003). The dual nature of glia in AD has been more investigated with respect to microglia: while some studies in mice models that recapitulate AD pathology have shown that microglia may contribute to neuronal loss (Furhmann et al., 2009), other studies support a role of activated microglia in Aβ phagocytosis and degradation (El Khoury et al., 2007; Bolmont et al., 2008), and other authors

defend the idea that microglia in AD is defective at clearing Aβ (Hickman et al., 2008; Grathwohl et al., 2009; Heneka et al., 2010). In the case of astrocytes, although they may be effective at forming a scar around plaques and preventing plaque growth, their recruitment by amyloid plaques may compromise their function at modulating synaptic activity and providing trophic support to neurons in areas distant from plaques.

Surprisingly, the progression of astrocytic and microglial responses through the course of AD and with respect to the other AD neuropathological hallmarks has not been described in detail in the literature, despite the fact that such data may shed light about their role in the disease and have both diagnostic (i.e. development of diagnostic and progression biomarkers) and therapeutic (i.e. development of anti-inflammatory drugs) implications. Following our two-stage model of the AD natural history, we hypothesized that glial responses, although initially directed towards amyloid plaques, become independent of plaques and spread throughout the neuropil, paralleling the neurodegenerative process downstream Aβ rather than the extent of Aβ deposition. Thus, at some point during the progression of the disease, glial responses could behave as a surrogate marker of neurodegeneration or even contribute to the neurodegenerative cascade.

2.3. Effects of anti-Aβ immunization on the Alzheimer brain.

The finding that monoclonal antibodies directed against the Aβ peptide sequence are able to dissolve pre-formed Aβ fibrils and prevent the polymerization of monomeric Aβ *in vitro* (Solomon et al., 1996 y 1997), prompted the study of the efficacy of immunotherapy in APP-overexpresing mouse models, that recapitulate the amyloid deposits of human AD. Both active and passive immunization (with aggregates prepared with synthetic Aβ and with anti-Aβ monoclonal antibodies, respectively) rendered excellent results in these murine models. Both approaches were effective to prevent the amyloid deposition in young mice and to clear existing deposits in aged animals (Schenk et al., 1999; Janus et al., 2000; Morgan et al., 2000; Bard et al., 2000; Bacskai et al., 2001; DeMattos et al., 2001; Dodart et al., 2002). Moreover, anti-Aβ immunization was able to prevent synaptic loss and to restore plaque-associated neuritic

dystrophies (Buttini et al., 2005; Brendza et al., 2005; Spires-Jones et al. 2009; Rozkalne et al. 2009). These animal studies led to the design of clinical trials in patients with mild-to-moderate AD. However, after a phase 1 trial without significant adverse effects, the first active immunotherapy trial with a preparation of Aβ aggregates (AN1792) had to be halted in its phase 2a after 6% of patients in the treatment group developed an autoimmune meningoencephalitis (Orgogozo et al., 2003). Currently, several clinical trials with passive immunotherapy have been completed or are ongoing (for updated information, see the website: http://clinicaltrials.gov/ct2/results?term=Alzheimer+disease).

The effects of anti-Aβ active immunization on the neuropathology of AD observed can be summarized as: 1) significant reduction in amyloid load, with a relative abundance of collapsed "moth-eaten" plaques among the remaining ones; 2) increased severity of cerebral amyloid angiopathy (CAA), with increased frequency of CAA-related microbleeds; 3) decrease in the density of clusters of neuritic dystrophies, reactive astrocytes and activated microglia, due to an effective clearance of plaques; and 4) a number and distribution of NFTs typical of advance AD (Braak stage V or VI in most cases) (Nicoll et al., 2003; Ferrer et al., 2004; Masliah et al., 2005; Bombois et al., 2007; Boche et al., 2008; Uro-Coste et al., 2010).

Although there is a substantial evidence of the beneficial effects of both active and passive anti-Aβ immunization on the integrity of synapses and the morphology of neurites (dendrites and axons) in animal models that develop amyloid plaques, little is known about these effects in the brain of patients with AD. In addition, besides the original description of collapsed "moth-eaten" amyloid plaques, the characteristics and properties of plaques remaining after immunization have not been fully documented. Lastly, the effect of the reduction of amyloid plaques on the tau pathology, and specifically on the aberrant misfolding, hyperphosphorylation and aggregation of tau in NFTs, beyond the application of Braak staging, has not been investigated with detail. According to our two-stage model of the pathophysiology of AD, we hypothesized that removing plaques at the stage of mild-to-moderate AD, may improve neuropil changes that are directly induced by plaques and closely associated to them, but may not be effective at restoring more downstream pathological events such as the aggregation of tau within the neurons.

3

HYPOTHESIS AND AIMS

3.1. Hypothesis.

We postulate the existence of two phases in the pathophysiology of AD (Hyman, 2011):

1. **Amyloid-dependent stage:** this initial phase is characterized by the widespread deposition of amyloid plaques in the cerebral cortex, where they will trigger a local cascade of adverse events including pro-inflammatory glial responses, oxidative stress, hyperphosphorylation and aggregation of tau in dystrophic neurites, and synaptic dysfunction and loss around them (Figure 1). This stage largely predates the appearance of the cognitive symptoms that characterize the disease, but represents a window of opportunity to prevent the onset of cognitive deficits through anti-Aβ therapies.

2. **Amyloid-independent stage:** at this stage, the cascade of adverse events becomes independent of Aβ, its initial trigger, and is not restricted to the local environment around the plaques but extends to distant regions. This stage is characterized by an increasing accumulation of hyperphosphorylated tau in neurofibrillary tangles and a massive loss of

synapses and neurons extending through the association cortex, which leads to the disconnection of distant areas of the neural network. This stage parallels the development and progression of the constellation of cognitive symptoms that ultimately will conform the dementia syndrome associated to AD. As this cascade runs independently of Aβ, at this stage the therapies directed to remove amyloid plaques and/or soluble Aβ oligomers (i.e. anti-Aβ immunization) will be ineffective to arrest the clinical progression of the disease.

3.2. Overall and specific aims.

Overall aim#1

To characterize the progression of the pathological hallmarks of AD (amyloid plaques and NFTs), the glial responses to these lesions, and the cortical atrophy.

Specific aims:

1.1. To address the temporal progression of these pathological lesions through the correlation of their quantitative measures with the duration of clinical disease;

1.2. To evaluate whether glial responses correlate and remain associated to amyloid plaques through the disease course or whether, according to our hypothesis, they become independent of Aβ deposition.

Overall aim#2

To characterize the effect of anti-Aβ active immunization in the brain of patients with AD who participated in a phase 2a clinical trial with this disease-modifying therapy (AN1792, Elan Pharmaceuticals Inc.).

Specific aims:

2.1. To assess its effect on the amyloid plaque burden;

2.2. To evaluate its effect on plaque-associated neuritic changes;

2.3. To describe the properties of amyloid plaques remaining after immunization (size, proportion of diffuse versus dense-core plaques, plaque-associated neuritic dystrophies and glial responses);

2.4. To investigate the characteristics of neurofibrillary tangles (misfolding, hyperphosphorylation and aggregation of tau).

4

METHODOLOGICAL CONSIDERATIONS

4.1. Postmortem brain tissue.

Brains from patients with AD and from subjects without evidence of neurodegenerative disease were obtained from the Massachusetts General Hospital Brain Bank. Specifically, formalin-fixed, paraffin-embedded eight-micron-thick sections were obtained from the hippocampus at the level of the lateral geniculate nucleus and from the temporal association cortex (Brodmann Area 38).

4.2. Immunohistochemistry.

Sections were deparaffinized with xylenes and hydrated with increasing concentrations of ethanol before performing immunohistochemical techniques to reveal the AD pathological hallmarks. The antibodies used in these immunostainings, the antigen retrieval methods, and the visualization strategies are depicted in Table 1. The counterstaining procedures used in this study are described in Table 2.

Table 1. Description of immunohistochemical methods used.

Antibody	Source	Antigen	Host species/ Ig isotype	Dilution	Antigen retrieval method	Visualization method
10D5	Elan Pharmaceuticals	Aβ, N-terminus	Mouse / IgG1 monoclonal	1:50	Citrate buffer + microwave + formic acid	DAB
3D6	Elan Pharmaceuticals	Aβ, N-terminus	Mouse / IgG1 monoclonal	1:1000	Citrate buffer + microwave	Cy3
Nab61	Dr. Virginia Lee (University of Pensylvannia, PA)	Oligomeric Aβ	Mouse / IgG1 monoclonal	1:500	--------	Cy3
Alz50	Dr. Peter Davies (Albert Einstein College, Bronx, NY)	Misfolded Tau	Mouse / IgM monoclonal	1:50	Citrate buffer + microwave	Cy3
PHF1	Dr. Peter Davies (Albert Einstein College, Bronx, NY)	Hyperphosphorylated Tau (Serine 396/404)	Mouse / IgG1 monoclonal	1:200	Citrate buffer + microwave	ABC+DAB
GFAP	Sigma-Aldrich (G9269)	Glial Fibrillar Acidic Protein (reactive astrocytes)	Rabbit / IgG1 polyclonal	1:1000	Citrate buffer + microwave	ABC+DAB / Cy3
CD68	Dako (Clone KP1, M-0814)	Activated / phagocytic microglia	Mouse / IgG1 monoclonal	1:100	Citrate buffer + microwave	ABC+DAB / Cy3
IBA1	Wako (019-19741)	Ionized calcium Binding Adaptor molecule 1 (activated microglia)	Rabbit / IgG1 polyclonal	1:250	Citrate buffer + microwave	Cy3
SMI-312	Covance (SMI-312R)	Non-phosphorylated neurofilament (axons and dystrophic neurites)	Mouse / IgG1 monoclonal	1:1000	Citrate buffer + microwave	Cy3
NF-H	Abcam (ab40796)	Neurofilament heavy chain (axons and dendrites)	Rabbit / IgG1 policlonal	1:100	Citrate buffer + microwave	Cy3
VDAC1 / porin	Abcam (ab15895)	Voltage-dependent anion channel 1, porin (mitochondria)	Rabbit / IgG1 polyclonal	1:1000	Citrate buffer + microwave	Cy3

Table 2. Description of the counterstaining histochemical methods used.

Staining	Brand/Catalog number	Method	Target	Results of staining
Thioflavin-S	Sigma-Aldrich / T1892	0.05% in ethanol 50%, 8 min., followed by clearance with ethanol 80% 30 s.	Fibrillar aggregates of proteins with abnormal conformation (β-pleated sheet structure)	Dense-core amyloid plaques and neurofibrillary tangles
4′,6-diamidino-2-phenylindole (DAPI)	Fisher Scientific	Solution in TBS, 10 min.	DNA	Fluorescent ultraviolet nuclear staining
Hematoxyline	Sigma-Aldrich / MHS32	Mayer's Hematoxyline, 30 s.	Acids, including DNA	Visible nuclear staining
Periodic Acid-Schiff (P.A.S.)	Sigma-Aldrich / P5463 and 3952016	Periodic Acid 0.5%, 5 min, followed by Schiff's reagent 15 min. (dilution 1:20)	Glycogen, mucine and other polysaccharides	Basement membranes of capillaries and other blood vessels

4.3. Neuropathological quantitative analyses.

Cortical thickness

In AD there is a progressive cortical atrophy resulting from the loss of synapses, neurons and neurites. This cortical atrophy follows a hierarchical temporal and spatial pattern that starts in the medial temporal lobe and spreads towards the association temporal, frontal, parietal and occipital cortices. In this study, cortical thickness was used as a global parameter of the neurodegenerative process associated to AD progression. Cortical thickness was measured in the temporal cortex (BA38) on sections stained with hematoxylin, eosin, and Luxol Fast Blue, using an Olympus BX51 microscope, equipped with a motorized stage and a video camera and coupled with the computer software CAST. The average of 20 measures randomly distributed along the cortical ribbon of the specimen was obtained under the 1.6x objective, using the appropriate tool of CAST software.

Amyloid burden

The amyloid burden was measured as the percent of cortical surface occupied by amyloid plaques in sections immunostained with the mouse monoclonal anti-Aβ antibody 10D5 (Elan Pharmaceuticals), using the peroxidase technique with DAB as a substrate. Sections were place under the 10x objective on the motorized stage of a Leica microscope model DRMB equipped a video camera and coupled with the computer software BIOQUANT Nova Prime. The optical threshold application of this software was used to capture the particles (plaques) stained. The calibration was kept constant at a magnification factor of 1.6158 μm^2/pixel.

Stereology-based quantification of neuropathology

Stereology is a technique that, when applied to histology, enables to obtain quantitative unbiased results of any given object (i.e. amyloid plaques or NFTs), by performing a systematic and random sampling of the specimen under the microscope and, then, extrapolating this result to the entire specimen (Hyman et al., 1998). Modern stereology is performed with microscopes equipped with a motorized stage and a videocamera and coupled with computer software.

Stereology-based analyses on sections stained with the peroxidase-DAB technique were performed with a Leica-BIOQUANT system, whereas those conducted on fluorescently stained sections were performed with a Olympus-CAST system. In both cases, the densities of total (10D5+) amyloid plaques, dense-core (ThioS+) amyloid plaques, oligomeric Aβ-enriched (NAB61+) plaques, NFTs (PHF1+), activated (CD68+, IBA1+) microglial cells, and reactive (GFAP+) astrocytes, were obtained. These densities were then corrected by the cortical thickness of each specimen to prevent bias due to disease-related atrophy.

Quantitative characterization of the properties of amyloid plaques

Plaque size distribution

The size distribution of total (10D5+) amyloid plaques was obtained with the Leica-BIOQUANT system that provides not only the quantification of amyloid burden, but also the size of each of the particles captured above the optical threshold. The size distribution of dense-core (ThioS+) plaques was obtained using the appropriate tool of the public domain sotware ImageJ (http://rsbweb.nih.gov/ij/). The selection of fields with dense-core plaques included in this analysis was performed in a random fashion using the system Olympus-CAST.

Percent of dense-core plaques

For this analysis, plaques were immunostained with the anti-Aβ monoclonal antibody 3D6 and counterstained with Thioflavin-S. The plaques were randomly selected using the optical dissector technique in the stereology software CAST.

Neuritic changes

The plaques and neuritis included in these analyses were also randomly selected with the system Olympus-CAST. The quantification of the number of neuritic dystrophies per plaque and of the percent of dense-core plaques with mitochondrial accumulation in those dystrophic neurites was performed on sections double-stained with Thioflavin-S and the anti-SMI312 or the anti-VDAC1 antibodies, respectively. In addition, the curvature ratio of neurites surrounding dense-core plaques was measured in sections doubly stained with Thioflavin-S and the anti-NF-H antibody, which labels both dendrites and axons. The curvature ratio was calculated as a

fraction with the neurite length as numerator and the end-to-end distance as the denominator. Therefore, if a neurite is completely straight, its curvature ratio will equal 1, and the more tortuous the neurite the higher will be its curvature ratio. Prior studies have demonstrated that the neurite curvature ratio is higher in AD patients compared to non-demented subjects and in plaque-bearing transgenic mice than in their wild-type littermates. Moreover, these studies have shown that the curvature ratio is higher in the vicinity of dense-core plaques (≤ 50 μm) than far away from them (Knowles et al., 1999; D'Amore et al., 2003). Thus, the curvature ratio is a measure of the toxic effect of amyloid plaques on the trajectory of surrounding neurites that is much more subtle than the notorious neuritic changes present within the plaques.

Glial responses

Plaque-associated glial responses were quantified in sections doubly stained with Thioflavin-S and an antibody against GFAP (reactive astrocytes) or Iba1 or CD68 (activated microglia). Again, plaques and glial cells were randomly selected using the Olympus-CAST system. Only glial cells with a DAPI-positive nucleus were counted and only the soma (not the processes) was used to refer the location of the glial cell with respect to the closest plaque or NFT. A boundary of 50 μm from the edge of the closest plaque was used to consider a glial cell close to a plaque. The same boundary was considered to quantify glial cells located in the vicinity of NFTs but far from dense-core plaques.

5

RESULTS

5.1. Review article:

Serrano-Pozo A, Frosch MP, Masliah E, Hyman BT. Neuropathological alterations in Alzheimer's disease. *Cold Spring Harb Perspect Med* 2011; 1(1): a006189.

Neuropathological Alterations in Alzheimer Disease

Alberto Serrano-Pozo[1], Matthew P. Frosch[1,2], Eliezer Masliah[3], and Bradley T. Hyman[1]

[1]Alzheimer Research Unit of the MassGeneral Institute for Neurodegenerative Disease, Department of Neurology of the Massachusetts General Hospital, and Harvard Medical School, Charlestown, Massachusetts 02129-4404

[2]C.S. Kubik Laboratory for Neuropathology, Massachusetts General Hospital, Boston, Massachusetts 02114

[3]Department of Neuroscience and Department of Pathology, University of California-San Diego School of Medicine, La Jolla, California 92093-0624

Correspondence: bhyman@partners.org

The neuropathological hallmarks of Alzheimer disease (AD) include "positive" lesions such as amyloid plaques and cerebral amyloid angiopathy, neurofibrillary tangles, and glial responses, and "negative" lesions such as neuronal and synaptic loss. Despite their inherently cross-sectional nature, postmortem studies have enabled the staging of the progression of both amyloid and tangle pathologies, and, consequently, the development of diagnostic criteria that are now used worldwide. In addition, clinicopathological correlation studies have been crucial to generate hypotheses about the pathophysiology of the disease, by establishing that there is a continuum between "normal" aging and AD dementia, and that the amyloid plaque build-up occurs primarily before the onset of cognitive deficits, while neurofibrillary tangles, neuron loss, and particularly synaptic loss, parallel the progression of cognitive decline. Importantly, these cross-sectional neuropathological data have been largely validated by longitudinal in vivo studies using modern imaging biomarkers such as amyloid PET and volumetric MRI.

The neuropathological changes of Alzheimer disease (AD) brain include both positive and negative features. Classical positive lesions consist of abundant amyloid plaques and neurofibrillary tangles, neuropil threads, and dystrophic neurites containing hyperphosphorylated tau (see Box 1 for glossary) (Terry et al. 1994, Mandelkow and Mandelkow 1998, Trojanowski and Lee 2000; Iqbal and Grundke-Iqbal 2002; Crews and Masliah 2010), that are accompanied by astrogliosis (Beach et al. 1989; Itagaki et al. 1989), and microglial cell activation (Rogers et al. 1988; Itagaki et al. 1989; Masliah et al. 1991). Congophilic amyloid angiopathy is a frequent concurrent feature. Unique lesions, found primarily in the hippocampal formation, include Hirano bodies and granulovacuolar degeneration. In addition to these positive lesions, characteristic losses of neurons, neuropil, and synaptic elements are core negative features of AD (Scheff et al. 1990, 2006, 2007; DeKosky and Scheff 1990;

Terry et al. 1991; Masliah et al. 1993b; Scheff and Price 1993, 1994; Gomez-Isla et al. 1996, 1997; Knowles et al. 1999). Each of these lesions has a characteristic distribution, with plaques found throughout the cortical mantle, and tangles primarily in limbic and association cortices (Arnold et al. 1991; Braak and Braak 1991; Thal et al. 2002). The hierarchical pattern of neurofibrillary degeneration among brain regions is so consistent that a staging scheme based on early lesions in the entorhinal/perirhinal cortex, then hippocampal Ammon subfields, then association cortex, and finally primary neocortex is well accepted as part of the 1997 NIA-Reagan diagnostic criteria (NIA-RI Consensus 1997). Neuronal loss and synapse loss largely parallel tangle formation, although whether tangles are causative of neuronal loss or synaptic loss remains uncertain (Gómez-Isla et al. 1997; Iqbal and Grundke-Iqbal 2002; Bussière et al. 2003; Hof et al. 2003; Yoshiyama et al. 2007; Spires-Jones et al. 2008; de Calignon et al. 2009, 2010; Kimura et al. 2010).

BOX 1. Glossary

Amyloid plaques: extracellular deposits of amyloid β abundant in the cortex of AD patients. Amyloid plaques are commonly classified in diffuse and dense-core based on their morphology and positive or negative staining with Thioflavin-S or Congo Red.

Dense-core plaques: fibrillar amyloid deposits with compact core that stains with Thioflavin-S and Congo Red. Dense-core plaques are typically surrounded by dystrophic neurites (neuritic plaques), reactive astrocytes and activated microglial cells, and associated with synaptic loss. A semi-quantitative score of neuritic plaques is used for the pathological diagnosis of AD because their presence is generally associated with the presence of cognitive impairment.

Diffuse plaques: amorphous amyloid deposits with ill-defined contours that are Congo Red and Thioflavin S negative. Diffuse plaques are usually nonneuritic and not associated with glial responses or synaptic loss. This plaque type is not considered for the pathological diagnosis of AD because it is a relatively common finding in the brain of cognitively intact elderly people.

Cerebral amyloid angiopathy (CAA): deposits of amyloid β in the tunica media of leptomeningeal arteries and cortical capillaries, small arterioles and medium-size arteries, particularly in posterior areas of the brain. Some degree of CAA, usually mild, is present in ≈80% of AD patients. If severe, CAA can weaken the vessel wall and cause life-threatening lobar hemorrhages.

Amyloid β: a 40 or 42 amino acid peptide derived from amyloid precursor protein (APP) after its sequential cleavage by β- and γ-secretases. Its physiological role is likely related to the modulation of synaptic activity although still controversial. In AD Aβ accumulates forming intermediate soluble oligomers that are synaptotoxic as well as insoluble β-sheet pleated amyloid fibrils that are the main constituent of dense-core plaques (mainly Aβ42) and cerebral amyloid angiopathy (primarily Aβ40).

Neurofibrillary tangles (NFTs): intraneuronal aggregates of hyperphosphorylated and misfolded tau that become extraneuronal ("ghost" tangles) when tangle-bearing neurons die. NFTs have a stereotypical spatiotemporal progression that correlates with the severity of the cognitive decline. In fact, a topographic staging of NFTs (Braak and Braak 1991) is used for the pathological diagnosis of AD.

Neuropil threads: axonal and dendritic segments containing aggregated and hyperphosphorylated tau that invariably accompany neurofibrillary tangles in AD.

Tau: a microtubule-associated protein normally located to the axon, where it physiologically facilitates the axonal transport by binding and stabilizing the mictrotubules. In AD, tau is translocated to the somatodendritc compartment and undergoes hyperphosphorylation, misfolding, and aggregation, giving rise to neurofibrillary tangles and neuropil threads.

Although all these neuropathological characteristics are useful diagnostic markers, the cognitive impairment in patients with AD is closely associated with the progressive degeneration of the limbic system (Arnold et al. 1991; Klucken et al. 2003), neocortical regions (Terry et al. 1981), and the basal forebrain (Teipel et al. 2005). This neurodegenerative process is characterized by early damage to the synapses (Masliah and Terry 1993, 1994; Masliah 2000; Crews and Masliah 2010) with retrograde degeneration of the axons and eventual atrophy of the dendritic tree (Coleman and Perry 2002; Higuchi et al. 2002; Grutzendler et al. 2007; Perlson et al. 2010) and perikaryon (Hyman et al. 1986; Lippa et al. 1992). Indeed, the loss of synapses in the neocortex and limbic system is the best correlate of the cognitive impairment in patients with AD (DeKosky and Scheff 1990; Terry et al. 1991; DeKosky et al. 1996).

In addition to the lesions detected by classical histopathological stains, including silver stains for tangles and plaques or immunostaining and quantitative analysis (or quantitative EM) for synaptic alterations, several lines of investigation now support the view that increased levels of soluble amyloid-β_{1-42} (Aβ) oligomers, might lead to synaptic damage and neurodegeneration (Lambert et al. 1998; Klein et al. 2001; Klein 2002; Walsh et al. 2002; Walsh and Selkoe 2004; Glabe 2005; Lesne et al. 2006; Townsend et al. 2006; Lacor et al. 2007). In experimental models, it has been shown that transsynaptic delivery of Aβ, for example from the entorhinal cortex to the molecular layer of the dentate gyrus, promotes neurodegeneration characterized by synapse loss (Harris et al. 2010a) and alterations to calbindin-positive neurons (Palop et al. 2003). This is accompanied by circuitry dysfunction and aberrant innervation of the hippocampus by NPY-positive fibers among others (Harris et al. 2010b; Palop et al. 2011). The Aβ oligomers secreted by cultured neurons inhibit long-term potentiation (LTP), damage spines and interfere with activity-regulated cytoskeleton associated protein (Arc) distribution (Klein et al. 2001; Walsh and Selkoe 2004; Townsend

et al. 2006; Selkoe 2008). Together, these studies indicate that Aβ oligomers ranging in size from 2 to 12 subunits might be responsible for the synaptic damage and memory deficits in AD (Lacor et al. 2007). Similar neurotoxic Aβ oligomers found in vitro and in APP transgenic models have been also identified in the CSF (Klyubin et al. 2008) and in the brains of patients with AD (Shankar et al. 2008; McDonald et al. 2010; Pham et al. 2010). These studies have shown that Aβ oligomers progressively accumulate in the brains of AD patients, although their relationship to the severity of the cognitive impairment remains uncertain.

In summary, in recent years, the concept of neurodegeneration in AD has been expanded from the idea of general neuronal loss and astrogliosis to include earlier alterations such as synaptic and dendritic injury and disturbances in the process of adult neurogenesis (Jin et al. 2004; Li et al. 2008; Crews et al. 2010), circuitry dysfunction, and aberrant innervation. All of these factors are important targets to consider when developing neuroprotective treatments for AD.

MACROSCOPIC FEATURES

Although the gross visual examination of the AD brain is not diagnostic, a typical symmetric pattern of cortical atrophy predominantly affecting the medial temporal lobes and relatively sparing the primary motor, sensory, and visual cortices, is considered strongly suggestive of AD being the condition underlying the patient's dementia. As a result of this pattern of cortical thinning, the lateral ventricules, particularly their temporal horns, can appear prominently dilated (ex vacuo hydrocephalus). This pattern is stereotypic and can be recognized early in the clinical course of the disease by MRI scan (Dickerson et al. 2009, 2011). Cerebrovascular disease, usually in the form of small vessel occlusive disease caused by chronic hypertension and other vascular risk factors, is a condition that frequently accompanies aging in general and also AD in particular. Thus, it is relatively common to find some cortical

microinfarcts, lacunar infarcts in the basal ganglia, and demyelination of the periventricular white matter. The presence of cortical petechial microbleeds or even evident lobar hemorrhages, particularly in the posterior parietal and occipital lobes, should lead to the suspicion of a concurrent severe cerebral amyloid angiopathy. Unless there is a concomitant Parkinson's disease or dementia with Lewy bodies, the substantia nigra shows a normal coloration; in contrast, the locus coeruleus is affected in the early stages of AD (Braak and Del Tredici 2011).

MICROSCOPIC FEATURES

Neurofibrillary Tangles

Composition

The neurofibrillary tangles (NFTs) were first described by Alois Alzheimer in his original autopsy case report as intraneuronal filamentous inclusions within the perikaryal region of pyramidal neurons. Ultrastructural studies on AD brain specimens revealed that NFTs are primarily made of paired helical filaments (PHFs), that is, fibrils of ≈10 nm in diameter that form pairs with a helical tridimensional conformation at a regular periodicity of ≈65 nm (Kidd 1963, 1964; Wisniewski et al. 1976). A small proportion of fibrils within the NFTs do not form pairs, but give the appearance of straight filaments without the periodicity of PHFs (Crowther 1991). Occasional hybrid filaments, with a sharp transition between a paired helical segment and a straight segment, have also been described within NFTs (Crowther 1991). Recently, modern high-resolution molecular microscopy techniques have revealed the presence of twisted ribbon-like assemblies of tau fibrils in vitro, thus challenging the PHF concept (Wegmann et al. 2010). Regardless of the morphology of their structural units, the major constituent of NFTs was found to be the microtubule-associated protein tau, which is aberrantly misfolded and abnormally hyperphosphorylated. Invariably accompanying NFTs are the neuropil threads, which are thought to

result from the breakdown of dendrites and axons of the tangle-bearing neurons.

Morphological Characteristics

The NFTs are argyrophilic and can be shown by silver impregnation methods such as the Gallyas technique (Braak and Braak 1991). An alternative method to examine NFTs is their staining with fluorescent dyes such as Thioflavin-S, which recognize the β-sheet pleated structure of the paired helical filaments (Arnold et al. 1991), or by immunostaining with anti-tau antibodies (Fig. 1). Three morphological stages have been distinguished: (1) Pre-NFTs or diffuse NFTs are defined by a diffuse, sometimes punctate, tau staining within the cytoplasm of otherwise normal-looking neurons, with well-preserved dendrites and a centered nucleus; (2) Mature or fibrillar intraneuronal NFTs (iNFTs) consist of cytoplasmic filamentous aggregates of tau that displace the nucleus toward the periphery of the soma and often extend to distorted-appearing dendrites and to the proximal segment of the axon; (3) extraneuronal "ghost" NFTs (eNFTs) result from the death of the tangle-bearing neurons and are identifiable by the absence of nucleus and stainable cytoplasm (Su et al. 1993; Braak et al. 1994; Augustinack et al. 2002). Both silver and Thioflavin-S stains, as well as some phosphotau antibodies such as AT8 and PHF1, preferentially identify the iNFTs and the eNFTs (Braak et al. 1994; Augustinack et al. 2002). By contrast, other phosphoepitopes (e.g., pThr153, pSer262, pThr231) and a certain conformational epitope recognized by the antibodies MC1 and Alz50 also recognize pre-NFTs, suggesting that the misfolding of the tau molecule and its phosphorylation in certain sites represent an early step prior to tau aggregation (Carmel et al. 1996; Weaver et al. 2000; Augustinack et al. 2002). Interestingly, the immunoreactivity for a caspase-cleaved form of tau with a faster rate of fibrillization than the full length molecule in vitro colocalize with Alz50 immunoreactivity in pre-NFTs, suggesting that the caspase-mediated cleavage of the carboxy-terminal region of the tau molecule is
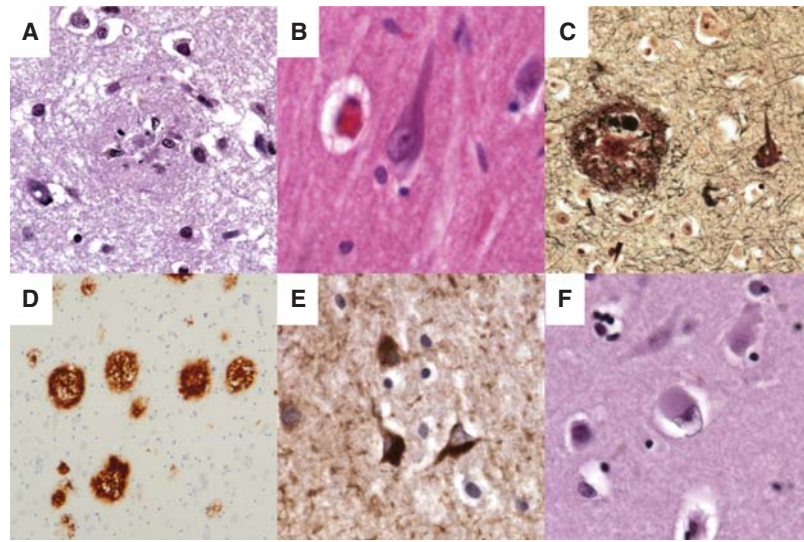
Figure 1. Photomicrographs of the core pathological lesions observed in Alzheimer and Lewy body diseases. (*A*) Plaque evident on routine H&E stained section of frontal cortex; (*B*) tangle in a hippocampal pyramidal neuron on routine H&E stained section; (*C*) silver stain highlights both a plaque and a tangle; (*D*) immunohistochemistry against Aβ highlights plaques; (*E*) immunohistochemistry against tau highlights tangles; (*F*) a cortical Lewy body can be seen in a layer V neuron on a routine H&E stained section of frontal cortex.

also a necessary step prior to further aggregation (Guillozet-Bongaarts et al. 2005).

Topographical Distribution

The spatiotemporal pattern of progression of NFTs (and neuropil threads in parallel) is rather stereotypical and predictable (Arnold et al. 1991; Braak and Braak 1991; Braak et al. 2006). Briefly, the neurofibrillary degeneration starts in the allocortex of the medial temporal lobe (entorhinal cortex and hippocampus) and spreads to the associative isocortex, relatively sparing the primary sensory, motor, and visual areas. In their clinicopathological study, Braak and Braak distinguished six stages that can be summarized in three: entorhinal, limbic, and isocortical (Fig. 2). The first NFTs consistently appear in the transentorhinal (perirhinal) region (stage I) along with the entorhinal cortex proper, followed by the CA1 region of the hippocampus (stage II). Next, NFTs develop and accumulate in limbic structures such as the subiculum of the hippocampal formation (stage III) and the amygdala, thalamus, and claustrum (stage IV). Finally, NFTs spread to all isocortical areas (isocortical stage), with the associative areas being affected prior and more severely (stage V) than the primary sensory, motor, and visual areas (stage VI). A severe involvement of striatum and substantia nigra can occur during the late isocortical stage. Of note, this neurofibrillary degeneration follows a laminar pattern affecting preferentially the stellate neurons of layer II, the superficial portion of layer III, and the large multipolar neurons of layer IV within the entorhinal cortex; the stratum pyramidale of CA1 and subiculum within the hippocampal formation, and the pyramidal neurons of layers III and V within the isocortical areas (Hyman et al. 1984; Arnold et al. 1991; Braak and Braak 1991).

Clinicopathological Correlations

Multiple clinicopathological studies from different groups have established that the amount and distribution of NFTs correlate with the severity and the duration of dementia (Arriagada et al. 1992a; Bierer et al. 1995; Gómez-Isla et al.
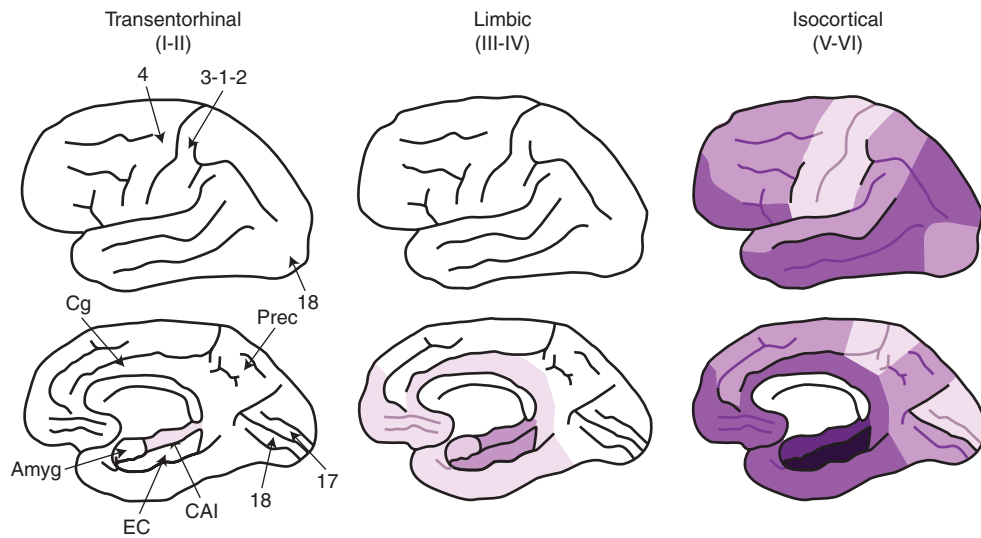
Figure 2. Spatiotemporal pattern of neurofibrillary degeneration. Shading indicates the distribution of NFTs with darker colors representing increasing densities. Amyg = Amygdala; EC = Entorhinal cortex; CA1 = Cornus ammonis 1 hippocampal subfield; Cg = Cingulate cortex; Prec = Precuneus; 4 = Primary motor cortex; 3-1-2 = Primary sensory cortex; 17 = Primary visual cortex; 18 = Associative visual cortex (data based on Arnold et al. 1991; Braak and Braak 1991; Arrigada et al 1992a,b; Braak et al. 1994).

1997; Giannakopoulos et al. 2003; Ingelsson et al. 2004). Moreover, the selective rather than widespread topographical distribution of NFTs described above matches with the hierarchical neuropsychological profile typical of the AD-type dementia syndrome. The prominent initial impairment of episodic memory characteristic of AD is explained by the isolation of the medial temporal lobe structures from the association isocortex and the subcortical nuclei because of the ongoing massive neurofibrillary degeneration. Next, the involvement of multimodal high-order association isocortical areas accounts for the progressive impairment of additional cognitive domains, including executive dysfunction (prefrontal cortex), apraxias (parietal cortex), visuospatial navigation deficits (occipitoparietal cortex), visuoperceptive deficits (occipitotemporal cortex), and semantic memory (anterior temporal cortex), giving rise to the full-blown dementia syndrome. By contrast, the late involvement of primary motor, sensory, and visual isocortical areas explains the sparing of motor, sensory, and

primary visual functions (Hyman et al. 1984; Arnold et al. 1991; Braak and Braak 1991). However, as discussed below, whether NFT formation is a necessary precursor of the neuronal death in AD or represents a protective response of damaged neurons (and thus more of a surrogate marker of the ongoing pathological process) is still controversial.

Amyloid Plaques

Composition

The senile plaques described by Alois Alzheimer in his original case report result from the abnormal extracellular accumulation and deposition of the amyloid-β peptide (Aβ) with 40 or 42 amino acids (Aβ40 and Aβ42), two normal byproducts of the metabolism of the amyloid precursor protein (APP) after its sequential cleavage by the enzymes β- and γ-secretases in neurons. Because of its higher rate of fibrillization and insolubility, Aβ42 is more abundant than Aβ40 within the plaques.

Morphological Characteristics

Attempts to understand the evolution of the amyloid plaque after its formation based on morphological criteria gave rise to a number of terms, including "primitive," "classical," and "burn-out" plaques. However, a more practical and widely used morphological classification distinguishes only two types of amyloid plaques–diffuse versus dense-core plaques-based on their staining with dyes specific for the β-pleated sheet conformation such as Congo Red and Thioflavin-S. This simpler categorization is relevant to the disease because, unlike diffuse Thioflavin-S negative plaques, Thioflavin-S positive dense-core plaques are associated with deleterious effects on the surrounding neuropil including increased neurite curvature and dystrophic neurites, synaptic loss, neuron loss, and recruitment and activation of both astrocytes and microglial cells (Itagaki et al. 1989; Masliah et al. 1990, 1994; Pike et al. 1995; Knowles et al. 1999; Urbanc et al. 2002; Vehmas et al. 2003). Indeed, diffuse amyloid plaques are commonly present in the brains of cognitively intact elderly people, whereas dense-core plaques, particularly those with neuritic dystrophies, are most often found in patients with AD dementia. However, the pathological boundaries between normal aging and AD dementia are not clear-cut and, as we will further discuss below, many cognitively normal elderly people have substantial amyloid burden in their brains.

Electron microscopy studies revealed that the ultrastructure of dense-core plaques is comprised of a central mass of extracelullar filaments that radially extend toward the periphery, where they are intermingled with neuronal, astrocytic, and microglial processes. These neuronal processes, known as dystrophic neurites, often contain packets of paired helical filaments, as well as abundant abnormal mitochondria and dense bodies of probable mitochondrial and lysosomal origin (Kidd 1964; Hirai et al. 2001; Fiala et al. 2007). Plaque-associated neuritic dystrophies represent the most notorious evidence of Aβ-induced neurotoxicity and feature many of the pathophysiological processes downstream Aβ. Their origin can be axonal or dendritic and their morphology can be either elongated and distorted or bulbous (Su et al. 1993). They can be argyrophylic (Fig. 1C) and Thioflavin-S positive because of the aggregation of β-sheet pleated tau fibrils, which can also be shown with many phosphotau and conformation-specific tau antibodies (Su et al. 1993, 1994, 1996). Interestingly, dystrophic neurites can also be immunoreactive for APP (Cras et al. 1991; Su et al. 1998). Cytoskeletal abnormalities in dystrophic neurites explain their immunoreactivity for neurofilament proteins (Su et al. 1996, 1998; Dickson et al. 1999; Knowles et al. 1999). These cytoskeletal abnormalities can lead to a disruption of the normal axonal transport and, indeed, a subset of dystrophic neurites are positive for mitochondrial porin and chromogranin-A because of the abnormal accumulation of mitochondria and large synaptic vesicles, respectively (Dickson et al. 1999; Woodhouse et al. 2006a; Pérez-Gracia et al. 2008). Moreover, some axonal dystrophic neurites contain either cholinergic, glutamatergic, or gabaergic markers, suggesting a plaque-induced aberrant sprouting (Benzing et al. 1993; Ferrer et al. 1993; Masliah et al. 2003; Bell et al. 2007). Finally, dystrophic neurites can be displayed with immunohistochemical studies for ubiquitin and lysosomal proteins, indicating that there is a compensatory attempt to degrade and clear the abnormal accumulation of proteins and organelles (Dickson et al. 1990; Barrachina et al. 2006). A less-evident expression of the plaque-induced neuritic changes is the increase in the curvature of neurites located in the proximity of dense-core plaques (Knowles et al. 1999).

Topographic Distribution

Unlike NFTs, amyloid plaques accumulate mainly in the isocortex. Although the spatiotemporal pattern of progression of amyloid deposition is far less predictable than that of NFTs, in general the allocortex (including entorhinal cortex and hippocampal formation), the basal ganglia, relevant nuclei of the

brainstem, and the cerebellum, are involved to a lesser extent and later than the associative isocortex. The dissociation between amyloid and NFT burdens in the medial temporal lobe is particularly noticeable. Among the isocortical areas, likewise NFTs, primary sensory, motor, and visual areas tend to be less affected as compared to association multimodal areas. (Arnold et al. 1991; Braak and Braak 1991). Despite this poorer predictability of the progression of amyloid deposition, two staging systems have been proposed. Braak and Braak distinguished three stages: (1) Stage A, with amyloid deposits mainly found in the basal portions of the frontal, temporal, and occipital lobes; (2) Stage B, with all isocortical association areas affected while the hippocampal formation is only mildly involved, and the primary sensory, motor, and visual cortices are devoid of amyloid; and (3) Stage C, characterized by the deposition of amyloid in these primary isocortical areas and, in some cases, the appearance of amyloid deposits in the molecular layer of the cerebellum and subcortical nuclei such as striatum, thalamus, hypothalamus, subthalamic nucleus, and red nucleus (Braak and Braak 1991). Thal et al. proposed a descendent progression of amyloid deposition in five stages: (1) Stage 1 or isocortical; (2) Stage 2, with additional allocortical deposits (entorhinal cortex, hippocampal formation, amygdala, insular, and cingulated cortices); (3) Stage 3, with additional involvement of subcortical nuclei including striatum, basal forebrain cholinergic nuclei, thalamus and hypothalamus, and white matter; (4) Stage 4, characterized by the involvement of brainstem structures, including red nucleus, substantia nigra, reticular formation of the medulla oblongata, superior and inferior colliculi; and (5) Stage 5, with additional amyloid deposits in the pons (reticular formation, raphe nuclei, locus ceruleus) and the molecular layer of the cerebellum (Thal et al. 2002). These five Thal stages can be summarized in three: stage 1 or isocortical; stage 2, allocortical or limbic, and stage 3 or subcortical (Fig. 3).

Amyloid deposits usually involve the six layers of the isocortex, although layers I and VI are usually relatively more spared than layers II-V (Arnold et al. 1991; Braak and Braak 1991). However, in advanced cases it is frequent to observe band-like diffuse amyloid deposits in the subpial surface of the cortex and even a few amyloid deposits in the white matter close to its transition with the cortical layer VI.
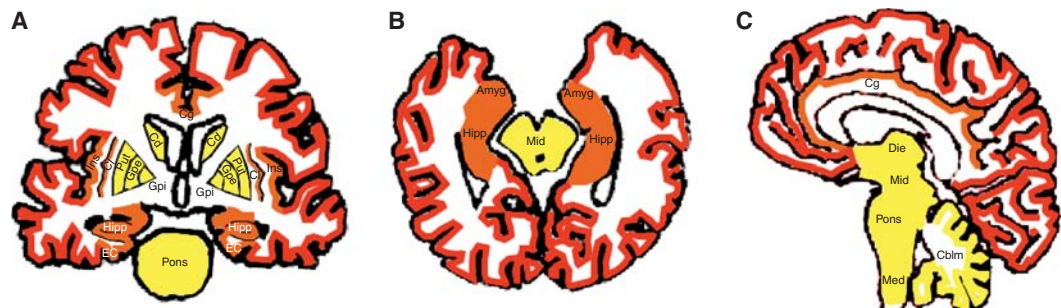

Figure 3. Spatiotemporal pattern of amyloid plaque deposition according to Thal et al. (2002). Coronal (*A*), axial (*B*), and sagittal (*C*) views of the brain. The five Thal stages of amyloid deposition are here summarized in three stages. Amyloid deposits accumulate first in isocortical areas (stage 1 or isocortical, in red), followed by limbic and allocortical structures (stage 2 or limbic, in orange), and in a later stage, by subcortical structures including basal ganglia, selected nuclei in diencephalon and brainstem, and the cerebellar cortex (stage 3 or subcortical, in yellow). Amyg = Amygdala; EC = Entorhinal cortex; Hipp = Hippocampus; Cg = Cingulate cortex; Cd = Caudate nucleus; Put = Putamen; Gpe = Globus pallidus externus; Gpi = Globus pallidus internus; Cl = Claustrum; Ins = Insular cortex; Die = Diencephalon; Mid = Midbrain; Med = Medulla oblongata; Cblm = Cerebellum.

Clinicopathological Correlations

Clinicopathological studies have established that the amyloid burden (either total amyloid plaques, dense-core plaques or only neuritic plaques) does not correlate with the severity or the duration of dementia (Arriagada et al. 1992a, Hyman et al. 1993; Bierer et al. 1995; Gómez-Isla et al. 1997; Giannakopoulos et al. 2003; Ingelsson et al. 2004). Indeed, in a region of early amyloid deposition such as the temporal associative isocortex, the amyloid burden reaches a plateau early after the onset of the cognitive symptoms or even in the preclinical phase of the disease (Ingelsson et al. 2004; Serrano-Pozo et al. 2011) and not even the size of the plaques grows significantly with the progression of the disease (Hyman et al. 1993). However, it is possible that the amount of amyloid measured over the entire cortical mantle does increase during the clinical course of the disease as the distribution of amyloid deposits "spread" following the above stages. Preliminary data from longitudinal amyloid PET imaging studies in living patients have recently supported this possibility (Jack et al. 2009).

Cerebral Amyloid Angiopathy

Composition

The amyloid-β peptide not only deposits in the brain parenchyma in the form of amyloid plaques but also in the vessel walls in the form of cerebral amyloid angiopathy (CAA). Indeed, the more insoluble and aggregation-prone Aβ42 peptide tends to accumulate in the core of senile plaques, while the more soluble Aβ40 peptide is the major constituent of CAA, accumulating mainly in the interstitium between the smooth muscle cells of the tunica media. Although CAA can also appear in isolation (pure CAA), it is more common in the context of AD, with ≈80% of AD patients showing some degree, usually mild, of CAA at autopsy,

Morphological Characteristics

The same methods described for the examination of amyloid plaques are valid for CAA, that is Thioflavin-S or Congo red staining or immunohistochemical studies with anti-Aβ

antibodies. A morphological staging system has been implemented to describe the severity of CAA within a single vessel: grade 0 or absence of staining; grade 1 or congophilic rim around an otherwise nomal-appearance vessel; grade 2 or complete replacement of the tunica media by congophilic material; grade 3 or cracking of ≥50% of the circumference of the vessel, giving a "vessel-within-vessel" or "double-barrel" appearance; and grade 4 or fibrinoid necrosis of the vessel wall, often accompanied by additional amyloid deposits in the surrounding neuropil ("dyshoric" changes) (Greenberg and Vonsattel 1997). In this severe stage, Prussian blue (Perl's) staining is useful to show hemosiderin-laden macrophages in the parenchyma surrounding CAA-affected vessels, indicative of chronic microbleeds.

Topographic Distribution

CAA usually affects cortical capillaries, small arterioles and middle-size arteries as well as leptomeningeal arteries, whereas venules, veins, and white-matter arteries are rarely involved. For unknown reasons, posterior parietal and occipital areas are usually more prominently affected than frontal and temporal lobes, and within the same area, leptomeningeal arteries usually show more severe CAA than cortical arteries. A semiquantitative scoring system has been proposed to characterize the severity of CAA within a region of the cortex: 0 = no Thioflavin-S-stained leptomeningeal or cortical vessels; 1 = scattered positivity in either leptomeningeal or cortical vessels; 2 = strong circumferential positivity in at least some vessels either leptomeningeal or cortical; 3 = widespread circumferential staining in many leptomeningeal and cortical vessels, and 4 = presence of "dyshoric" perivascular amyloid deposits in addition to score 3. A global severity score can be obtained by averaging the scores from several regions (Olichney et al. 2000).

Clinicopathological Correlations

According to the Boston criteria, CAA should be suspected after one or multiple major symptomatic lobar hemorrhages in an elderly patient

(Knudsen et al. 2001). But in the context of AD, unless it becomes symptomatic because of this hemorrhagic complication, CAA is usually diagnosed at autopsy. However, three independent postmortem longitudinal studies have revealed that the otherwise apparently asymptomatic CAA can also be a synergistic contributor to cognitive decline in AD (MRC CFAS 2001; Pfeifer et al. 2002; Greenberg et al, 2004; Arvanitakis et al. 2011).

Granuovacuolar Degeneration and Hirano Bodies

Granulovacuolar degeneration (GVD) and Hirano bodies are two poorly understood lesions present in the cytoplasm of hippocampal pyramidal neurons of AD patients. Although they are increasingly observed with aging in cognitively intact elderly people, these two lesions are more severe and frequent in age-matched AD patients. (Ball 1978; Xu et al. 1992).

GVD consists of the accumulation of large double-membrane bodies. Their origin and significance are uncertain. Early immunohistochemical studies reported immunoreactivity of GVD bodies for cytoskeletal proteins including tubulin, neurofilament proteins and tau (Kahn et al. 1985; Price et al. 1986; Dickson et al. 1987; Bondareff et al. 1991; Mena et al. 1992; Ikegami et al. 1996). Because GVD bodies are also positive for some tau kinases, a role in tangle formation has been proposed (Ghoshal et al. 1999; Leroy et al. 2002; Kannanayakal et al. 2006). Other authors have postulated a role in the apoptotic cell death because of their immunoreactivity for activated caspase-3 (Selznick et al. 1999; Stadelmann et al. 1999; Su et al. 2002). More recent studies have suggested that these bodies might derive from the endoplasmic reticulum and represent the stress granules that feature the unfolded protein response, because they are positive for several stress kinases (Zhu et al. 2001; Lagalwar et al. 2007; Thakur et al. 2007; Hoozemans et al. 2009). Finally, based on their positivity for ubiquitin and autophagic markers, it has been proposed that these granules are late-stage autophagic vacuoles (Okamoto et al. 1991;

Barrachina et al. 2006; Yamazaki et al. 2010; Funk et al. 2011).

Hirano bodies are eosinophilic rod-like cytoplasmic inclusions relatively common in the stratum lacunosum of the hippocampal CA1 region in the elderly. However, in AD patients the number of Hirano bodies is abnormally high and they are translocated to the neurons of the stratum pyramidale (Gibson and Tomlison 1977). Although the significance of Hirano bodies in AD is not completely understood, they are recognized by antibodies against tau, neurofilament proteins, actin, and other cytoskeletal proteins (Goldman 1983; Galloway et al. 1987a,b; Schmidt et al. 1989; Maciver and Harrington 1995; Rossiter et al. 2000). Other immunoreactivities associated with Hirano bodies are inducible nitric oxide synthase (Lee et al. 1999), advanced glycation endproducts (Münch et al. 1998), and the carboxy-terminal fragments of APP (Muñoz et al. 1993).

Glial Responses

Reactive astrocytes and activated microglial cells are commonly associated to dense-core amyloid plaques, indicating that amyloid-β is a major trigger of this glial response (Itagaki et al. 1989; Pike et al. 1995; Vehmas et al. 2003). However, we have recently observed a linear increase in reactive astrocytes and activated microglial cells through the entire disease course despite an early plateau in amyloid deposition in the temporal associative isocortex. Indeed, we found a highly significant positive correlation between both astrocytosis and microgliosis and NFT burden but not between both reactive glial cell types and amyloid burden, suggesting that glial responses are also related to neurofibrillary degeneration (Ingelsson et al. 2004; Serrano-Pozo et al. 2011).

Neuronal Loss

Neuronal loss is the main pathological substrate of cortical atrophy and, although usually evident in sections stained with hematoxylin and eosin, it can be more readily shown with a Nissl staining or a NeuN immunohistochemistry. Nissl staining (for example with cresyl

violet) reveals the negatively charged ribosomic RNA present in the ribosomes of the rough endoplasmic reticulum (Nissl substance or granules), giving a dark blue appearance to the perinuclear region of neurons. By contrast, NeuN is a neuronal-specific nuclear antigen, although NeuN immunohistochemistry also stains the perinuclear region and some proximal processes of neurons.

The regional and laminar pattern of neuronal loss matches that of NFTs, but, importantly, within the same region neuronal loss exceeds the numbers of NFTs, so that it is a better correlate of cognitive deficits than the number of NFTs (Gómez-Isla et al. 1996, 1997). Indeed, quantitative stereology-based studies of neurons, iNFTs and eNFTs have concluded that iNFTs can last for up to two decades and that neurons bearing iNFTs might still be viable as evidenced by their positive Nissl staining (Bussiére et al. 2003; Hof et al. 2003). This dissociation between the extent of neuronal loss and that of NFTs suggests that there are least two mechanisms of neuronal death in AD: one affecting tangle-bearing neurons, that will lead to the appearance of ghost extracellular tangles, and another affecting tangle-free neurons. Although the mechanisms of neuronal death in AD are beyond the scope of this article, it will be noted that postmortem studies on apoptosis have yielded controversial results, with some studies showing a widespread distribution of apoptotic markers (Troncoso et al. 1996; Su et al. 2001), while others have only reported a scattered distribution (Selznick et al. 1999; Woodhouse et al. 2006b).

Synapse Loss

Besides neuronal loss, synapse loss is another contributor to the cortical atrophy of the AD brain. Synapse loss in AD was shown with immunohistochemical studies using antibodies against pre- or postsynaptic proteins—typically the presynaptic protein synaptophysin—and with electron microscopy studies.

The spatiotemporal and laminar pattern of synapse loss matches that of neuron loss. Synaptic loss is not only caused by neuronal loss but

can exceed the existing neuronal loss within a particular cortical area. This indicates that synapse loss predates neuronal loss and that the remaining neurons become less well connected to their synaptic partners than expected just by the number of viable neurons surviving in a particular circuit. Likely this is why synaptic density is the best correlate of cognitive decline in AD (DeKosky and Scheff 1990; Scheff et al. 1990, 1993, 2007; Terry et al. 1991; Masliah et al. 1994; Ingelsson et al. 2004). Interestingly, an inverse correlation has been observed between synaptic density and the size of remaining synapses as measured by the length of the postsynaptic density. This enlargement of remaining synapses has been interpreted as a compensatory response, rather than as selective loss of small synapses (DeKosky and Scheff 1990; Scheff et al. 1990; Scheff and Price 1993).

CRITERIA FOR THE PATHOLOGICAL DIAGNOSIS OF ALZHEIMER DISEASE

Of all pathological features described above, amyloid plaques and NFTs are the most characteristic of AD and, understandably, the criteria for the pathological diagnosis of AD rely on their amount and/or distribution.

The first pathological criteria for the diagnosis of AD were based on the highest density of total amyloid plaques (both diffuse and neuritic) in any cortical field, adjusted for age so that the older the patient at death, the greater the density required for diagnosis (Khachaturian 1985). The presence of NFTs was not required and diffuse plaques—relatively frequent in nondemented elderly people—had the same consideration as neuritic plaques. Although meritorious, these criteria were soon abandoned because, despite a very high sensitivity to diagnose AD dementia, they lacked sufficient specificity (Geddes et al. 1997). In 1991, the Consortium to Establish a Registry for Alzheimer Disease (CERAD) proposed more specific diagnostic criteria by emphasizing the importance of neuritic plaques over diffuse plaques (Mirra et al. 1991, 1997). CERAD criteria use a semiquantitative score of the density of neuritic plaques in the most severely affected region of

the isocortex (frontal, temporal, or parietal) and the patient's age at death to obtain an age-related plaque score. This score is then integrated with clinical information regarding the presence or absence of dementia to establish one of three levels of certainty that dementia is explained by the AD pathological changes: possible, probable, and definite. A diagnosis of AD is made if the criteria for probable or definite AD are met. Although higher than that of Khachaturian criteria, the specificity of CERAD criteria proved to be still insufficient because they did not incorporate the scoring of the severity of NFTs (Geddes et al. 1997). By contrast, the use of Braak and Braak staging of NFTs alone—with the isocortical stages V and VI as criteria of definite AD—showed a high specificity at the expense of a low sensitivity (Geddes et al. 1997).

Current pathological criteria for AD were defined in 1997 by a workshop of the National Institute of Aging and the Reagan Institute. The NIA-RI consensus recommendations combine the CERAD semiquantitative score of neuritic plaques and the Braak and Braak staging of NFTs to distinguish three probabilistic diagnostic categories: (1) high likelihood, if there are frequent neuritic plaques (CERAD definite) and abundant isocortical NFTs (Braak stage V/VI); (2) intermediate likelihood, if there are moderate neuritic plaques (CERAD probable) and NFTs are restricted to limbic regions (Braak III/IV), and (3) low likelihood, if there are infrequent neuritic plaques (CERAD possible) and NFTs are restricted to the entorhinal cortex and/or hippocampus (Braak I/II). A diagnosis of AD is made when the criteria for intermediate or high likelihood of AD are met and the patient had a clinical history of dementia (NIA-RI Consensus 1997). Because experience has revealed infrequent cases with many AD pathological lesions but no or few cognitive symptoms (and vice versa) and these circumstances were not addressed by the NIA-RI consensus workgroup, these diagnostic criteria are currently under review.

Both CERAD and NIA-RI criteria also incorporated the assessment of other pathologies, particularly vascular and Lewy body diseases, already recognizing the high prevalence of mixed pathologies underlying dementia in elderly people, a circumstance well documented by more recent longitudinal community-based clinicopathological studies (MRC CFAS 2001; Schneider et al. 2007). Thus, in many practical instances, the CERAD criteria for "possible AD" and the NIA-RI criteria for "intermediate probability of AD" are not only based on a moderate amount and distribution of AD pathology but also on the coexistence of vascular or Lewy body pathology with sufficient severity to contribute to the patient's dementia.

NEUROPATHOLOGY OF MILD COGNITIVE IMPAIRMENT AND EARLY ALZHEIMER DISEASE

Clinicopathological correlation studies have taught us that at the moment of the clinical diagnosis, patients with AD-type dementia often already have a Braak stage V or VI of neurofibrillary degeneration and a substantial and widespread synaptic and neuronal loss. To anticipate the clinical diagnosis of AD before the stage of full-blown dementia, a new clinical construct was needed. Petersen et al. proposed the concept of "mild cognitive impairment" (MCI) as a new diagnostic entity for the transition between normal aging and AD dementia. Patients with MCI have already some cognitive complaints that are detectable with the appropriate cognitive tests and represent a decline from a previous higher baseline level but that, unlike the definition of dementia, do not interfere with their activities of daily life. Importantly, MCI patients have an increased risk of developing dementia, which has been reported between 10% and 15% per year (Petersen et al. 1999, 2001; Petersen 2004).

Autopsy studies on MCI patients are scarce but they have reproducibly found a stage of AD pathology intermediate between cognitively intact subjects and demented patients, particularly regarding neurofibrillary degeneration, that is consistent with the idea of a transition phase between normal aging and definite AD (Jicha et al. 2006; Markesbery et al. 2006; Petersen et al. 2006; Schneider et al. 2009). Specifically, MCI patients usually have

a moderate number of neuritic plaques and a limbic stage of NFTs (Braak stage III or IV), fitting into the NIA-RI category of intermediate likelihood of AD (sufficient to cause dementia) and providing a pathological validation for this clinical construct. Along the same lines, patients with a Clinical Dementia Rating score of 0.5 (equivalent to MCI or very mild AD) have already a ≈30% of neuron loss in the entorhinal cortex compared to cognitively intact controls (CDR = 0), but still no evident neuronal loss in the superior temporal sulcus (Gómez-Isla et al. 1996, 1997). Moreover, electron microscopy studies have shown that MCI patients also have an intermediate number of synapses between nondemented controls and mild AD patients in the hippocampus, further indicating that many individuals with the clinical symptoms of MCI have early AD (Scheff et al. 2006, 2007). Of note, a paradoxical, presumably compensatory, up-regulation in the density of presynaptic glutamatergic boutons has been reported in the frontal cortex of MCI patients compared to nondemented controls and mild AD patients (Bell et al. 2007).

Although AD was the most common pathological diagnosis underlying MCI in the above case series, it should be noted that there was a high degree of pathological heterogeneity underlying the clinical diagnosis of MCI, with vascular disease, Lewy body disease, argyrophilic grain disease, and hippocampal sclerosis as major concurrent or alternative pathologies (Jicha et al. 2006; Petersen et al. 2006; Schneider et al. 2009). In addition, in the largest study a high proportion (up to 25%) of MCI patients had no pathology at autopsy (Schneider et al. 2009). Finally, no significant pathological differences have been observed between the amnestic and the nonamnestic subtypes of MCI nor in their pathological outcome after conversion to dementia (Jicha et al. 2006; Schneider et al. 2009).

ALZHEIMER NEUROPATHOLOGY IN "NORMAL AGING"

Longitudinal prospective clinicopathological studies in nondemented elderly people have revealed that up to 45% of nondemented elderly would meet the NIA-RI criteria for AD had they been demented, usually the intermediate likelihood category of these criteria, and rarely the high likelihood category (Schmitt et al. 2000; Knopman et al. 2003; Bennet et al. 2006; Price et al. 2009; Schneider et al. 2009). Moreover, the pattern of regional distribution of pathological changes in nondemented controls matches that of AD patients (Arriagada et al. 1992b). Thus, mounting evidence from clinicopathological studies support the view that AD is a continuous spectrum between asymptomatic lesions in cognitively normal elderly and dementia, with MCI as a transition phase between these two ends.

The apparent dissociation between AD pathology and cognitive status in some elderly people is remarkable because these so-called "high-pathology nondemented controls" or "individuals with asymptomatic AD" seem to be resilient to the neurotoxic effects of amyloid plaques and NFTs and to contradict the aforementioned positive correlation between NFT burden and cognitive decline. Understanding the biochemical and morphological substrates of this resilience to cognitive decline in the presence of abundant AD pathology might be crucial to discover new therapeutic targets for the disease. As expected from the highly significant clinicopathological correlations of synaptic and neuronal loss in AD, high-pathology controls have preserved synaptophysin levels compared to AD patients with a similar burden of plaques and NFTs (Lue et al. 1996), and they do not seem to have significant neuronal loss, not even in vulnerable regions such as the entorhinal cortex and the hippocampus (Price et al. 2001; West et al. 2004). Moreover, they have lower levels of neuroinflammatory markers than pathology-matched AD patients (Lue et al. 1996). This resistance to AD pathology has also been related to a nucleolar, nuclear, and cell body hypertrophy of the hippocampal and cortical neurons, suggestive of a compensatory metabolic activation to face the neurotoxic effects of AD lesions (Riudavets et al. 2007; Iacono et al. 2008). In keeping with these pathological reports, a MRI-neuropathological correlation study revealed larger brain and hippocampal

volumes in high-pathology controls than in pathology-matched demented patients, further supporting the preservation of both neurons and synapses (Erten-Lyons et al. 2009).

OVERLAP OF AD WITH LEWY BODY DISEASE

Alzheimer disease and Parkinson's disease (PD) are the leading causes of dementia and movement disorders in the aging population. It is estimated that over 10 million people live with these devastating neurological conditions in the United States. It is estimated that over 10 million people live with these devastating neurological conditions in the United States, and that this country alone will see a 50% annual increase of AD and PD by the year 2025 (Herbert et al. 2001).

PD and AD are two distinct clinicopathological entities. While in AD, abnormal accumulation of misfolded Aβ protein in the neocortex and limbic system is thought to be responsible for the neurodegenerative pathology (Selkoe 1990; Sisodia and Price 1995), intracellular accumulation of α-synuclein has been centrally implicated in the pathogenesis of PD (Spillantini et al. 1997; Hashimoto et al. 1998; Trojanowski and Lee 1998). In AD, Aβ protein accumulates in the intracellular (LaFerla et al. 1995; Skovronsky et al. 1998) and extracellular space, leading to the formation of plaques, whereas intracellular polymerization of phosphorylated cytoskeletal molecules such as tau results in the formation of neurofibrillary tangles (Greenberg and Davies 1990; Lee et al. 2001). In PD, intracellular accumulation of α-synuclein—an abundant synaptic terminal protein (Iwai et al. 1995)—results in the formation of characteristic inclusions called Lewy bodies (LBs) (Fig. 1F) (Spillantini et al. 1997; Wakabayashi et al. 1997; Takeda et al. 1998). The new consortium criteria for the classification of Lewy body diseases (LBD) recognizes two clinical entities, the first denominated dementia with LBs (DLB) and the second PD dementia (PDD) (McKeith et al. 1996; Aarsland et al. 2004; Burn 2006; McKeith 2006; Lippa et al. 2007). While in patients with

DLB, the clinical presentation is of dementia followed by parkinsonism, in patients with PDD the initial signs are of parkinsonism followed by dementia (Litvan et al. 1998; Janvin et al. 2006; McKeith 2006). Interestingly, the brains of patients with DLB and PDD display very similar pathology, with the exception that recent studies have shown extensive deposition of Aβ and α-synuclein in the striatum and hippocampus in DLB compared to only α-synuclein in PDD cases (Duda et al. 2002; Jellinger and Attems 2006). Because of the implications for the management and treatment of parkinsonism and dementia in patients with PD and DLB, loss of dopaminergic neurons in the midbrain (Dickson et al. 1994; Tsuboi and Dickson 2005) and cholinergic cells in the nucleus basalis of Meynert have been characterized in detail (Perry et al. 1978; Hansen et al. 1990). Although the severity of the neuronal loss within these subcortical regions might explain some of the neurological deficits in patients with PD and DLB, the neuronal populations responsible for the more complex cognitive and psychiatric alterations have not been completely characterized. Abnormal accumulation of α-synuclein in the CA2-3 region of the hippocampus (Harding and Halliday 2001; Bertrand et al. 2004), insula, amygdala and cingulate cortex has been shown to be an important neuropathological feature (Dickson et al. 1994; Spillantini et al. 1997; Trojanowski et al. 1998; Aarsland et al. 2004).

Remarkably, despite being initially considered distinct clinicopathological conditions, several studies have now confirmed that the clinical features and the pathology of AD and PD can overlap (McKeith 2000, 2006; Lippa et al. 2007). Approximately 25% of all patients with AD develop parkinsonism, and about 50% of all cases of PD develop AD-type dementia after 65 years of age (Hansen et al. 1990). Moreover, 70% of patients with sporadic AD display the formation of α-synuclein-positive LB-like inclusions in the amygdala and limbic structures (Lippa et al. 1998; Trojanowski et al. 1998; Hamilton 2000). Similarly, in patients with familial AD (FAD) and Down syndrome, LB-like pathology and parkinsonism have

been reported (Lippa et al. 1999). Last, as mentioned above, the single most important neuropathological finding that distinguishes PDD from DLB is the presence of Aβ deposits in the striatum (Duda et al. 2002) and in the hippocampus (Masliah et al. 1993a).

A number of studies provide extensive support for an interaction between pathogenic pathways in AD and LBD and argue against a coincidental concurrence of both disorders (i.e., merely because of their high prevalence in the elderly). FAD cases with presenilin mutations that present with significant LB pathology strongly support an interaction between Aβ and α-synuclein (Rosenberg 2005; Snider et al. 2005; Leverenz et al. 2006). Although plaques, tangles and LBs are useful neuropathological and diagnostic markers of these disorders, the initial injury that results in the cognitive and movement alterations is likely the damage of the synaptic terminals in selected circuitries (DeKosky and Scheff 1990; Masliah and Terry 1993; Masliah et al. 1994, 2001a, Klucken et al. 2003). Several lines of investigation support the notion that oligomeric forms of Aβ and α-synuclein, rather than the polymers and fibrils associated with plaques and LBs, accumulate in the neuronal membranes and lead to the characteristic synaptic pathology (Lambert et al. 1998; Conway et al. 2000; Lashuel et al. 2002; Haass and Selkoe 2007; Kramer and Schulz-Schaeffer 2007; Koffie et al. 2009; Scott et al. 2010). Some studies have shown that underlying interactions between α-synuclein and Aβ play a fundamental role in the pathogenesis of LBD (Lippa et al. 1998; Hashimoto et al. 2000; Masliah et al. 2001b, Pletnikova et al. 2005). Specifically, Aβ promotes the oligomerization and toxic conversion of α-synuclein (Masliah et al. 2001b; Mandal et al. 2006), Aβ exacerbates the deficits associated with α-synuclein accumulation, Aβ and α-synuclein colocalize in membrane and caveolar fractions, and Aβ stabilizes α-synuclein multimers that might form channel-like structures in the membrane (Tsigelny et al. 2007, 2008). Both lysosomal leakage (Nixon and Cataldo 2006) and oxidative stress (Smith et al. 1996) appear to be involved in the process of neurotoxicity and

pathological interactions between Aβ and α-synuclein (Rockenstein et al. 2005).

Therefore, it is possible that the combined effects of α-synuclein and Aβ might lead to synaptic damage and selective degeneration of neurons in the neocortical, limbic, and subcortical regions. A more precise mapping of the neuronal populations affected in these regions is needed to understand the cellular basis for the characteristic cognitive dysfunction in PDD and DLB and to develop new treatments for these conditions.

CONCLUSIONS

Classical neuropathological lesions including senile amyloid plaques and neurofibrillary tangles define AD but they likely represent the "tip of the iceberg" of the pathological alterations that cause the cognitive decline associated with AD. Indeed, the development of new biomarkers and imaging tools has made evident that these neuropathological stigmata of AD begin to accumulate a decade or more prior to a clinical diagnosis of dementia. Synaptic loss, plasticity changes, neuronal loss, and the presence of soluble microscopic oligomeric forms of Aβ and even of tau, likely contribute to the progressive neural system failure that occurs over decades. An understanding of this natural history of the disease is critical to design primary or secondary prevention strategies to halt the disease progression before the damage to the neural system becomes irreversible.

REFERENCES

Aarsland D, Ballard CG, Halliday G. 2004. Are Parkinson's disease with dementia and dementia with Lewy bodies the same entity? *J Geriatr Psychiatry Neurol* **17:** 137–145.

Arnold SE, Hyman BT, Flory J, Damasio AR, Van Hoesen GW. 1991. The topographical and neuroanatomical distribution of neurofibrillary tangles and neuritic plaques in the cerebral cortex of patients with Alzheimer's disease. *Cereb Cortex* **1:** 103–116.

Arriagada PV, Growdon JH, Hedley-Whyte ET, Hyman BT. 1992a. Neurofibrillary tangles but not senile plaques parallel duration and severity of Alzheimer's disease. *Neurology* **42:** 631–639.

Arriagada PV, Marzloff K, Hyman BT. 1992b. Distribution of Alzheimer-type pathologic changes in non-demented elderly individuals matches the pattern in Alzheimer's disease. *Neurology* **42:** 1681–1688.

Arvanitakis Z, Leurgans SE, Wang Z, Wilson RS, Bennet DA, Schneider JA. 2011. Cerebral amyloid angiopathy pathology and cognitive domains in older persons. *Ann Neurol* **69:** 320–327.

Augustinack JC, Schneider A, Mandelkow EM, Hyman BT. 2002. Specific tau-phosphorylation sites correlate with severity of neuronal cytopathology in Alzheimer's disease. *Acta Neuropathol* **103:** 26–35.

Ball MJ, Nuttal K. 1978. Topographic distribution of neurofibrillary tangles and granulovacuoles in hippocampal cortex of aging and demented patients. A quantitative study. *Acta Neuropathol* **42:** 73–80.

Barrachina M, Maes T, Buesa C, Ferrer I. 2006. Lysosome-associated membrane protein 1 (LAMP-1) in Alzheimer's disease. *Neuropathol Appl Neurobiol* **32:** 505–516.

Beach T, Walker R, McGeer E. 1989. Patterns of gliosis in Alzheimer's disease and aging cerebrum. *Glia* **2:** 420–436.

Bell KFS, Bennet DA, Cuello AC. 2007. Paradoxical upregulation of glutamatergic presynaptic boutons during mild cognitive impairment. *J Neurosci* **27:** 10810–10817.

Bennet DA, Schneider JA, Arvanitakis Z, Kelly JF, Aggarwal NT, Shah RC, Wilson RS. 2006. Neuropathology of older persons without cognitive impairment from two community-based studies. *Neurology* **66:** 1837–1844.

Benzing WC, Ikonomovic MD, Brady DR, Mufson EJ, Armstrong DM. 1993. Evidence that transmitter-containing dystrophic neurites precede paired helical filament and Alz-50 formation within senile plaques in the amygdala of nondemented elderly and patients with Alzheimer's disease. *J Comp Neurol* **334:** 176–191.

Bertrand E, Lechowicz W, Szpak GM, Lewandowska E, Dymecki J, Wierzba-Bobrowicz T. 2004. Limbic neuropathology in idiopathic Parkinson's disease with concomitant dementia. *Folia Neuropathol* **42:** 141–150.

Bierer LM, Hof PR, Purohit DP, Carlin L, Schneider J, Davis KL, Perl DP. 1995. Neocortical neurofibrillary tangles correlate with dementia severity in Alzheimer's disease. *Arch Neurol* **52:** 81–88.

Bondareff W, Wischik CM, Novak M, Roth M. 1991. Sequestration of tau by granulovacuolar degeneration in Alzheimer's disease. *Am J Pathol* **139:** 641–647.

Braak H, Braak E. 1991. Neuropathological stageing of Alzheimer-related changes. *Acta Neuropathol* **82:** 239–259.

Braak H, Del Tredici K. 2011. The pathological process underlying Alzheimer's disease in individuals under thirty. *Acta Neuropathol* **121:** 171–181.

Braak E, Braak H, Mandelkow EM. 1994. A sequence of cytoskeleton changes related to the formation of neurofibrillary tangles and neuropil threads. *Acta Neuropathol* **87:** 554–567.

Braak H, Alafuzoff I, Arzberger T, Kretzschmanr H, Del Tredici K. 2006. Staging of Alzheimer disease-associated neurofibrillary pathology using paraffin sections and immunhistochemistry. *Acta Neuropathol* **112:** 389–404.

Burn DJ. 2006. Parkinson's disease dementia: What's in a Lewy body? *J Neural Transm Suppl* **70:** 361–365.

Bussière T, Gold G, Kövari E, Giannakopoulos P, Bouras C, Perl DP, Morrison JH, Hof PR. 2003. Stereologic analysis of neurofibrillary tangle formation in prefrontal cortex area 9 in aging and Alzheimer's disease. *Neuroscience* **117:** 577–592.

Carmel G, Mager EM, Binder LI, Kuret J. 1996. The structural basis of monoclonal antibody Alz50's selectivity for Alzheimer's disease pathology. *J Biol Chem* **271:** 32789–32795.

Coleman MP, Perry VH. 2002. Axon pathology in neurological disease: A neglected therapeutic target. *Trends Neurosci* **25:** 532–537.

Conway KA, Lee SJ, Rochet JC, Ding TT, Williamson RE, Lansbury PT Jr. 2000. Acceleration of oligomerization, not fibrillization, is a shared property of both α-synuclein mutations linked to early-onset Parkinson's disease: Implications for pathogenesis and therapy. *Proc Natl Acad Sci* **97:** 571–576.

Cras P, Kawai M, Lowery D, Gonzalez-DeWhitt P, Greenberg B, Perry G. 1991. Senile plaque neurites in Alzheimer disease accumulate amyloid precursor protein. *Proc Natl Acad Sci* **88:** 7552–7556.

Crews L, Masliah E. 2010. Molecular mechanisms of neurodegeneration in Alzheimer's disease. *Hum Mol Genet* **19:** R12–R20.

Crews L, Rockenstein E, Masliah E. 2010. APP transgenic modeling of Alzheimer's disease: Mechanisms of neurodegeneration and aberrant neurogenesis. *Brain Struct Funct* **214:** 111–126.

Crowther RA. 1991. Straight and paired helical filaments in Alzheimer disease have a common structural unit. *Proc Natl Acad Sci* **88:** 2288–2292.

de Calignon A, Spires-Jones TL, Pitstick R, Carlson GA, Hyman BT. 2009. Tangle-bearing neurons survive despite disruption of membrane integrity in a mouse model of tauopathy. *J Neuropathol Exp Neurol* **68:** 757–761.

de Calignon A, Fox LM, Pitstick R, Carlson GA, Bacskai BJ, Spires-Jones TL, Hyman BT. 2010. Caspase activation precedes and leads to tangles. *Nature* **464:** 1201–1204.

DeKosky ST, Scheff SW. 1990. Synapse loss in frontal cortex biopsies in Alzheimer's disease: Correlation with cognitive severity. *Ann Neurol* **27:** 457–464.

DeKosky ST, Scheff SW, Styren SD. 1996. Structural correlates of cognition in dementia: Quantification and assessment of synapse change. *Neurodegeneration* **5:** 417–421.

Dickerson BC, Bakkour A, Salat DH, Feczko E, Pacheco J, Greve DN, Grodstein F, Wright CI, Blacker D, Rosas HD, et al. 2009. The cortical signature of Alzheimer's disease: Regionally specific cortical thinning relates to symptom severity in very mild to mild AD dementia and is detectable in asymptomatic amyloid-positive individuals. *Cereb Cortex* **19:** 497–510.

Dickerson BC, Stoub TR, Shah RC, Sperling RA, Killiany RJ, Albert MS, Hyman BT, Blacker D, Detoledo-Morrell L. 2011. Alzheimer-signature MRI biomarker predicts AD dementia in cognitively normal adults. *Neurology* **76:** 1395–1402.

Dickson DW, Ksiezak-Reding H, Davies P, Yen SH. 1987. A monoclonal antibody that recognizes a phosphorylated epitope in Alzheimer neurofibrillary tangles, neurofilaments and tau proteins immunostains granulovacuolar degeneration. *Acta Neuropathol* **73:** 254–258.

Dickson DW, Wertkin A, Mattiace LA, Fier E, Kress Y, Davies P, Yen SH. 1990. Ubiquitin immunoelectron microscopy of dystrophic neurites in cerebellar senile plaques of Alzheimer's disease. *Acta Neuropathol* **79:** 486–493.

Dickson DW, Schmidt ML, Lee VM, Zhao ML, Yen SH, Trojanowski JQ. 1994. Immunoreactivity profile of hippocampal CA2/3 neurites in diffuse Lewy body disease. *Acta Neuropathol* **87:** 269–276.

Dickson TC, King CE, McCormack GH, Vickers JC. 1999. Neurochemical diversity of dystrophic neurites in the early and late stages of Alzheimer's disease. *Exp Neurol* **1:** 100–110.

Duda JE, Giasson BI, Mabon ME, Lee VM, Trojanowski JQ. 2002. Novel antibodies to synuclein show abundant striatal pathology in Lewy body diseases. *Ann Neurol* **52:** 205–210.

Duda JE, Giasson B, Lee V-M, Trojanowski JQ. 2003. Is the initial insult in Parkinson's disease and Dementia with Lewy bodies a neuritic dystrophy? *Ann NY Acad Sci* **991:** 295.

Erten-Lyons D, Woltjer RL, Dodge H, Nixon R, Vorobik R, Calvert JF, Leahy M, Montine T, Kaye J. 2009. Factors associated with resistance to dementia despite high Alzheimer disease pathology. *Neurology* **72:** 354–360.

Ferrer I, Zújar MJ, Rivera R, Soria M, Vidal A, Casas R. 1993. Parvalbumin-immunoreactive dystrophic neurites and aberrant sprouts in the cerebral cortex of patients with Alzheimer's disease. *Neurosci Lett* **158:** 163–166.

Fiala JC, Feinberg M, Peters A, Barbas H. 2007. Mitochondrial degeneration in dystrophic neurites of senile plaques may lead to extracellular deposition of fine filaments. *Brain Struct Funct* **212:** 195–207.

Funk KE, Mrak RE, Kuret J. 2011. Granulovacuolar degeneration bodies of Alzheimer's disease resemble late-stage autophagic organelles. *Neuropathol Appl Neurobiol* **37:** 295–306.

Galloway PG. Perry G, Gambetti P. 1987a. Hirano bodies filaments contain actin and actin-associated proteins. *J Neuropathol Exp Neurol* **46:** 185–199.

Galloway PG, Perry G, Gambetti P. 1987b. Hirano bodies contain tau protein. *Brain Res* **403:** 337–340.

Geddes JW, Tekirian TL, Soultanian NS, Ashford JW, Davis DG, Markesbery WR. 1997. Comparison of neuropathologic criteria for the diagnosis of Alzheimer's disease. *Neurobiol Aging* **18:** S99–S105.

Ghoshal N, Smiley JF, DeMaggio AJ, Hoekstra MF, Cochran EJ, Binder LI, Kuret J. 1999. A new molecular link between fibrillar and granulovacuolar lesions of Alzheimer's disease. *Am J Pathol* **155:** 1163–1172.

Giannakopoulos P, Herrmann FR, Bussière T, Bouras C, Kövari E, Perl DP, Morrison JH, Gold G, Hof PR. 2003.

Tangle and neuron numbers, but not amyloid load, predict cognitive status in Alzheimer's disease. *Neurology* **60:** 1495–1500.

Gibson PH, Tomlison BE. 1977. Numbers of Hirano bodies in the hippocampus of normal and demented people with Alzheimer's disease. *J Neurol Sci* **33:** 199–206.

Glabe CC. 2005. Amyloid accumulation and pathogensis of Alzheimer's disease: Significance of monomeric, oligomeric and fibrillar Aβ. *Subcell Biochem* **38:** 167–177.

Goldman JE. 1983. The association of actin with Hirano bodies. *J Neuropathol Exp Neurol* **42:** 146–152.

Gómez-Isla T, Price JL, McKeel DW Jr, Morris JC, Growdon JH, Hyman BT. 1996. Profound loss of layer II entorhinal cortex neurons occurs in very mild Alzheimer's disease. *J Neurosci* **16:** 4491–4500.

Gómez-Isla T, Hollister R, West H, Mui S, Growdon JH, Petersen RC, Parisi JE, Hyman BT. 1997. Neuronal loss correlates with but exceeds neurofibrillary tangles in Alzheimer's disease. *Ann Neurol* **41:** 17–24.

Greenberg SG, Davies P. 1990. A preparation of Alzheimer paired helical filaments that displays distinct tau proteins by polyacrylamide gel electrophoresis. *Proc Natl Acad Sci* **87:** 5827–5831.

Greenberg SM, Vonsattel JPG. 1997. Diagnosis of cerebral amyloid angiopathy: Sensitivity and specificity of cortical biopsy. *Stroke* **28:** 1418–1422.

Greenberg SM, Gurol ME, Rosand J, Smith EE. 2004. Amyloid angiopathy-related vascular cognitive impairment. *Stroke* **35:** 2616–2619.

Grutzendler J, Helmin K, Tsai J, Gan WB. 2007. Various dendritic abnormalities are associated with fibrillar amyloid deposits in Alzheimer's disease. *Ann NY Acad Sci* **1097:** 30–39.

Guillozet AL, Weintraub S, Mash DC, Mesulam MM. 2003. Neurofibrillary tangles, amyloid, and memory in aging and mild cognitive impairment. *Arch Neurol* **60:** 729–736.

Guillozet-Bongaarts AL, García-Sierra F, Reynolds MR, Horowitz PM, Fu Y, Wang T, Cahill ME, Bigio EH, Berry RW, Binder LI. 2005. Tau truncation during neurofibrillary tangle evolution in Alzheimer's disease. *Neurobiol Aging* **26:** 1015–1022.

Haass C, Selkoe DJ. 2007. Soluble protein oligomers in neurodegeneration: Lessons from the Alzheimer's amyloid β-peptide. *Nat Rev Mol Cell Biol* **8:** 101–112.

Hamilton RL. 2000. Lewy bodies in Alzheimer's disease: A neuropathological review of 145 cases using α-synuclein immunohistochemistry. *Brain Pathol* **10:** 378–384.

Hansen L, Salmon D, Galasko D, Masliah E, Katzman R, DeTeresa R, Thal L, Pay MM, Hofstetter R, Klauber M, et al. 1990. The Lewy body variant of Alzheimer's disease: A clinical and pathologic entity. *Neurology* **40:** 1–8.

Harding AJ, Halliday GM. 2001. Cortical Lewy body pathology in the diagnosis of dementia. *Acta Neuropathol* **102:** 355–363.

Harris JA, Devidze N, Verret L, Ho K, Halabisky B, Thwin MT, Kim D, Hamto P, Lo I, Yu GQ, et al. 2010a. Trans-synaptic progression of amyloid-β-induced neuronal dysfunction within the entorhinal-hippocampal network. *Neuron* **68:** 428–441.

Harris JA, Devidze N, Halabisky B, Lo I, Thwin MT, Yu GQ, Bredesen DE, Masliah E, Mucke L. 2010b. Many neuronal and behavioral impairments in transgenic mouse models of Alzheimer's disease are independent of caspase cleavage of the amyloid precursor protein. *J Neurosci* **30:** 372–381.

Hashimoto M, Hernandez-Ruiz S, Hsu L, Sisk A, Xia Y, Takeda A, Sundsmo M, Masliah E. 1998. Human recombinant NACP/α-synuclein is aggregated and fibrillated in vitro: Relevance for Lewy body disease. *Brain Res* **799:** 301–306.

Hashimoto M, Takenouchi T, Mallory M, Masliah E, Takeda A. 2000. The role of NAC in amyloidogenesis in Alzheimer's disease. *Am J Pathol* **156:** 734–736.

Hebert LE, Beckett LA, Scherr PA, Evans DA. 2001. Annual incidence of Alzheimer disease in the United States projected to the years 2000 through 2050. *Alzheimer Dis Assoc Disord* **15:** 169–173.

Higuchi M, Lee VM, Trojanowski JQ. 2002. Tau and axonopathy in neurodegenerative disorders. *Neuromolecular Med* **2:** 131–150.

Hirai K, Aliev G, Nunomura A, Fujioka H, Russell RL, Atwood CS, Johnson AB, Kress Y, Vinters HV, Tabaton M, et al. 2001. Mitochondrial abnormalities in Alzheimer's disease. *J Neurosci* **21:** 3017–3023.

Hof PR, Bussière T, Gold G, Kövari E, Giannakopoulos P, Bouras C, Perl DP, Morrison JH. 2003. Stereologic evidence for persistence of viable neurons in layer II of the entorhinal cortex and the CA1 field in Alzheimer disease. *J Neuropathol Exp Neurol* **62:** 55–67.

Hoozemans JJ, van Haastert ES, Nijholt DA, Rozemuller AJ, Eikelenboom P, Scheper W. 2009. The unfolded protein response is activated in pretangle neurons in Alzheimer's disease hippocampus. *Am J Pathol* **174:** 1241–1251.

Hyman BT, Van Hoesen GW, Damasio AR, Barnes CL. 1984. Alzheimer's disease: Cell-specific pathology isolates the hippocampal formation. *Science* **225:** 1168–1170.

Hyman BT, Van Hoesen GW, Kromer LJ, Damasio AR. 1986. Perforant pathway changes in the memory impairment of Alzheimer's disease. *Ann Neurol* **20:** 472–481.

Hyman BT, Marzloff K, Arriagada PV. 1993. The lack of accumulation of senile plaques or amyloid burden in Alzheimer's disease suggests a balance between amyloid deposition and resolution. *J Neuropathol Exp Neurol* **52:** 594–600.

Iacono D, O'Brien R, Resnick SM, Zonderman AB, Pletnikova O, Rudow G, An Y, West MJ, Crain B, Troncoso JC. 2008. Neuronal hypertrophy in asymptomatic Alzheimer disease. *J Neuropathol Exp Neurol* **67:** 578–589.

Ikegami K, Kimura T, Katsuragi S, Ono T, Yamamoto H, Miyamoto E, Miyakawa T. 1996. Immunohistochemical examination of phophorylated tau in granulovacuolar degeneration granules. *Psychiatry Clin Neurosci* **50:** 137–140.

Ingelsson M, Fukumoto H, Newell KL, Growdon JH, Hedley-Whyte ET, Frosch MP, Albert MS, Hyman BT, Irizarry MC. 2004. Early Aβ accumulation and progressive synaptic loss, gliosis, and tangle formation in AD brain. *Neurology* **62:** 925–931.

Iqbal K, Grundke-Iqbal I. 2002. Neurofibrillary pathology leads to synaptic loss and not the other way around in Alzheimer disease. *J Alzheimers Dis* **4:** 235–238.

Itagaki S, McGeer PL, Akiyama H, Zhu S, Selkoe D. 1989. Relationship of microglia and astrocytes to amyloid deposits of Alzheimer disease. *J Neuroimmunol* **24:** 173–182.

Iwai A, Masliah E, Yoshimoto M, Ge N, Flanagan L, de Silva HA, Kittel A, Saitoh T. 1995. The precursor protein of non-Aβ component of Alzheimer's disease amyloid is a presynaptic protein of the central nervous system. *Neuron* **14:** 467–475.

Jack CR Jr, Lowe VJ, Weigand SD, Wiste HJ, Senjem ML, Knopman DS, Shiung MM, Gunter JL, Boeve BF, Kemp BJ, et al. 2009. Serial PIB and MRI in normal, mild cognitive impairment and Alzheimer's disease: Implications for sequence of pathological events in Alzheimer's disease. *Brain* **132:** 1355–1365.

Janvin CC, Larsen JP, Salmon DP, Galasko D, Hugdahl K, Aarsland D. 2006. Cognitive profiles of individual patients with Parkinson's disease and dementia: Comparison with dementia with Lewy bodies and Alzheimer's disease. *Mov Disord* **21:** 337–342.

Jellinger KA, Attems J. 2006. Does striatal pathology distinguish Parkinson disease with dementia and dementia with Lewy bodies? *Acta Neuropathol* **112:** 253–260.

Jicha GA, Parisi JE, Dickson DW, Johnson K, Cha R, Ivnik RJ, Tangalos EG, Boeve BF, Knopman DS, Braak H, et al. 2006. Neuropathologic outcome of mild cognitive impairment following progression to clinical dementia. *Arch Neurol* **63:** 674–681.

Jin K, Peel AL, Mao XO, Xie L, Cottrell BA, Henshall DC, Greenberg DA. 2004. Increased hippocampal neurogenesis in Alzheimer's disease. *Proc Natl Acad Sci* **101:** 343–347.

Kahn J, Anderton BH, Probst A, Ulrich J, Esiri MM. 1985. Immunohistological study of granulovacuolar degeneration sing monoclonal antibodies to neurofilaments. *J Neurol Neurosurg Psychiatry* **48:** 924–926.

Kannanayakal TJ, Tao H, Vandre DD, Kuret J. 2006. Casein kinase-1 isoforms differentially associate with neurofibrillary and granulovauoclar degeneration lesions. *Acta Neuropathol* **111:** 413–421.

Khachaturian ZS. 1985. Diagnosis of Alzheimer's disease. *Arch Neurol* **42:** 1092–1105.

Kidd M. 1963. Paired helical filaments in electron microscopy of Alzheimer's disease. *Nature* **197:** 192–193.

Kidd M. 1964. Alzheimer's disease: An electron microscopy study. *Brain* **87:** 307–320.

Kimura T, Fukuda T, Sahara N, Yamashita S, Murayama M, Mirozoki T, Yoshiike Y, Lee B, Sotiropoulos I, Maeda S, et al. 2010. Aggregation of detergent-insoluble tau is involved in neuronal loss but not in synaptic loss. *J Biol Chem* **285:** 38692–38699.

Klein WL. 2002. Aβ toxicity in Alzheimer's disease: Globular oligomers (ADDLs) as new vaccine and drug targets. *Neurochem Int* **41:** 345–352.

Klein WL, Krafft GA, Finch CE. 2001. Targeting small Aβ oligomers: The solution to an Alzheimer's disease conundrum? *Trends Neurosci* **24:** 219–224.

Klucken J, McLean PJ, Gomez-Tortosa E, Ingelsson M, Hyman BT. 2003. Neuritic alterations and neural system dysfunction in Alzheimer's disease and dementia with Lewy bodies. *Neurochem Res* **28:** 1683–1691.

Klyubin I, Betts V, Welzel AT, Blennow K, Zetterberg H, Wallin A, Lemere CA, Cullen WK, Peng Y, Wisniewski T, et al. 2008. Amyloid β protein dimer-containing human CSF disrupts synaptic plasticity: Prevention by systemic passive immunization. *J Neurosci* **28:** 4231–4237.

Knopman DS, Parisi JE, Salviati A, Floriach-Robert M, Boeve BF, Ivnik RJ, Smith GE, Dickson DW, Johnson KA, Petersen LE, et al. 2003. Neuropathology of cognitively normal elderly. *J Neuropathol Exp Neurol* **62:** 1087–1095.

Knowles RB, Wyart C, Buldyrev SV, Cruz L, Urbanc B, Hasselmo ME, Stanley HE, Hyman BT. 1999. Plaque-induced neurite abnormalities: implications for disruption of neural networks in Alzheimer's disease. *Proc Natl Acad Sci* **96:** 5274–5279.

Knudsen KA, Rosand J, Karluk D, Greenberg SM. 2001. Clinical diagnosis of cerebral amyloid angiopathy: Validation of the Boston criteria. *Neurology* **56:** 537–539.

Koffie RM, Meyer-Luehmann M, Hashimoto T, Adams KW, Mielke ML, Garcia-Alloza M, Micheva KD, Smith SJ, Kim ML, Lee VM, et al. 2009. Oligomeric amyloid β associates with postsynaptic densities and correlates with excitatory synapse loss near senile plaques. *Proc Natl Acad Sci* **106:** 4012–4017.

Kramer ML, Schulz-Schaeffer WJ. 2007. Presynaptic α-synuclein aggregates, not Lewy bodies, cause neurodegeneration in dementia with Lewy bodies. *J Neurosci* **27:** 1405–1410.

Lacor PN, Buniel MC, Furlow PW, Clemente AS, Velasco PT, Wood M, Viola KL, Klein WL. 2007. Aβ oligomer-induced aberrations in synapse composition, shape, and density provide a molecular basis for loss of connectivity in Alzheimer's disease. *J Neurosci* **27:** 796–807.

LaFerla F, Tinkle B, Bieberich C, Haudenschild C, Jay G. 1995. The Alzheimer's Aβ peptide induces neurodegeneration and apoptotic cell death in transgenic mice. *Nat Genet* **9:** 21–30.

Lagalwar S, Berry RW, Binder LI. 2007. Regulation of hippocampal phospho-SAPK/JNK granules in Alzheimer's disease and tauopathies to granulovacuolar degeneration bodies. *Acta Neuropathol* **113:** 63–73.

Lambert MP, Barlow AK, Chromy BA, Edwards C, Freed R, Liosatos M, Morgan TE, Rozovsky I, Trommer B, Viola KL, et al. 1998. Diffusible, nonfibrillar ligands derived from Aβ1–42 are potent central nervous system neurotoxins. *Proc Natl Acad Sci* **95:** 6448–6453.

Lashuel HA, Petre BM, Wall J, Simon M, Nowak RJ, Walz T, Lansbury PT Jr. 2002. α-synuclein, especially the Parkinson's disease-associated mutants, forms pore-like annular and tubular protofibrils. *J Mol Biol* **322:** 1089–1102.

Lee SC, Zhao ML, Hirano A, Dickson DW. 1999. Inducible nitric oxide synthase immunoreactivity in the Alzheimer disease hippocampus: Association with Hirano bodies, neurofibrillary tangles, and senile plaques. *J Neuropathol Exp Neurol* **58:** 1163–1169.

Lee VM, Goedert M, Trojanowski JQ. 2001. Neurodegenerative tauopathies. *Annu Rev Neurosci* **24:** 1121–1159.

Leroy K, Boutajangout A, Authelet M, Woodgett JR, Anderton BH, Brion JP. 2002. The active form of glycogen synthase kinase-3β is associated with granulovacuolar degeneration in neurons in Alzheimer's disease. *Acta Neuropathol* **103:** 91–99.

Lesne S, Koh MT, Kotilinek L, Kayed R, Glabe CG, Yang A, Gallagher M, Ashe KH. 2006. A specific amyloid-β protein assembly in the brain impairs memory. *Nature* **440:** 352–357.

Leverenz JB, Fishel MA, Peskind ER, Montine TJ, Nochlin D, Steinbart E, Raskind MA, Schellenberg GD, Bird TD, Tsuang D. 2006. Lewy body pathology in familial Alzheimer disease: Evidence for disease- and mutation-specific pathologic phenotype. *Arch Neurol* **63:** 370–376.

Li B, Yamamori H, Tatebayashi Y, Shafit-Zagardo B, Tanimukai H, Chen S, Iqbal K, Grundke-Iqbal I. 2008. Failure of neuronal maturation in Alzheimer disease dentate gyrus. *J Neuropathol Exp Neurol* **67:** 78–84.

Lippa CF, Hamos JE, Pulaski-Salo D, DeGennaro LJ, Drachman DA. 1992. Alzheimer's disease and aging: Effects on perforant pathway perikarya and synapses. *Neurobiol Aging* **13:** 405–411.

Lippa CF, Fujiwara H, Mann DM, Giasson B, Baba M, Schmidt ML, Nee LE, O'Connell B, Pollen DA, St George-Hyslop P, et al. 1998. Lewy bodies contain altered α-synuclein in brains of many familial Alzheimer's disease patients with mutations in presenilin and amyloid precursor protein genes. *Am J Pathol* **153:** 1365–1370.

Lippa CF, Schmidt ML, Lee VM, Trojanowski JQ. 1999. Antibodies to α-synuclein detect Lewy bodies in many Down's syndrome brains with Alzheimer's disease. *Ann Neurol* **45:** 353–357.

Lippa CF, Duda JE, Grossman M, Hurtig HI, Aarsland D, Boeve BF, Brooks DJ, Dickson DW, Dubois B, Emre M, et al. 2007. DLB and PDD boundary issues: Diagnosis, treatment, molecular pathology, and biomarkers. *Neurology* **68:** 812–819.

Litvan I, MacIntyre A, Goetz CG, Wenning GK, Jellinger K, Verny M, Bartko JJ, Jankovic J, McKee A, Brandel JP, et al. 1998. Accuracy of the clinical diagnoses of Lewy body disease, Parkinson disease, and dementia with Lewy bodies: A clinicopathologic study. *Arch Neurol* **55:** 969–978.

Lue LF, Brachova L, Civin WH, Rogers J. 1996. Inflammation, Aβ deposition, and neurofibrillary tangle formation as correlates of Alzheimer's disease neurodegeneration. *J Neuropathol Exp Neurol* **55:** 1083–1088.

Maciver SK, Harrington CR. 1995. Two actin binding proteins, actin depolymerizing factor and cofilin, are associated with Hirano bodies. *Neuroreport* **6:** 1985–1988.

Mandal PK, Pettegrew JW, Masliah E, Hamilton RL, Mandal R. 2006. Interaction between Aβ peptide and α synuclein: Molecular mechanisms in overlapping pathology of Alzheimer's and Parkinson's in dementia with Lewy body disease. *Neurochem Res* **31:** 1153–1162.

Mandelkow EM, Mandelkow E. 1998. Tau in Alzheimer's disease. *Trends Cell Biol* **8:** 425–427.

Markesbery WR, Schmitt FA, Kryscio RJ, Davis DG, Smith CD, Wekstein DR. 2006. Neuropathologic substrate of mild cognitive impairment. *Arch Neurol* **63:** 38–46.

Masliah E. 2000. The role of synaptic proteins in Alzheimer's disease. *Ann NY Acad Sci* **924:** 68–75.

Masliah E, Terry R. 1993. The role of synaptic proteins in the pathogenesis of disorders of the central nervous system. *Brain Pathol* **3:** 77–85.

Masliah E, Terry R. 1994. The role of synaptic pathology in the mechanisms of dementia in Alzheimer's disease. *Clin Neurosci* **1:** 192–198.

Masliah E, Terry RD, Mallory M, Alford M, Hansen LA. 1990. Diffuse plaques do not accentuate synapse loss in Alzheimer's disease. *Am J Pathol* **137:** 1293–1297.

Masliah E, Mallory M, Hansen L, Alford M, Albright T, Terry R, Shapiro P, Sundsmo M, Saitoh T. 1991. Immunoreactivity of CD45, a protein phosphotyrosine phosphatase, in Alzheimer disease. *Acta Neuropathol* **83:** 12–20.

Masliah E, Mallory M, DeTeresa R, Alford M, Hansen L. 1993a. Differing patterns of aberrant neuronal sprouting in Alzheimer's disease with and without Lewy bodies. *Brain Res* **617:** 258–266.

Masliah E, Mallory M, Hansen L, DeTeresa R, Terry RD. 1993b. Quantitative synaptic alterations in the human neocortex during normal aging. *Neurology* **43:** 192–197.

Masliah E, Mallory M, Hansen L, DeTeresa R, Alford M, Terry R. 1994. Synaptic and neuritic alterations during the progression of Alzheimer's disease. *Neurosci Lett* **174:** 67–72.

Masliah E, Mallory M, Alford M, DeTeresa R, Hansen LA, McKeel DW Jr, Morris JC. 2001a. Altered expression of synaptic proteins occurs early during progression of Alzheimer's disease. *Neurology* **56:**127–129.

Masliah E, Rockenstein E, Veinbergs I, Sagara Y, Mallory M, Hashimoto M, Mucke L. 2001b. β-amyloid peptides enhance α-synuclein accumulation and neuronal deficits in a transgenic mouse model linking Alzheimer's disease and Parkinson's disease. *Proc Natl Acad Sci* **98:** 12245–12250.

Masliah E, Alford M, Adame A, Rockenstein E, Galasko D, Salmon D, Hansen LA, Thal LJ. 2003. Aβ1–42 promotes cholinergic sprouting in patients with AD and Lewy body variant of AD. *Neurology* **61:** 206–211.

McDonald JM, Savva GM, Brayne C, Welzel AT, Forster G, Shankar GM, Selkoe DJ, Ince PG, Walsh DM. 2010. The presence of sodium dodecyl sulphate-stable Aβ dimers is strongly associated with Alzheimer-type dementia. *Brain* **133:** 1328–1341.

McKeith IG. 2000. Spectrum of Parkinson's disease, Parkinson's dementia, and Lewy body dementia. *Neurol Clin* **18:** 865–902.

McKeith IG. 2006. Consensus guidelines for the clinical and pathologic diagnosis of dementia with Lewy bodies (DLB): Report of the Consortium on DLB International Workshop. *J Alzheimers Dis* **9:** 417–423.

McKeith IG, Galasko D, Kosaka K, Perry EK, Dickson DW, Hansen LA, Salmon DP, Lowe J, Mirra SS, Byrne EJ, et al. 1996. Consensus guidelines for the clinical and pathologic diagnosis of dementia with Lewy bodies (DLB): Report of the consortium on DLB international workshop. *Neurology* **47:** 1113–1124.

McKeith IG, Dickson DW, Lowe J, Emre M, O'Brien JT, Feldman H, Cummings J, Duda JE, Lippa C, Perry EK, et al. 2005. Diagnosis and management of dementia with Lewy bodies: Third report of the DLB consortium. *Neurology* **65:** 1863–1872.

Mena R, Robitaille Y, Cuello AC. 1992. New patterns of intraneuronal accumulation of the microtubular binding domain of tau in granulovacuolar degeneration. *J Geriatr Psychiatry Neurol* **5:** 132–141.

Mirra SS, Heyman A, McKeel D, Sumi SM, Crain BJ, Brownlee LM, Vogel FS, Hughes JP, van Belle G, Berg L. 1991. The Consortium to Establish a Registry for Alzheimer's Disease (CERAD). Part II. Standardization of the neuropathological assessment of Alzheimer's disease. *Neurology* **41:** 479–486.

Mirra SS, Gearing M, Nash F. 1997. Neuropathological assessment of Alzheimer's disease. *Neurology* **49:** S14–S16.

Münch G, Cunningham AM, Riederer P, Braak E. 1998. Advance glycation endproducts are associated with Hirano bodies in Alzheimer's disease. *Brain Res* **796:** 307–310.

Muñoz DG, Wang D, Greenberg BD. 1993. Hirano bodies accumulate C-terminal sequences of β-amyloid precursor protein (β-APP) epitopes. *J Neuropathol Exp Neurol* **52:** 14–21.

Neuropathology Group of the Medical Research Council Cognitive Function and Aging Study (MRC CFAS). 2001. Pathological correlates of late-onset dementia in a multicenter community-based population in England and Wales. *Lancet* **357:** 169–175.

Nixon RA, Cataldo AM. 2006. Lysosomal system pathways: Genes to neurodegeneration in Alzheimer's disease. *J Alzheimers Dis* **9:** 277–289.

Okamoto K, Hirai S, Iizuka T, Yanagisawa T, Watanabe M. 1991. Reexamination of granulovacuolar degeneration. *Acta Neuropathol* **82:** 340–345.

Olichney JM, Hansen LA, Hoffstetter CR, Lee JH, Katzman R, Thal LJ. 2000. Association between severe cerebral amyloid angiopathy and cerebrovascular lesions in Alzheimer disease is not a spurious one attributable to apolipoprotein E4. *Arch Neurol* **57:** 869–874.

Palop JJ, Jones B, Kekonius L, Chin J, Yu GQ, Raber J, Masliah E, Mucke L. 2003. Neuronal depletion of calcium-dependent proteins in the dentate gyrus is tightly linked to Alzheimer's disease-related cognitive deficits. *Proc Natl Acad Sci* **100:** 9572–9577.

Palop JJ, Mucke L, Roberson ED. 2011. Quantifying biomarkers of cognitive dysfunction and neuronal network hyperexcitability in mouse models of Alzheimer's disease: Depletion of calcium-dependent proteins and inhibitory hippocampal remodeling. *Methods Mol Biol* **670:** 245–262.

Pérez-Gracia E, Torrejón-Escribano B, Ferrer I. 2008. Dystrophic neurites of senile plaques in Alzheimer's disease are deficient in cytochrome c oxidase. *Acta Neuropathol* **116:** 261–268.

Perlson E, Maday S, Fu MM, Moughamian AJ, Holzbaur EL. 2010. Retrograde axonal transport: Pathways to cell death? *Trends Neurosci* **33:** 335–344

Perry EK, Tomlinson BE, Blessed G, Bergmann K, Gibson PH, Perry RH. 1978. Correlation of cholinergic abnormalities with senile plaques and mental test scores in senile dementia. *Br Med J* **2:** 1457–1459.

Petersen RC. 2004. Mild cognitive impairment as a diagnostic entity. *J Intern Med* **256:** 183–194.

Petersen RC, Smith GE, Waring SC, Ivnik RJ, Tangalos EG, Kokmen E. 1999. Mild cognitive impairment: Clinical characterization and outcome. *Arch Neurol* **56:** 303–308.

Petersen RC, Doody R, Kurz A, Mohs RC, Morris JC, Rabins PV, Ritchie K, Rossor M, Thal L, Winblad B. 2001. Current concepts in mild cognitive impairment. *Arch Neurol* **58:** 1985–1992

Petersen RC, Parisi JE, Dickson DW, Johnson KA, Knopman DS, Boeve BF, Jicha GA, Ivnik RJ, Smith GE, Tangalos EG, et al. 2006. Neuropathologic features of amnestic mild cognitive impairment. *Arch Neurol* **63:** 665–672.

Pfeifer LA, White LR, Ross GW, Petrovich H, Launer LJ. 2002. Cerebral amyloid angiopathy and cognitive function: The HAAS autopsy study. *Neurology* **58:** 1629–1634.

Pham E, Crews L, Ubhi K, Hansen L, Adame A, Cartier A, Salmon D, Galasko D, Michael S, Savas JN, et al. 2010. Progressive accumulation of amyloid-β oligomers in Alzheimer's disease and in amyloid precursor protein transgenic mice is accompanied by selective alterations in synaptic scaffold proteins. *FEBS J* **277:** 3051–3067.

Pike CJ, Cummings BJ, Cotman CW. 1995. Early association of reactive astrocytes with senile plaques in Alzheimer's disease. *Exp Neurol* **132:** 172–179.

Pletnikova O, West N, Lee MK, Rudow GL, Skolasky RL, Dawson TM, Marsh L, Troncoso JC. 2005. Aβ deposition is associated with enhanced cortical α-synuclein lesions in Lewy body diseases. *Neurobiol Aging* **26:** 1183–1192.

Price DL, Altschuler RJ, Struble RG, Casanova MF, Cork LC, Murphy DB. 1986. Sequestration of tubulin in neurons in Alzheimer's disease. *Brain Res* **385:** 305–310.

Price JL, Ko AI, Wade MJ, Tsou SK, McKeel DW, Morris JC. 2001. Neuron number in the entorhinal cortex and CA1 in preclinical Alzheimer disease. *Arch Neurol* **58:** 1395–1402.

Price JL, McKeel DW Jr, Buckles VD, Roe CM, Xiong C, Grundman M, Hansen LA, Petersen RC, Parisi JE, Dickson DW, et al. 2009. Neuropathology of nondemented aging: Presumptive evidence for preclinical Alzheimer disease. *Neurobiol Aging* **30:** 1026–1036.

Riudavets MA, Iacono D, Resnick SM, O'Brien R, Zonderman AB, Martin LJ, Rudow G, Pletnikova O, Troncoso JC. 2007. Resistance to Alzheimer's pathology is associated with nuclear hypertrophy in neurons. *Neurobiol Aging* **28:** 1484–1492.

Rockenstein E, Schwach G, Ingolic E, Adame A, Crews L, Mante M, Pfragner R, Schreiner E, Windisch M, Masliah E. 2005. Lysosomal pathology associated with alpha-synuclein accumulation in transgenic models using an eGFP fusion protein. *J Neurosci Res* **80:** 247–259.

Rogers J, Luber-Narod J, Styren S, Civin W. 1988. Expression of immune system-associated antigens by cells of the human central nervous system: Relationship to the pathology of Alzheimer's disease. *Neurobiol Aging* **9:** 339–349.

Rosenberg RN. 2005. New presenilin 1 mutation with Alzheimer disease and Lewy bodies. *Arch Neurol* **62:** 1808.

Rossiter JP, Anderson LL, Yang F, Cole GM. 2000. Caspase-cleaved actin (fractin) immunolabeling of Hirano bodies. *Neuropathol Appl Neurobiol* **26:** 342–346.

Scheff SW, Price DA. 1993. Synapse loss in the temporal lobe in Alzheimer's disease. *Ann Neurol* **33:** 190–199.

Scheff SW, DeKosky ST, Price DA. 1990. Quantitative assessment of cortical synaptic density in Alzheimer's disease. *Neurobiol Aging* **11:** 29–37.

Scheff SW, Price DA, Schmitt FA, Mufson EJ. 2006. Hippocampal synaptic loss in early Alzheimer's disease and mild cognitive impairment. *Neurobiol Aging* **27:** 1372–1384.

Scheff SW, Price DA, Schmitt FA, DeKosky ST, Mufson EJ. 2007. Synaptic alterations in CA1 in mild Alzheimer disease and mild cognitive impairment. *Neurology* **68:** 1501–1508.

Schmidt ML, Lee VM, Trojanowski JQ. 1989. Analyses of epitopes shared by Hirano bodies and neurofilament proteins in normal and Alzheimer's disease hippocampus. *Lab Invest* **60:** 513–522.

Schmitt FA, Davis DG, Wekstein DR, Smith CD, Ashford JW, Markesbery WR. 2000. "Preclinical" AD revisited. Neuropathology of cognitively normal older adults. *Neurology* **55:** 370–376.

Schneider JA, Arvanitakis Z, Bang W, Bennet DA. 2007. Mixed brain pathologies account for most dementia cases in community-dwelling older persons. *Neurology* **69:** 2197–2204.

Schneider JA, Arvanitakis Z, Leurgans SE, Bennet DA. 2009. The neuropathology of probable Alzheimer's disease and mild cognitive impairment. *Ann Neurol* **66:** 200–208.

Scott DA, Tabarean I, Tang Y, Cartier A, Masliah E, Roy S. 2010. A pathologic cascade leading to synaptic dysfunction in α-synuclein-induced neurodegeneration. *J Neurosci* **30:** 8083–8095.

Selkoe D. 1989. Amyloid β protein precursor and the pathogenesis of Alzheimer's disease. *Cell* **58:** 611–612.

Selkoe D. 1990. Amyloid β-protein deposition as a seminal pathogenic event in AD: An hypothesis. *Neurobiol Aging* **11:** 299.

Selkoe D. 1993. Physiological production of the β-amyloid protein and the mechanisms of Alzheimer's disease. *Trends Neurosci* **16:** 403–409.

Selkoe DJ. 2008. Soluble oligomers of the amyloid β-protein impair synaptic plasticity and behavior. *Behav Brain Res* **192:** 106–113.

Selznick LA, Holtzman DM, Han BH, Gökden M, Srinivasan AN, Johnson EM Jr, Roth KA. 1999. In situ immunodetection of neuronal caspase-3 activation in Alzheimer disease. *J Neuropathol Exp Neurol* **58:** 1020–1026.

Serrano-Pozo A, Mielke ML, Gómez-Isla E, Betensky RA, Growdon JH, Frosch MP, Hyman BT. 2011. Reactive glia not only associates with plaques but also parallels tangles in Alzheimer's disease. *Am J Pathol* **179**. doi: 10.1016/j.ajpath.2011.05.047.

Shankar GM, Li S, Mehta TH, García-Munoz A, Shepardson NE, Smith I, Brett FM, Farrell MA, Rowan MJ, Lemere CA, et al. 2008. Amyloid-beta protein dimers isolated directly from Alzheimer's brains impair synaptic plasticity and memory. *Nat Med* **14:** 837–842.

Sisodia SS, Price DL. 1995. Role of the β-amyloid protein in Alzheimer's disease. *FASEB J* **9:** 366–370.

Skovronsky DM, Doms RW, Lee VM-Y. 1998. Detection of a novel intraneuronal pool of insoluble amyloid β-protein that accumulates with time in culture. *J Cell Biol* **141:** 1031–1039.

Smith MA, Perry G, Richey PL, Sayre LM, Anderson VE, Beal MF, Kowall N. 1996. Oxidative damage in Alzheimer's. *Nature* **382:** 120–121.

Snider BJ, Norton J, Coats MA, Chakraverty S, Hou CE, Jervis R, Lendon CL, Goate AM, McKeel DW Jr, Morris JC. 2005. Novel presenilin 1 mutation (S170F) causing Alzheimer disease with Lewy bodies in the third decade of life. *Arch Neurol* **62:** 1821–1830.

Spillantini M, Schmidt M, Lee V-Y, Trojanowski J, Jakes R, Goedert M. 1997. α-Synuclein in Lewy bodies. *Nature* **388:** 839–840.

Spires-Jones TL, de Calignon A, Matsui T, Zehr C, Pitstick R, Wu HY, Osetek JD, Jones PB, Bacskai BJ, Feany MB, et al. 2007. In vivo imaging reveals dissociation between caspase activation and acute neuronal death in tangle-bearing neurons. *J Neurosci* **28:** 862–867.

Stadelmann C, Deckwerth TL, Srinivasan A, Bancher C, Brück W, Jellinger K, Lassmann H. 1999. Activation of caspase-3 in single neurons and autophagic vacuoles of granulovacuolar degeneration in Alzheimer's disease. Evidence for apoptotic cell death. *Am J Pathol* **155:** 1459–1466.

Su JH, Cummings BJ, Cotman CW. 1993. Identification and distribution of axonal dystrophic neurites in Alzheimer's disease. *Brain Res* **625:** 228–237.

Su JH, Cummings BJ, Cotman CW. 1994. Subpopulations of dystrophic neuritis in Alzheimer's brain with distinct immunocytochemical and argentophilic characteristics. *Brain Res* **637:** 37–44.

Su JH, Cummings BJ, Cotman CW. 1996. Plaque biogenesis in brain aging and Alzheimer's disease. I. Progressive changes in phosphorylation states of paired helical filaments and neurofilaments. *Brain Res* **739:** 79–87.

Su JH, Cummings BJ, Cotman CW. 1998. Plaque biogenesis in brain aging and Alzheimer's disease. II. Progressive transformation and developmental sequence of dystrophic neurites. *Acta Neuropathol* **96:** 463–471.

Su JH, Zhao M, Anderson AJ, Srinivasan A, Cotman CW. 2001. Activated-caspase-3 expression in Alzheimer's and aged control brain: Correlation with Alzheimer pathology. *Brain Res* **898:** 350–357.

Su JH, Kesslak JP, Head E, Cotman CW. 2002. Caspase-cleaved amyloid precursor protein and activated caspase-3 are co-localized in the granules of granulovacuolar degeneration in Alzheimer's disease and Down's syndrome brain. *Acta Neuropathol* **104:** 1–6.

Takeda A, Mallory M, Sundsmo M, Honer W, Hansen L, Masliah E. 1998. Abnormal accumulation of NACP/α-synuclein in neurodegenerative disorders. *Am J Pathol* **152:** 367–372.

Teipel SJ, Flatz WH, Heinsen H, Bokde AL, Schoenberg SO, Stockel S, Dietrich O, Reiser MF, Moller HJ, Hampel H. 2005. Measurement of basal forebrain atrophy in Alzheimer's disease using MRI. *Brain* **128:** 2626–2644.

Terry R, Peck A, DeTeresa R, Schechter R, Horoupian D. 1981. Some morphometric aspects of the brain in senile dementia of the Alzheimer type. *Ann Neurol* **10:** 184–192.

Terry RD, Masliah E, Salmon DP, Butters N, DeTeresa R, Hill R, Hansen LA, Katzman R. 1991. Physical basis of cognitive alterations in Alzheimer's disease: Synapse loss is the major correlate of cognitive impairment. *Ann Neurol* **30:** 572–580.

Terry R, Hansen L, Masliah E. 1994. Structural basis of the cognitive alterations in Alzheimer disease. In *Alzheimer disease* (ed. R. Terry, R. Katzman), pp. 179–196. Raven, New York.

Thakur A, Wang X, Siedlak SL, Perry G, Smith MA, Zhu X. 2007. c-Jun phosphorylation in Alzheimer disease. *J Neurosci Res* **85:** 1668–1673.

Thal DR, Rüb U, Orantes M, Braak H. 2002. Phases of Aβ-deposition in the human brain and its relevance for the development of AD. *Neurology* **58:** 1791–1800.

The National Institute of Aging, and Reagan Institute working group on the diagnostic criteria for the neuropathological assessment of Alzheimer's disease. 1997. Consensus recommendations for the postmortem diagnosis of Alzheimer's disease. *Neurobiol Aging* **18:** S1–S2.

Townsend M, Shankar GM, Mehta T, Walsh DM, Selkoe DJ. 2006. Effects of secreted oligomers of amyloid β-protein on hippocampal synaptic plasticity: A potent role for trimers. *J Physiol* **572:** 477–492.

Trojanowski JQ, Lee VM. 1998. Aggregation of neurofilament and α-synuclein proteins in Lewy bodies: Implications for the pathogenesis of Parkinson disease and Lewy body dementia. *Arch Neurol* **55:** 151–152.

Trojanowski JQ, Lee VM. 2000. "Fatal attractions" of proteins. A comprehensive hypothetical mechanism underlying Alzheimer's disease and other neurodegenerative disorders. *Ann NY Acad Sci* **924:** 62–67.

Trojanowski JQ, Goedert M, Iwatsubo T, Lee VM. 1998. Fatal attractions: Abnormal protein aggregation and neuron death in Parkinson's disease and Lewy body dementia. *Cell Death Differ* **5:** 832–837.

Troncoso JC, Sukhov RR, Kawas CH, Koliatsos VE. 1996. In situ labeling of dying cortical neurons in normal aging and in Alzheimer's disease: Correlations with senile plaques and disease progression. *J Neuropathol Exp Neurol* **55:** 1134–1142.

Tsigelny IF, Bar-On P, Sharikov Y, Crews L, Hashimoto M, Miller MA, Keller SH, Platoshyn O, Yuan JX, Masliah E. 2007. Dynamics of α-synuclein aggregation and inhibition of pore-like oligomer development by β-synuclein. *FEBS J* **274:** 1862–1877.

Tsigelny IF, Crews L, Desplats P, Shaked GM, Sharikov Y, Mizuno H, Spencer B, Rockenstein E, Trejo M, Platoshyn O, et al. 2008. Mechanisms of hybrid oligomer formation in the pathogenesis of combined Alzheimer's and Parkinson's diseases. *PLoS One* **3:** e3135.

Tsuboi Y, Dickson DW. 2005. Dementia with Lewy bodies and Parkinson's disease with dementia: Are they different? *Parkinsonism Relat Disord* **11:** S47–S51.

Uboga NV, Price JL. 2000. Formation of diffuse and fibrillar tangles in aging and early Alzheimer's disease. *Neurobiol Aging* **21:** 1–10.

Urbanc B, Cruz L, Le R, Sanders J, Hsiao-Ashe K, Stanley HE, Irizarry MC, Hyman BT. 2002. Neurotoxic effects of thioflavin S-positive amyloid deposits in transgenic mice and Alzheimer's disease. *Proc Natl Acad Sci* **99:** 13990–13995.

Vehmas AK, Kawas CH, Stewart WF, Troncoso JC. 2003. Immune reactive cells in senile plaques and cognitive decline in Alzheimer's disease. *Neurobiol Aging* **24:** 321–331.

Wakabayashi K, Matsumoto K, Takayama K, Yoshimoto M, Takahashi H. 1997. NACP, a presynaptic protein, immunoreactivity in Lewy bodies in Parkinson's disease. *Neurosci Lett* **239:** 45–48.

Walsh DM, Selkoe DJ. 2004. Oligomers on the brain: The emerging role of soluble protein aggregates in neurodegeneration. *Protein Pept Lett* **11:** 213–228.

Walsh DM, Klyubin I, Fadeeva JV, Cullen WK, Anwyl R, Wolfe MS, Rowan MJ, Selkoe DJ. 2002. Naturally secreted oligomers of amyloid β protein potently inhibit hippocampal long-term potentiation in vivo. *Nature* **416:** 535–539.

Weaver CL, Espinoza M, Kress Y, Davies P. 2000. Conformational change as one of the earliest alterations of tau in Alzheimer's disease. *Neurobiol Aging* **21:** 719–727.

Wegmann S, Jung YJ, Chinnathambi S, Mandelkow EM, Mandelkow E, Muller DJ. 2010. Human tau isoforms assemble into ribbon-like fibrils that display polymorphic structure and stability. *J Biol Chem* **285:** 27302–27313.

West MJ, Kawas CH, Stewart WF, Rudow GL, Troncoso JC. 2004. Hippocampal neurons in pre-clinical Alzheimer's disease. *Neurobiol Aging* **25:** 1205–1212.

Wisniewski HM, Narang HK, Terry RD. 1976. Neurofibrillary tangles of paired helical filaments. *J Neurol Sci* **27:** 173–181.

Woodhouse A, Vickers JC, Dickson TC. 2006a. Cytoplasmic cytochrome c immunolabeling in dystrophic neurites in Alzheimer's disease. *Acta Neuropathol* **112:** 429–437.

Woodhouse A, Dickson TC, West AK, McLean CA, Vickers JC. 2006b. No difference in expression of apoptosis-related proteins and apoptotic morphology in control, pathologically aged and Alzheimer's disease cases. *Neurobiol Dis* **22:** 323–333.

Xu M, Shibayama H, Kobayashi H, Yamada K, Ishihara R, Zhao P, Takeuchi T, Yoshida K, Inagaki T, Nokura K. 1992. Granulovacuolar degeneration in the hippocampal cortex of aging and demented patients: A quantitative study. *Acta Neuropathol* **85:** 1–9.

Yamazaki Y, Takahashi T, Hiji M, Kurashige T, Izumi Y, Yamawaki T, Matsumoto M. 2010. Immunopositivity for ESCRT-III subunit CHMP2B in granulovacuolar degeneration of neurons in the Alzheimer's disease hippocampus. *Neurosci Lett* **477:** 86–90.

Yoshiyama Y, Higucho M, Zhang B, Huang SM, Iwata N, Saido TC, Maeda J, Suhara T, Trojanowski JQ, Lee VM. 2007. Synapse loss and microglial activation precede tangles in a P301S tauopathy mouse model. *J Neuron* **53:** 337–351.

Zhu X, Raina AK, Rottkamp CA, Aliev G, Perry G, Boux H, Smith MA. 2001. Activation and redistribution of c-jun N-terminal kinase/stress activated protein kinase in degenerating neurons in Alzheimer's disease. *J Neurochem* **76:** 435–441.

5.2. Original article#1:

Serrano-Pozo A, Mielke ML, Gómez-Isla T, Betensky RA, Growdon JH, Frosch MP, Hyman BT. Reactive glia not only associates with plaques but also parallels tangles in Alzheimer's disease. *Am J Pathol* 2011; 179(3): 1373-84.

Neurobiology

Reactive Glia not only Associates with Plaques but also Parallels Tangles in Alzheimer's Disease

Alberto Serrano-Pozo,*† Matthew L. Mielke,*
Teresa Gómez-Isla,*† Rebecca A. Betensky,†‡
John H. Growdon,*† Matthew P. Frosch,*†¶ and
Bradley T. Hyman*†

*From the Massachusetts General Hospital Institute for
Neurodegenerative Disease,* Massachusetts General Hospital, and
the Massachusetts Alzheimer Disease Research Center,†
Charlestown; the Harvard School of Public Health,‡ Boston; and
the C.S. Kubik Laboratory for Neuropathology,¶ Massachusetts
General Hospital, Boston, Massachusetts*

**Senile plaques are a prominent pathological feature
of Alzheimer's disease (AD), but little is understood
about the association of glial cells with plaques or
about the dynamics of glial responses through the
disease course. We investigated the progression of
reactive glial cells and their relationship with AD
pathological hallmarks to test whether glial cells are
linked only to amyloid deposits or also to tangle de-
position, thus integrating both lesions as a marker of
disease severity. We conducted a quantitative stereol-
ogy-based post-mortem study on the temporal neo-
cortex of 15 control subjects without dementia and 91
patients with AD, including measures of amyloid load,
neurofibrillary tangles, reactive astrocytes, and acti-
vated microglia. We also addressed the progression of
glial responses in the vicinity (≤50 μm) of dense-core
plaques and tangles. Although the amyloid load
reached a plateau early after symptom onset, astrocy-
tosis and microgliosis increased linearly throughout
the disease course. Moreover, glial responses corre-
lated positively with tangle burden, whereas astrocy-
tosis correlated negatively with cortical thickness.
However, neither correlated with amyloid load.
Glial responses increased linearly around existing
plaques and in the vicinity of tangles. These results
indicate that the progression of astrocytosis and
microgliosis diverges from that of amyloid deposi-
tion, arguing against a straightforward relationship
between glial cells and plaques. They also suggest
that reactive glia might contribute to the ongoing
neurodegeneration.   (Am J Pathol 2011, 179:1373–1384;
DOI: 10.1016/j.ajpath.2011.05.047)**

Activated glia is a prominent feature of Alzheimer's dis-
ease (AD) neuropathological features, with both reactive
astrocytes and activated microglia clustering around and
within dense-core amyloid plaques (ie, thioflavin-S–pos-
itive plaques).[1] A better understanding of how these reac-
tive glial cells accrue during the disease course and how
they relate to the classic AD pathological hallmarks [ie,
amyloid plaques and neurofibrillary tangles (NFTs)] is cru-
cial for the following reasons: i) a body of preclinical evi-
dence implicates these glial cells in AD pathophysiological
features; ii) new positron emission tomographic (PET) radio-
tracers for amyloid plaques, NFTs, and, particularly, acti-
vated glial cells are being developed as diagnostic and
progression biomarkers; and iii) clinical trials with anti-in-
flammatory therapies, ranging from nonsteroidal anti-inflam-
matory drugs (NSAIDs) to i.v. Ig, are under development.

In a previous quantitative neuropathological study,[2] we
observed a positive linear correlation between astrocytosis
in the temporal neocortex, as measured with a glial fibrillary
acidic protein (GFAP) enzyme-linked immunosorbent as-
say, and the duration of the disease from the onset of
cognitive symptoms, despite the plaque burden remaining
stable throughout the course of the disease. We hypothe-
sized that a certain threshold of amyloid burden might be
needed to trigger glial responses within a particular region
of the cortex and that, once triggered, glial responses would
reflect a pathogenic cascade increasingly independent of
plaques. In the present study, we sought to extend that
observation and test the hypothesis that, although initially
linked to plaques, glial responses increasingly reflect the
widespread ongoing neurodegenerative process. We
quantified the number of reactive astrocytes and activated
microglial cells in the temporal neocortex of a large cohort of
controls without dementia and subjects with AD at different
stages of the disease and investigated both their apparent

progression throughout the disease course and their relation to the local burden of amyloid plaques and NFTs. Although glial association with amyloid plaques has long been assumed, we found a dissociation between these pathological features, with a linear increase of reactive glia despite a relatively stable plaque burden. The magnitude of these glial changes correlated with the burden of NFTs. A closer analysis in a subset of subjects with AD revealed that reactive glial cells increased both in the proximity of dense-core plaques and near NFTs, thus supporting a previously not described association between glial responses and neurofibrillary degeneration.

Materials and Methods

Brain Specimens and Immunohistochemical Studies

Formalin-fixed, paraffin-embedded tissue specimens from the temporal association isocortex (Brodmann area 38) of 91 patients with AD and 15 controls without dementia were obtained from the Massachusetts Alzheimer Disease Research Center Brain Bank. They were consecutively selected by tissue availability. All of the study subjects or their next of kin gave written informed consent for the brain donation, and the Massachusetts General Hospital Institutional Review Board approved the study protocol. The demographic characteristics of both groups are depicted in Table 1. All of the patients with AD fulfilled the National Institute of Neurological and Communicative Disorders and Stroke–Alzheimer's Disease and Related Disorders Associations criteria for probable AD[3] and the National Institute on Aging–Reagan criteria for high likelihood of AD.[4] Cases with cerebrovascular disease considered severe enough to contribute to the dementia syndrome were excluded because cerebrovascular disease is a major cause of focal gliosis. Cases with Lewy body pathological features were also excluded. Sections (8-μm thick) were deparaffinized for immunohistochemistry by standard methods. Primary and secondary antibodies, pretreatments for antigen retrieval, and visualization strategies are summarized in Table 2. For stereological quantitative studies, immunostained sections were developed with 3,3′-diaminobenzidine (Vector Laboratories, Burlingame, CA), lightly counterstained with Mayer's hematoxylin, dehydrated with increasing concentrations of ethanol, cleared with xylene, and cover-slipped with Permount mounting media (Fisher Scientific, Fair Lawn, NJ). Nearly adjacent temporal sections from a subset of 40 subjects with AD and six controls without dementia were immunostained using fluorescently labeled secondary antibodies, counterstained with 0.05% thioflavin-S (Sigma, St Louis, MO) in 50% ethanol for 8 minutes, and cover-slipped with Vectashield mounting media with 4′,6-diamidino-2-phenylindole (DAPI) (Vector Laboratories).

Quantitative Neuropathological Analyses

We took advantage of stereology tools to perform unbiased quantitative neuropathological studies in these brain specimens. All analyses were conducted blinded to disease status.

Cortical Thickness

Cortical thickness was measured in sections stained with Luxol fast blue H&E, as previously described.[5] Briefly, the image analysis software CAST (Olympus, Copenhagen, Denmark), mounted on an upright BX51 Olympus microscope (Olympus) and coupled with a motorized stage and a charge-coupled device camera, was used to randomly sample the cortex of the entire section and measure the thickness of the full cortex. The measurements of full cortical thickness in 20 random sites were averaged.

Amyloid Load and Number of Total Amyloid Plaques

Amyloid load and stereology-based studies on 3,3′-diaminobenzidine sections were conducted in an upright Leica DMRB microscope (Leica, Wetzlar, Germany) equipped with a motorized stage and a charge-coupled device camera (model DC330; DAGE-MTI, Inc., Michigan City, IN) and coupled with the software BIOQUANT NOVA PRIME, version 6.90.10 (MBSR, Nashville, TN). Amyloid load was measured as the percentage of total surface

Table 1. Demographic Characteristics of the Cohorts without Dementia and with AD and Their Corresponding Subsets Included in the Quantitative Neuropathological Study

Characteristics	Control cohort (n = 15)	AD cohort (n = 91)	P value	Control subset (n = 6)	AD subset (n = 40)	P value
Age at death (years)*	79.9 ± 13.3	79.0 ± 7.8	NS	83.7 ± 14.0	77.6 ± 8.6	**0.0429**
Female sex†	10 (66.7)	58 (63.7)	NS	4 (66.7)	26 (65.0)	NS
Disease duration (years)‡	NA	9.8 (6.8–13.7)	NA	NA	9.9 (5.4–15.5)	NA
APOE genotype†						
APOEε4 carriers	4 (26.7)	59 (64.8)	**0.0090**	2 (33.3)	21 (52.5)	NS
APOEε4 alleles§	4 (13.3)	70 (38.5)	**0.0070**	2 (16.7)	25 (31.2)	NS
Post-mortem interval (hours)*	22.3 ± 12.8	13.9 ± 9.1	**0.0085**	21.0 ± 11.1	14.1 ± 6.2	NS

    Information about cause of death was available in only 44 of the 91 subjects with AD because nursing homes are the main source of our brain donation program. Patients with protracted death (mostly aspirative pneumonia and cancer, n = 31) did not differ from patients with sudden death (mostly pulmonary emboli and myocardial infarction, n = 13) regarding their age at death (P = 0.2261), disease duration (P = 0.9898), or amount of astrocytosis (P = 0.1870) and microgliosis (P = 0.9180). Statistically significant P values are boldfaced.
    *Data are given as mean ± SD. P values were obtained using the two-tailed Mann-Whitney U-test.
    †Data are given as number (percentage) of each group. P values were obtained using the two-tailed χ^2 test with Fisher's exact test.
    ‡Data are given as median (interquartile range).
    §To obtain percentages, the denominators for this row were doubled.
    NA, not applicable; NS, not significant.

Table 2.   Antibodies, Antigen Retrieval Protocols, and Visualization Strategies Used in the IHC Studies

Primary antibody	Host	Dilution	Antigen retrieval*	Secondary antibody[†]	Visualization strategy
10D5 (Elan Pharmaceuticals, Inc.)	Ms	1:50	Citrate buffer + MW and 90% formic acid for 5 minutes	HRP anti-Ms (1:200)	DAB (Vector Laboratories)
PHF1 (gift from Dr. Peter Davies)	Ms	1:200	Citrate buffer + MW	Biotin anti-Ms (1:200)	ABC kit + DAB (Vector Laboratories for both)
GFAP (catalogue no. G9269; Sigma)	Rb	1:1000	Citrate buffer + MW	i) Biotin anti-Rb (1:200) and ii) Cy3 anti-Rb (1:200)	i) ABC kit + DAB (Vector Laboratories for both) and ii) none
CD68 (catalogue no. M0814; Dako, Glostrup, Denmark)	Ms	1:100	Citrate buffer + MW	Biotin anti-Ms (1:200)	ABC kit + DAB (Vector Laboratories for both)
Iba1 (catalogue no. 019-19741; Wako)	Rb	1:250	Citrate buffer + MW	Cy3 anti-Rb (1:200)	None
NAB61 (gift from Dr. Virginia Lee)	Ms	1:500	None	Biotin anti-Ms (1:200)	ABC kit (Vector Laboratories) + streptavidin-Cy3 (1:200) (Invitrogen)

*Citrate buffer + MW indicates 0.01 mol/L citrate buffer (pH 6.0) with 0.05% Tween 20 in a microwave oven at 95°C for 20 minutes.
[†]All secondary antibodies were obtained from Jackson ImmunoResearch Labs (West Grove, PA).
ABC, avidin-biotin complex; DAB, 3,3′-diaminobenzidine; HRP, horseradish peroxidase; Ms, mouse; Rb, rabbit.

stained by the N-terminal–specific anti-amyloid β (Aβ) antibody 10D5 (Elan Pharmaceuticals, Inc., Dublin, Ireland) in a full-thickness strip of cortex (approximately 1-cm long) using the optical threshold application of the software. The total number of amyloid plaques in a 1-cm-long strip of cortex was calculated by dividing the total number of particles higher than the threshold by the area analyzed (both parameters provided by the software) and then correcting the resultant density by the cortical thickness.

Stereology-Based Quantitation of NFTs, Astrocytes, and Microglia

Paired helical filament 1–positive NFTs, GFAP-positive astrocytes, and CD68-positive microglial cells were counted with the optic dissector technique,[6] using either 100 cells or 1000 optical dissectors as the end point. The objective/dissector size used in each case was 40/150 × 150 μm for paired helical filament 1–positive neurons, 40/50 × 50 μm for GFAP-positive astrocytes, and 100/20 × 20 μm for CD68-positive microglial cells. Intraneuronal and extracellular ghost tangles were not distinguished. Because different pathological features tend to accumulate in specific layers of the cortex (ie, reactive astrocytes in layer I and NFTs in layers II and V), care was taken to cover all of the six cortical layers in the systematic random sampling to avoid selection bias. As with the amyloid plaques, the densities of NFTs, astrocytes, and microglial cells were calculated by dividing the number of cells counted in single sections by the total area of the dissectors analyzed. To avoid any overestimation of densities because of disease-related cortical atrophy, these densities were then corrected by the cortical thickness to estimate the total number of cells within a full-thickness 1-cm-long strip of cortex.

Stereology-Based Quantitation of Oligomeric Aβ-Positive and Dense-Core Plaques

We performed additional quantitative studies in a subset of 40 AD cases selected from the original AD cohort on the

basis of a wide range of disease duration and in a subset of six controls without dementia (ie, those with enough dense-core plaques). These subsets were representative of their corresponding cohorts in demographic characteristics, and the AD subset was also comparable to the entire AD cohort in neuropathological quantitative measures (Table 1; see also Supplemental Table S1 and Figure S1 at *http://ajp.amjpathol.org*). To study the progression of compact and oligomeric species of Aβ, we quantified the number of dense-core plaques and oligomeric Aβ-positive plaques in sections doubly stained with thioflavin-S and NAB61 antibody. The NAB61 antibody was provided by Dr. Virginia Lee (University of Pennsylvania, Philadelphia) and has been previously characterized. It is a conformation-specific anti-Aβ mouse monoclonal antibody that binds to Aβ dimers, small oligomers, and higher-order Aβ assemblies and stains a subset of mature dense-core plaques.[7] Virtually no thioflavin-S–negative plaque was immunoreactive for NAB61. In this study, 100 dense-core plaques per case were randomly sampled, as previously described, and their positivity for NAB61 was qualitatively assessed. The densities of dense-core plaques and NAB61-positive plaques obtained were corrected by the cortical thickness to calculate total numbers of plaques within a 1-cm-long full-thickness strip of cortex.

Spatial Relationships of Dense-Core Plaques, NFTs, Astrocytes, and Microglia

Single sections from the subset of 40 AD cases were also doubly stained with thioflavin-S and GFAP or Iba1 to investigate the spatial relationship between glial responses and dense-core plaques and NFTs along the course of the disease. Optimal fluorescent immunolabeling of activated microglia was achieved with antibody Iba1 (Wako, Osaka, Japan), another marker widely used for activated microglia. Sections were placed on the motorized stage of an upright BX51 Olympus microscope equipped with CAST stereology software. One hundred GFAP-positive astrocytes or Iba1-positive microglial cells per section were ran-
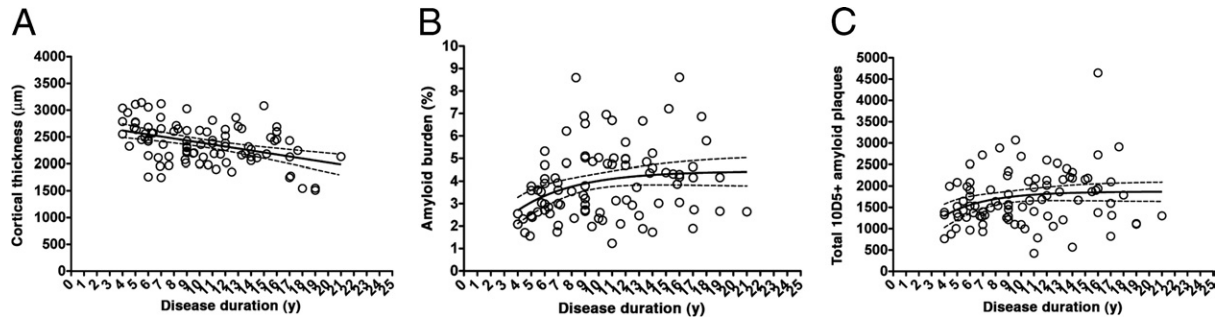
Figure 1. Progression of cortical atrophy and amyloid deposition in the temporal neocortex in AD (see also Table 3). **A:** Cortical thickness decreased linearly, along with the symptomatic disease duration, indicating that this is a reliable proxy of disease severity. Amyloid burden (**B**) and total number of plaques (**C**) increased during the first years of the clinical course of the disease but reached a plateau soon after.

domly selected under the ×20 or the ×40 objective, respectively, and their distance with respect to the closest dense-core plaque or NFT was measured with the appropriate tool of the software. For consistency, only cells with a visible nucleus in the DAPI staining

were considered. Astrocytes and microglial cells were classified into three categories: i) close to plaques, if located ≤50 μm from the edge of a plaque (regardless of the presence of an NFT within this boundary); ii) close to NFTs, if located ≤50 μm from an NFT but far

Table 3.   Summary of the Results from the AD and Control Cohorts

Variable	AD cohort (n = 91) Linear	AD cohort (n = 91) One-phase exponential	AD + CTRL with plaques (n = 101) Linear	AD + CTRL with plaques (n = 101) One-phase exponential	AD + all CTRL (n = 106) Linear	AD + all CTRL (n = 106) One-phase exponential
Cortical thickness (μm)						
ΔAICc		1.804		NA		NA
Probability (%)	71.13	28.87	100	Not converged	100	Not converged
Goodness (R²)	0.1797	0.1831	0.2130	NA	0.2296	NA
Slope ≠ 0? (P)	<0.0001	NA	<0.0001	NA	<0.0001	NA
Spearman's r	−0.3977	NA	−0.4523	NA	−0.4649	NA
Spearman's P	<0.0001	NA	<0.0001	NA	<0.0001	NA
Amyloid burden (%)						
ΔAICc		4.347		10.83		18.23
Probability (%)	10.22	**89.78**	0.44	**99.56**	0.01	**99.99**
Goodness (R²)	0.0657	**0.1093**	0.2317	**0.3099**	0.3117	**0.4205**
Slope ≠ 0? (P)	0.0142	**NA**	<0.0001	**NA**	<0.0001	**NA**
Total amyloid plaques						
ΔAICc		1.761		11.96		21.72
Probability (%)	29.31	**70.69**	0.25	**99.75**	<0.01	**>99.99**
Goodness (R²)	0.0391	**0.0575**	0.2101	**0.2983**	0.2952	**0.4258**
Slope ≠ 0? (P)	0.0602	**NA**	<0.0001	**NA**	<0.0001	**NA**
Total astrocytes						
ΔAICc		0.7545		3.005		3.953
Probability (%)	59.32	40.68	81.80	18.20	87.83	12.17
Goodness (R²)	0.1951	0.1884	0.2433	0.2204	0.2705	0.2428
Slope ≠ 0? (P)	<0.0001	NA	<0.0001	NA	<0.0001	NA
Spearman's r	0.4070	NA	0.5037	NA	0.5471	NA
Spearman's P	<0.0001	NA	<0.0001	NA	<0.0001	NA
Total microglia						
ΔAICc		5.171		33.18		42.25
Probability (%)	92.99	7.01	>99.99	<0.01	>99.99	<0.01
Goodness (R²)	0.0960	0.0431	0.1728	−0.1489	0.2109	−0.1755
Slope ≠ 0? (P)	0.0028	NA	<0.0001	NA	<0.0001	NA
Spearman's r	0.3545	NA	0.4326	NA	0.4728	NA
Spearman's P	0.0006	NA	<0.0001	NA	<0.0001	NA

   The probability of being correct and the goodness of fit (R²) of both the linear regression and the one-phase exponential association models (or decay, in the case of cortical thickness) are shown for the main neuropathological measures in the AD cohort alone, the AD cohort plus the controls without dementia and with plaques, and the AD cohort plus the entire control cohort. The best-fit model is boldfaced. In the linear regression model, P indicates whether the slope is significantly different from 0. When the linear regression model was the preferred-fit model, the correlation coefficient and the P value from the Spearman's rank correlation test are also shown. For the amyloid burden and the total number of amyloid plaques, the nonlinear model remains the best fit, despite the linear fit yielding a straight line with a slope significantly different from 0 (because of the anchoring effect of controls close to 0). Also, the R² of the one-phase exponential association model is negative for some neuropathological measures, indicating that the best-fit curve fits the data even worse than a horizontal line. *Statistics* in *Materials and Methods* provides further details.
   ΔAICc, magnitude of the difference between both fit models; CTRL, control without dementia; NA, not applicable.

(>50 μm) from dense-core plaques; and iii) far from plaques and NFTs, if the closest plaque and NFT to the glial cell were located >50 μm. Densities of glial cells in each of these categories were obtained as previously described.

APOE *Genotyping*

The *APOE* genotype was determined in all of the study subjects by restriction fragment length polymorphism analysis, as previously described.[8]

Statistics

Statistics were performed, and graphs were obtained with GraphPad Prism software for Mac, version 5.0. The normality of data sets was tested with the D'Agostino-Pearson omnibus test. For correlations of cortical thickness, amyloid load, and total number of astrocytes/microglia with disease duration, two different fit models were examined using the least-squares fitting method: linear regression versus one-phase exponential association (or decay in the case of cortical thickness). The first model assumes a linear increase of the pathological features over time, whereas the second model consists of an initial increase followed by a plateau. Next, these two fit models were compared using the Akaike's Informative Criteria method with no constraints, and the model most likely to have generated the data was selected based on the magnitude of the difference between both fit models, the probabilities of the models being correct (as calculated by the statistical software), and their goodness of fit (R^2). When the straight-line model was preferred, a *P* value indicating whether the slope of the straight line is significantly different from 0 and both the correlation coefficient (*r*) and the *P* value of Spearman's rank correlation test were also reported. Because none of the data sets was normally distributed, cross correlations between these pathological quantitative measures were investigated with the Spearman's rank correlation test. The significance level was set at a two-sided $P < 0.05$ in all statistical analyses.

Results

Disease Duration Is a Reliable Proxy of Disease Severity

We have previously used disease duration (defined from the onset of cognitive symptoms) as a proxy of disease severity to avoid the floor effects of neuropsychological tests in patients with advanced dementia, who are typically not testable. More important, the three major pathological correlates of cognitive decline (ie, NFT burden, neuron loss, and synaptic loss) also correlated with disease duration in our previous quantitative post-mortem studies[2,9,10] on the temporal neocortex. Herein, we measured the cortical thickness of the temporal neocortex specimens from the AD cohort as an index of synaptic, dendritic, and neuronal integrity. We found a significant negative correlation between cortical thickness and symptomatic disease duration, further validating the use of disease duration as a surrogate of disease severity ($r = -0.3977$, $P < 0.0001$) (Figure 1A and Table 3).

Progression of Amyloid Deposition in the Temporal Neocortex

Next, we traced the progression of amyloid deposition and patterns of glial immunostaining throughout the clinical disease course. Amyloid burden, determined as the percentage of cortical surface immunoreactive
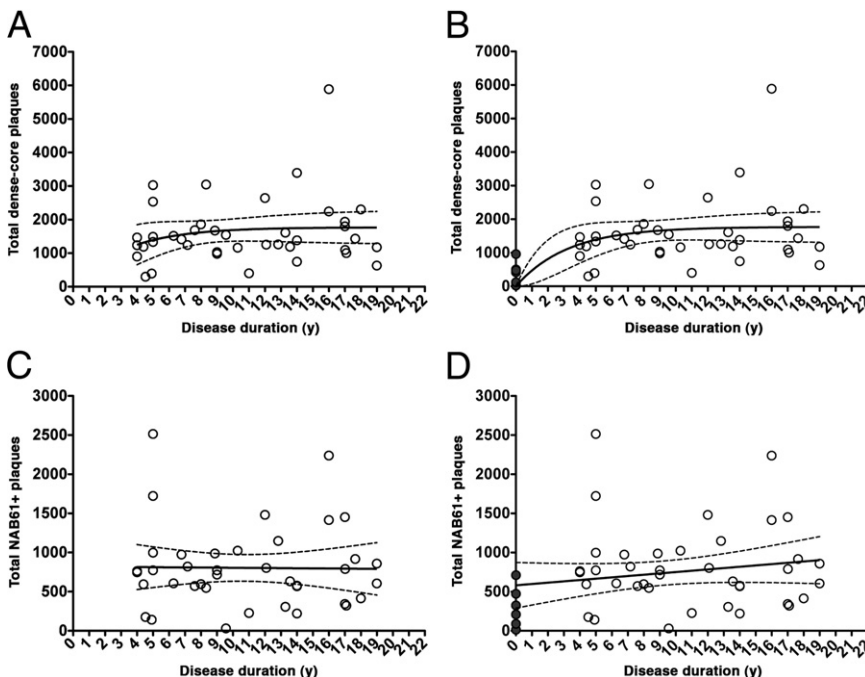
Figure 2. Progression of fibrillar and oligomeric Aβ burden in the temporal neocortex (see also Table 4). **A** and **C:** Only the AD subset is shown (open circles, *n* = 40). **B** and **D:** The highly selected subset of controls without dementia and with dense-core plaques is also included, with a disease duration of 0 years (dark gray circles, *n* = 6). In **A** and **B**, a small increase in the number of dense-core plaques was only detectable during the first years after the onset of cognitive symptoms. In **C** and **D**, the number of NAB61-positive oligomeric Aβ-enriched plaques remained unchanged after symptom onset.

Table 4.   Summary of the Results from the AD and Control Subsets Concerning Fibrillar and Oligomeric Aβ Burden

Variable	AD subset (n = 40)		AD + CTRL with dense-core plaques (n = 46)	
	Linear	One-phase exponential	Linear	One-phase exponential
Total dense-core plaques				
ΔAICc		0.2525		1.833
Probability (%)	46.85	**53.15**	28.57	**71.43**
Goodness (R^2)	0.0248	0.0310	0.1297	0.1637
Slope ≠ 0? (P)	0.3313	NA	0.0140	NA
Total NAB61 + plaques				
ΔAICc		NA		NA
Probability (%)	100	Not converged	100	Not converged
Goodness (R^2)	0.0002		0.0361	
Slope ≠ 0? (P)	0.9313		0.2060	
Spearman's r	−0.0037	NA	0.2267	NA
Spearman's P	0.9816	NA	0.1298	NA

The ΔAICc represents the magnitude of the difference between the two fit models compared. The best-fit model is boldfaced. In the linear model, P indicates whether the slope is significantly different from 0. When the linear regression model was the preferred-fit model, the correlation coefficient and the P value from the Spearman's rank correlation test are also shown. The nonlinear model is the best fit for total dense-core plaques in the AD + CTRL analysis, despite the linear fit yielding a straight line with a slope significantly different from 0 (likely because of the anchoring effect caused by the controls). *Statistics* in *Materials and Methods* provides further details.
    ΔAICc, magnitude of the difference between both fit models; CTRL, control without dementia; NA, not applicable.

for the anti-Aβ antibody 10D5, reached a plateau early after symptomatic onset and remained relatively stable thereafter (Figure 1B and Table 3). An analysis of total number of plaques yielded similar results (Figure 1C and Table 3). Like 10D5-immunoreactive plaques in the original AD cohort, the number of dense-core plaques determined in a subset of 40 AD cases remained relatively stable throughout the disease clinical course after an initial increase (Figure 2, A and B, and Table 4). Last, the amount of NAB61-positive oligomeric Aβ-enriched plaques also remained constant throughout the disease clinical course (Figure 2, C and D, and Table 4).

Progression of Glial Responses and Relationship to AD Pathological Hallmarks

Despite being traditionally regarded as plaque-associated pathological features, the progression of astrocytic and microglial responses differed from that of amyloid plaques both qualitatively and quantitatively. Both reactive glial cell types increased linearly through the entire clinical course of the disease, even when the amyloid burden was no longer increasing [r = 0.4070 (P < 0.0001) and r = 0.3545 (P = 0.0006) for astrocytes and microglia, respectively]. The inclusion in these analyses of either controls without dementia who
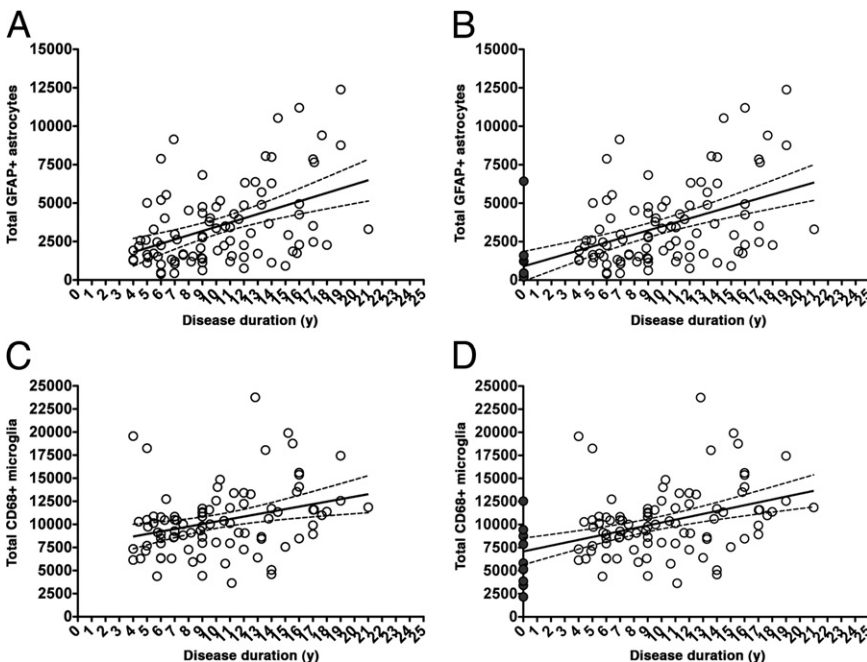
Figure 3. Progression of glial responses in the temporal neocortex (see also Table 3). **A** and **C:** Only the AD cohort is shown (open circles, n = 91). **B** and **D:** The controls without dementia and with plaques are also included, with a clinical disease duration of 0 years (dark gray circles, n = 10). Both astrocytosis (**A** and **B**) and microgliosis (**C** and **D**) significantly increased in a linear fashion, along with disease progression.
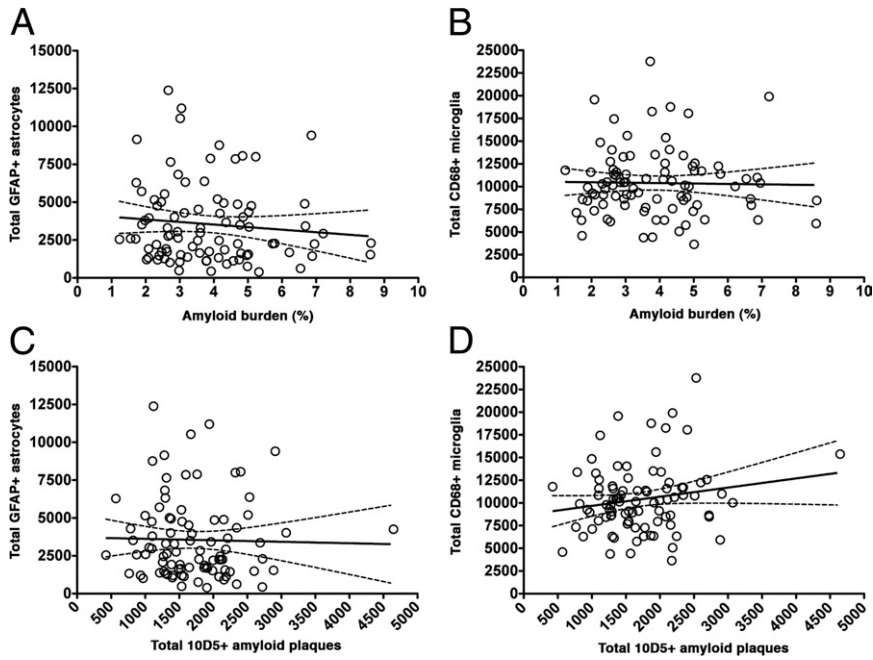
Figure 4. Correlations between glial responses and measures of amyloid deposition in AD. Neither astrocytosis nor microgliosis correlated with amyloid burden (**A** and **B**) or total number of plaques (**C** and **D**).

had plaques ($n = 10$) or all controls ($n = 15$) further accentuated the difference in the patterns of progression of amyloid burden and glial responses (Figure 3, A–D, and Table 3). Indeed, neither astrocytosis nor microgliosis correlated with the amyloid burden [$r = -0.0963$ ($P = 0.3637$) and $r = 0.0062$ ($P = 0.9538$), respectively] or the total number of plaques [$r = -0.0774$ ($P = 0.4660$) and $r = 0.1124$ ($P = 0.2888$), respectively] (Figure 4, A–D).

Unlike the measures of amyloid deposition, both astrocytosis and microgliosis correlated positively with the NFT burden [$r = 0.3419$ ($P = 0.0009$) and $r = 0.4635$ ($P < 0.0001$) respectively]. Also, astrocytosis, but not microgliosis, correlated negatively with cortical thickness [$r = -0.4647$ ($P < 0.0001$) and $r = -0.0199$ ($P = 0.8517$), respectively] (Figure 5, A–D), further arguing that the relationship between reactive glia and amyloid plaques might not be as straightforward as previously thought. Last, astrocytosis and microgliosis tightly covaried together ($r = 0.3377$, $P = 0.0011$) (data not shown).
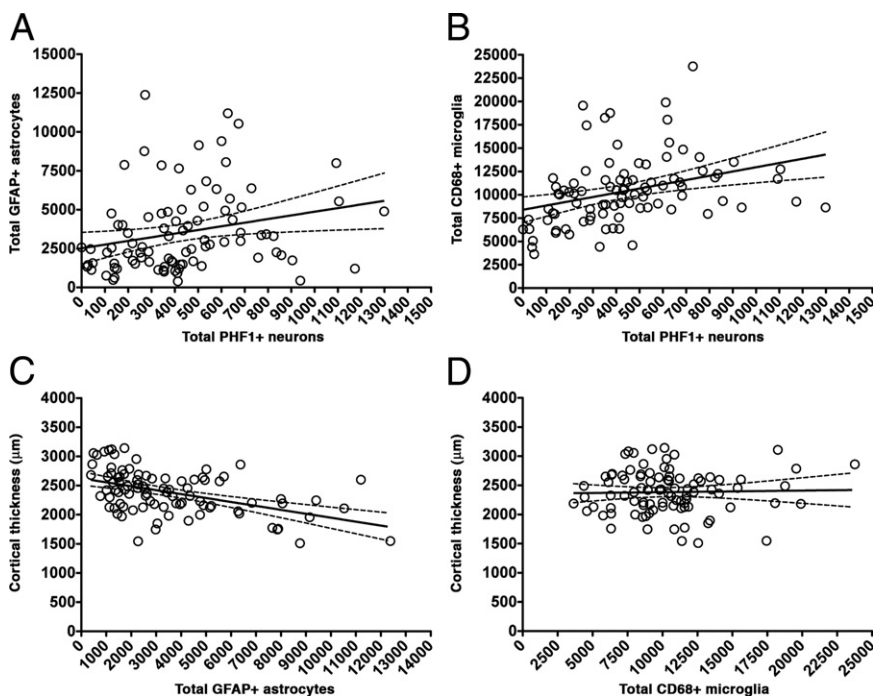
Figure 5. Correlations between glial responses and markers of neurodegeneration in AD. Astrocytosis (**A**) and microgliosis (**B**) correlated positively with the burden of NFTs. Patients with higher astrocytosis tended to have more cortical atrophy (**C**), but no association was observed between the extent of microgliosis and cortical thickness (**D**). PHF, paired helical filament.

The *APOE* genotype did not affect the magnitude of astrocytosis or microgliosis and did not significantly influence the progression of glial responses (see Supplemental Figure S2 at *http://ajp.amjpathol.org*).

Spatial Relationships between Glial Responses and Amyloid Plaques/NFTs

It is well established that activated glial cells are associated with individual senile plaques. In an attempt to better understand the previous results, we examined reactive glia in the microenvironment near plaques and tangles. We compared the progression of plaque-associated reactive glial cells with NFT-associated reactive glial cells and reactive glial cells in the neuropil not close to either a plaque or a tangle in the subset of 40 AD cases using the stereology-based procedures described in *Materials and Methods*. We observed a significant increase in the density of reactive astrocytes and, to a lesser extent, activated microglia in the proximity of dense-core plaques, along with disease progression [$r = 0.6275$ ($P < 0.0001$) and $r = 0.3073$ ($P = 0.0538$), respectively] (Figure 6, A, D, G, and J). We also observed a significant, although weaker, linear increase of astrocytosis and, particularly, microgliosis in the vicinity of NFTs as the disease progresses [$r = 0.3125$ ($P = 0.0497$) and $r = 0.3586$ ($P = 0.0231$), respectively] (Figure 6, B, E, H, and K), suggesting that a causal link underlies the positive correlations between accumulation of reactive glia and NFT burden previously shown. By contrast, the density of astrocytes and microglial cells not associated with either dense-core plaques or NFTs (ie, free in the neuropil) did not significantly correlate with the progression of the disease [$r = 0.1883$ ($P = 0.2447$) and $r = 0.0921$ ($P = 0.5720$), respectively] (Figure 6, C, F, I, and L).

Discussion

Much evidence from previous clinicopathological studies[9–15] has established that the NFT burden and both neuronal and synaptic loss, but not amyloid plaque burden, correlate with the severity of cognitive impairment in AD. However, despite invariably accompanying these classic hallmarks, particularly amyloid plaques, these previous reports have not addressed the progression of glial responses in AD. Although post-mortem studies are inherently cross-sectional and, therefore, any longitudinal extrapolation should be interpreted with caution, quantitative unbiased stereology-based analysis in a large cohort of subjects with a broad range of disease duration enabled us to track the progression of amyloid deposition, NFTs, and glial responses within the AD temporal neocortex and to investigate their relationships. Our findings can be summarized as follows: i) astrocytosis and microgliosis occur both around dense-core plaques and in the proximity of NFTs; ii) astrocytosis and microgliosis increase linearly with disease duration, despite amyloid burden reaching a plateau early in the clinical course of the disease; iii) astrocytosis and microgliosis covary with the burden of NFTs through the

entire clinical course of the disease. Taken together, the number of reactive astrocytes and activated microglial cells tracks better with tangles than with plaques (Figure 7).

Dynamics of Amyloid Deposition in the Temporal Neocortex

Previous post-mortem studies[2,9–13] have established that the amyloid burden remains relatively stable after the first stages of AD dementia and, thus, does not correlate with the severity of dementia. The inclusion of controls without dementia and with AD pathological changes and, particularly, of patients with AD who died shortly after the clinical onset enabled us to trace the natural history of brain β-amyloidosis as a continuum between normal aging and AD. Taken together, our analyses of amyloid deposition support a saturation model in which most amyloid accumulation occurs in the earliest phases, after which there is little or no further accumulation of total amyloid burden in a particular brain region (Figure 7). The pace at which this pattern of deposition and plateau occurs may well play out at different rates or times, depending on the brain region, as suggested by the hierarchical distribution of amyloid deposits previously described.[9,16–18] The type of amyloid plaque did not vary substantially once plaques were deposited. The natural history of fibrillar (thioflavin-S–positive) amyloid deposition paralleled that of total (10D5-immunoreactive) amyloid deposition, also in keeping with our previous results.[2] Interestingly, NAB61-positive oligomeric Aβ was readily observed in association with the dense-core plaques throughout the disease course.

Implications for the Role of Reactive Glial Cells in AD

Because the increase in reactive glial cells cannot be attributed to a progressive buildup of plaque burden, we reasoned that it might be explained by either the same original plaques accumulating more reactive glial cells as the disease advances or the reactive glial cells spreading throughout the neuropil, perhaps contributing to neuronal dysfunction and neurodegeneration as additional neuronal lesions and synaptic loss accrue. Both explanations are supported by our results. On one hand, we observed a progressive increase in the density of reactive astrocytes and activated microglial cells in the proximity (≤ 50 μm) of dense-core plaques, indicating that Aβ plaques are permanently recruiting and activating glial cells. On the other hand, both astrocytosis and microgliosis covaried with the number of NFTs and increased in their proximity, and astrocytosis also correlated negatively with cortical thickness, suggesting a partial emancipation of glial cells from amyloid plaques. Whether the increasing number of reactive glial cells is responding to the ongoing neurodegenerative process (and, thus, a surrogate marker of neurodegeneration) or actively contributes to neurodegeneration cannot be determined by cross-sectional human neuropathological studies. However, along this line, astrocytosis was the best correlate of neuron loss and cognitive deficits in an Aβ precursor
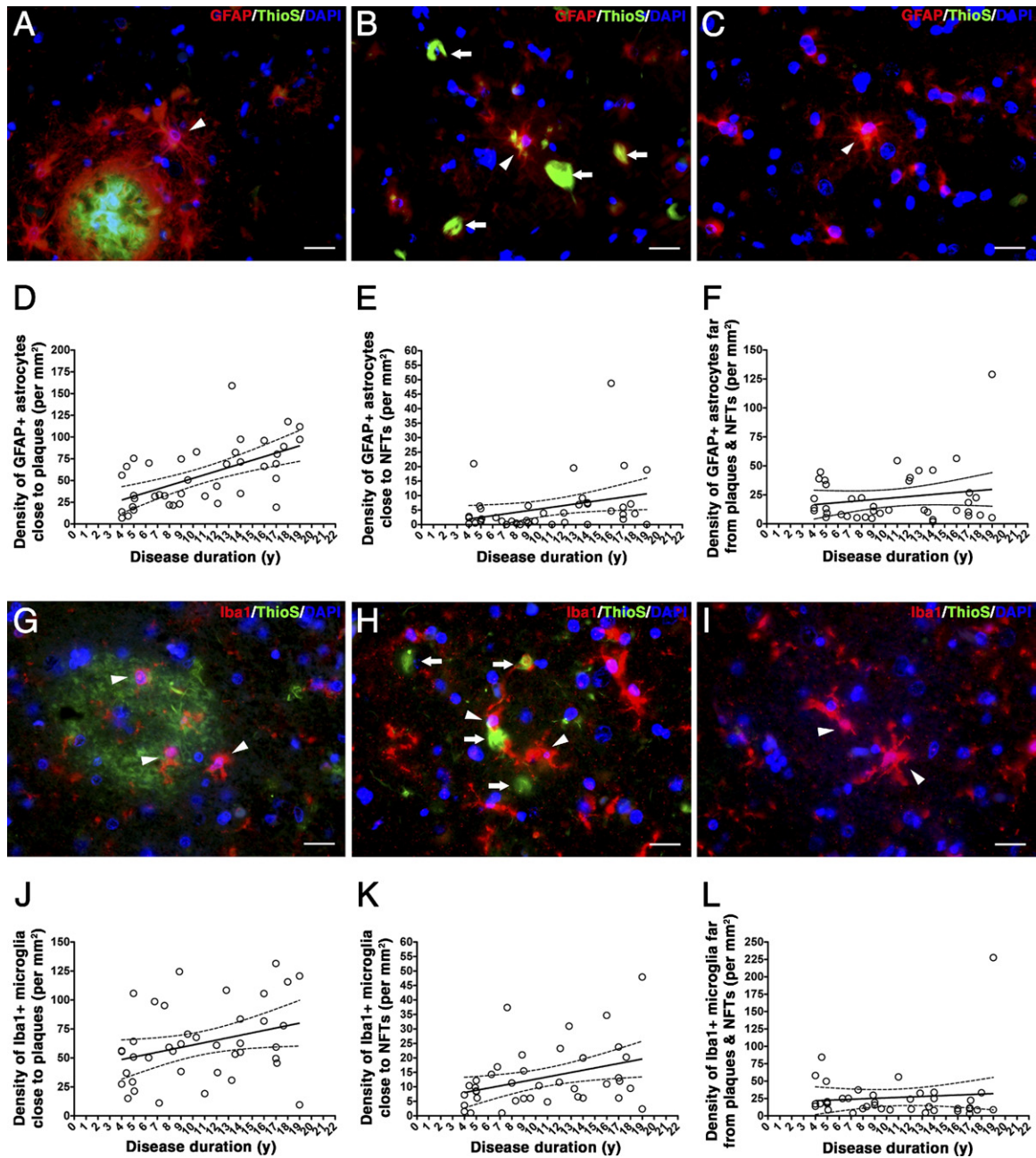
Figure 6. Spatial relationship of glial responses and dense-core plaques and NFTs. **A–C:** Photomicrographs of triple staining for GFAP (red), thioflavin-S (ThioS; green), and DAPI (blue) in an AD case. GFAP-positive reactive astrocytes (**arrowhead**) cluster in the vicinity (≤50 μm) of dense-core plaques (**A**), but they can also be seen in close association to NFTs (**B**, **arrows**) and free in the neuropil (**C**). Scale bar = 20 μm. The density of reactive astrocytes increased linearly in the proximity of dense-core plaques (**D**) and close to NFTs (**E**); by contrast, reactive astrocytes did not increase far (>50 μm) from dense-core plaques and NFTs (**F**). **G–I:** Photomicrographs of triple staining for Iba1 (red), ThioS (green), and DAPI (blue) in an AD case. Iba1-positive activated microglial cells (**arrowheads**) cluster in the vicinity (≤50 μm) of dense-core plaques (**G**), but they can also be found near NFTs (**H**, **arrows**) and free in the neuropil (**I**). Scale bar = 20 μm. Microgliosis increased linearly close to both plaques (**J**) and NFTs (**K**), but no significant increase in the number of activated microglial cells was observed far (>50 μm) from dense-core plaques and NFTs (**L**).

protein/τ double-transgenic mouse model that closely recapitulates the pathological features of human AD.[19] In addition, recent experimental studies with *in vitro* and mouse models of AD have linked both astrocytes and microglia to neurodegeneration[20–25] and have shown that activated microglia can lead to τ hyperphosphorylation and aggregation.[26,27]

The idea of reactive glia as a hostile environment for neurons in the context of neurodegeneration has been recently proposed by elegant studies[28,29] on amyotrophic lateral sclerosis and tauopathy mouse models. If this idea proves to apply to AD, an increasing number of reactive glial cells around dense-core plaques might well contribute to their local toxicity by releasing soluble biologically active toxic molecules, such as pro-inflammatory cytokines and reactive oxygen species. These toxic biomolecules, together with soluble Aβ oligomers existing around the plaques, might account for the plaque-
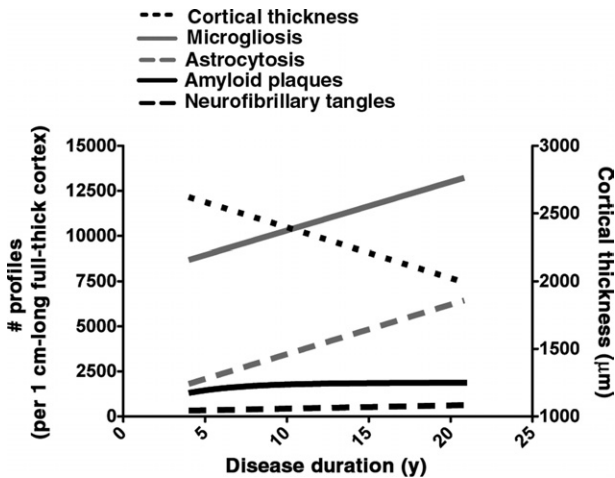
Figure 7. A model of the progression of AD-related pathological features in the temporal neocortex based on the present results. The regression lines for each of the pathological measures were plotted within a single graph. For clarity purposes, the regression line for cortical thickness was linked to the y axis with a different scale (**right**). Amyloid deposition reaches a plateau early after the onset of cognitive symptoms, whereas reactive astrocytes, activated microglial cells, and NFTs keep accumulating as the cortical mantle atrophies through the disease course. Remarkably, the slopes indicate that, within a reference area of 1-cm-long full-thickness temporal neocortex, activated microglia and reactive astrocytes accumulate at a strikingly similar average rate of 270 and 275 cells per year, respectively, which is >10-fold higher than the rate of neurofibrillary degeneration (average, 18 tangles per year). Last, cortical thickness decreased at an average rate of 37 μm/year.

associated neurodegenerative changes, including neuritic dystrophies, an increased neurite curvature ratio, and synaptic and neuron loss, which might be slowly progressive.

Diagnostic and Therapeutic Implications

Follow-up PET studies using the fibrillar amyloid-specific radiotracer Pittsburgh compound B (PiB) have yielded conflicting results regarding the progression of amyloid deposition *in vivo* in patients with AD-type dementia, with some studies[30,31] reporting little or no increase in PiB uptake over time and other studies[32,33] describing a significant increase in patients with dementia. Technical issues inherent to PET, such as test-retest reliability or a dynamic range of detection, might account for these divergent findings to some extent. Our post-mortem analyses argue against a marked increase in PiB uptake in a region with established amyloid deposition (eg, the temporal neocortex) once the dementia syndrome is overt. However, PiB might be useful to track the spreading of amyloid deposition to additional cortical areas *in vivo* in elderly controls without dementia, patients with mild cognitive impairment, and perhaps patients with mild dementia. It is also possible that regions of interest with later amyloid deposition, such as the occipital cortex, might still show increasing PiB uptake in patients with established dementia.[30] Longer serial PET studies,[34] combined with serial cognitive assessments in larger samples of elderly controls and patients with mild cognitive impairment and AD, will determine whether PiB PET is useful as a surrogate biomarker of progression at each stage of the disease. The current post-mortem quantitative analysis

suggests that imaging some sort of glial marker might also be a useful approach to track the progression of AD *in vivo*. A positive glial PET might also add diagnostic and prognostic specificity to a positive amyloid PET study at the preclinical and mild cognitive impairment phases of the disease. Our results predict that the pattern of glial radiotracer uptake would closely match those of PiB uptake and cortical atrophy. However, the first PET studies using [11C]-(R)-PK11195, a radiotracer for the peripheral benzodiazepine receptor expressed by activated microglia, have reported contradictory results: although the original study[35] described an abnormal uptake in vulnerable cortical regions of patients with mild AD but not in controls without dementia, more recent studies[36–38] have reported a great overlap between both groups and no correlation between [11C]-(R)-PK11195 uptake and severity of cognitive decline. Novel radioligands targeting the same receptor in microglia have recently proven to track considerably better with τ-induced neurodegeneration in mice overexpressing mutant human τ than with amyloid burden in animals modeling Aβ plaque deposition.[39]

If glial responses become partially independent from amyloid plaques and their contribution to neurodegeneration is relevant, then removal of amyloid plaques with anti-Aβ-directed therapies, such as passive or active immunization, might not be sufficient to block this neurotoxicity. In this scenario, the transient microglial response triggered by anti-Aβ immunization might have deleterious effects on the neuropil, even though there is an overall decrease in gliosis on clearance of amyloid plaques.[40,41] Glia-mediated inflammation has already been considered as a therapeutic target. NSAIDs became promising agents after the first large epidemiological studies[42,43] revealed that a long-term treatment substantially reduced the risk of AD. Preclinical research[44] has demonstrated that NSAIDs can decrease Aβ_{42} levels by modulating the activity of the γ-secretase complex, independently from their inhibitory effect on the pro-inflammatory cyclooxygenase and peroxisome proliferator-activated receptor-γ pathways. However, the clinical trials[44] with NSAIDs completed thus far have failed to delay the progression of cognitive decline in AD or the conversion from mild cognitive impairment to AD, and recent epidemiological studies have suggested that NSAIDs might have no effect on the risk of AD[45] or might even increase it.[46] Moreover, two neuropathological studies[45,47] found an increased burden of AD pathological features, particularly amyloid plaques, in NSAID users compared with nonusers. Other molecular targets involved in the first steps of glial activation, rather than in the production of singular pro-inflammatory cytokines, remain to be explored. Recently, the activation phenotype of both astrocytes and microglial cells was reported to be largely mediated through the calcineurin–nuclear factor of activated T cells pathway.[48,49] Fibrillar and particularly oligomeric Aβ can aberrantly activate this molecular signaling pathway in glial cells[48,50] and neurons, causing the morphological triad of dystrophic neurites, dendritic simplification, and loss of dendritic spines, subsequently leading to cognitive impairment.[51–53] More important, Food and Drug Administration–approved and available calcineurin inhibitors,

such as cyclosporine and FK-506 (tacrolimus), can revert these Aβ-related pathological changes both *in vitro* and *in vivo* and ameliorate both the neuropathological features and the memory deficits of AD mouse models.[26,51–53]

In summary, our findings indicate a major role of gliosis in the pathophysiological features of both amyloid plaques and NFTs, suggesting that glial cells might be proactive players linking Aβ with downstream neurodegenerative events beyond their role in the initial steps of the amyloid cascade. The implications of these results for the development of imaging biomarkers and disease-modifying drugs encourage further research.

Acknowledgments

References

1. Itagaki S, McGeer PL, Akiyama H, Zhu S, Selkoe D: Relationship of microglia and astrocytes to amyloid deposits of Alzheimer disease. J Neuroimmunol 1989, 24:173–182
2. Ingelsson M, Fukumoto H, Newell KL, Growdon JH, Hedley-Whyte ET, Frosch MP, Albert MS, Hyman BT, Irizarry MC: Early Aβ accumulation and progressive synaptic loss, gliosis, and tangle formation in AD brain. Neurology 2004, 62:925–931
3. McKhann G, Drachman D, Folstein M, Katzman R, Price D, Stadlan EM: Clinical diagnosis of Alzheimer's disease: report of the NINCDS-ADRDA Work Group under the auspices of the Department of Health and Human Services Task Force on Alzheimer's Disease. Neurology 1984, 34:939–944
4. The National Institute on Aging, and Reagan Institute Working Group on Diagnostic Criteria for the Neuropathological Assessment of Alzheimer's Disease. Consensus recommendations for the postmortem diagnosis of Alzheimer's disease. Neurobiol Aging 1997, 18(Suppl):S1–S2
5. Freeman SH, Kandel R, Cruz L, Rozkalne A, Newell K, Frosch MP, Hedley-Whyte ET, Locascio JJ, Lipsitz LA, Hyman BT: Preservation of neuronal number despite age-related cortical brain atrophy in elderly subjects without Alzheimer disease. J Neuropathol Exp Neurol 2008, 67:1205–1212
6. Hyman BT, Gómez-Isla T, Irizarry MC: Stereology: a practical primer for neuropathology. J Neuropathol Exp Neurol 1998, 57:305–310
7. Lee EB, Leng LZ, Zhang B, Kwong L, Trojanowski JQ, Abel T, Lee VM: Targeting amyloid-β peptide (Aβ) oligomers by passive immunization with a conformation-selective monoclonal antibody improves learning and memory in Aβ precursor protein (APP) transgenic mice. J Biol Chem 2006, 281:4292–4299
8. Ingelsson M, Shin Y, Irizarry MC, Hyman BT: Genotyping of apolipoprotein E: comparative evaluation of different protocols. Curr Protoc Hum Gen 2003, 38:1–13
9. Arriagada PV, Growdon JH, Hedley-Whyte ET, Hyman BT: Neurofibrillary tangles but not senile plaques parallel duration and severity of Alzheimer's disease. Neurology 1992, 42:631–639
10. Gómez-Isla T, Hollister R, West H, Mui S, Growdon JH, Petersen RC, Parisi JE, Hyman BT: Neuronal loss correlates with but exceeds neurofibrillary tangles in Alzheimer's disease. Ann Neurol 1997, 41:17–24
11. Hyman BT, Marzloff K, Arriagada PV: The lack of accumulation of senile plaques or amyloid burden in Alzheimer's disease suggests a dynamic balance between amyloid deposition and resolution. J Neuropathol Exp Neurol 1993, 52:594–600
12. Bierer LM, Hof PR, Purohit DP, Carlin L, Schmeidler J, Davis KL, Perl DP: Neocortical neurofibrillary tangles correlate with dementia severity in Alzheimer's disease. Arch Neurol 1995, 52:81–88
13. Giannakopoulos P, Herrmann FR, Bussière T, Bouras C, Kövari E, Perl DP, Morrison JH, Gold G, Hof PR: Tangle and neuron numbers, but not amyloid load, predict cognitive status in Alzheimer's disease. Neurology 2003, 60:1495–1500
14. DeKosky ST, Scheff SW: Synapse loss in frontal cortex biopsies in Alzheimer's disease: correlation with cognitive severity. Ann Neurol 1990, 27:457–464
15. Terry RD, Masliah E, Salmon DP, Butters N, DeTeresa R, Hill R, Hansen LA, Katzman R: Physical basis of cognitive alterations in Alzheimer's disease: synapse loss is the major correlate of cognitive impairment. Ann Neurol 1991, 30:572–580
16. Braak H, Braak E: Neuropathological stageing of Alzheimer-related changes. Acta Neuropathol 1991, 82:239–259
17. Arriagada PV, Marzloff K, Hyman BT: Distribution of Alzheimer-type pathologic changes in nondemented elderly individuals matches the pattern in Alzheimer's disease. Neurology 1992, 42:1681–1688
18. Thal DR, Rüb U, Orantes M, Braak H: Phases of Aβ-deposition in the human brain and its relevance for the development of AD. Neurology 2001, 58:1791–1800
19. DaRoucha-Souto B, Scotton TC, Coma M, Serrano-Pozo A, Hashimoto T, Serenó L, Rodríguez M, Sánchez MB, Hyman BT, Gómez-Isla T: Brain oligomeric Aβ but not total amyloid plaque burden correlates with neuronal loss and astrocyte inflammatory response in APP/tau-transgenic mice. J Neuropathol Exp Neurol 2011, 70:360–376
20. Fonseca MI, Zhou J, Botto M, Tenner AJ: Absence of C1q leads to less neuropathology in transgenic mouse models of Alzheimer's disease. J Neurosci 2004, 24:6457–6465
21. Ortinski PI, Dong J, Mungenast A, Yue C, Takano H, Watson DJ, Haydon PG, Coulter DA: Selective induction of astrocytic gliosis generates deficits in neuronal inhibition. Nat Neurosci 2010, 13:584–591
22. Allaman I, Gavillet M, Bélanger M, Laroche T, Viertl D, Lashuel HA, Magistretti PJ: Amyloid-β aggregates cause alterations of astrocytic metabolic phenotype: impact on neuronal viability. J Neurosci 2010, 30:3326–3338
23. Jana A, Pahan K: Fibrillar amyloid-β-activated human astroglia kill primary human neurons via neutral sphingomyelinase: implications for Alzheimer's disease. J Neurosci 2010, 30:12676–12689
24. Giulian D, Haverkamp LJ, Yu JH, Karshin W, Tom D, Li J, Kirkpatrick J, Kuo LM, Roher AE: Specific domains of β-amyloid from Alzheimer plaque elicit neuron killing in human microglia. J Neurosci 1996, 16:6021–6037
25. Fuhrmann M, Bittner T, Jung CK, Burgold S, Page RM, Mitteregger G, Haass C, LaFerla FM, Kretzschmar H, Herms J: Microglial Cx3cr1 knockout prevents neuron loss in a mouse model of Alzheimer's disease. Nat Neurosci 2010, 13:411–413
26. Yoshiyama Y, Higuchi M, Zhang B, Huang SM, Iwata N, Saido TC, Maeda J, Suhara T, Trojanowski JQ, Lee VM: Synapse loss and microglial activation precede tangles in a P301S tauopathy mouse model. Neuron 2007, 53:337–351
27. Bhaskar K, Konerth M, Kokiko-Cochran ON, Cardona A, Ransohoff RM, Lamb BT: Regulation of tau pathology by the microglial fractalkine receptor. Neuron 2010, 68:19–31
28. Yamanaka K, Chun SJ, Boillee S, Fujimori-Tonou N, Yamashita H, Gutmann DH, Takahashi R, Misawa H, Cleveland DW: Astrocytes as determinants of disease progression in inherited amyotrophic lateral sclerosis. Nat Neurosci 2008, 11:251–253
29. Hampton DW, Webber DJ, Bilican B, Goedert M, Spillantini MG, Chandran S: Cell-mediated neuroprotection in a mouse model of human tauopathy. J Neurosci 2010, 30:9973–9983
30. Engler H, Forsberg A, Almkvist O, Blomquist G, Larsson E, Savitcheva I, Wall A, Ringheim A, Längström B, Nordberg A: Two-year follow-up of amyloid deposition in patients with Alzheimer's disease. Brain 2006, 129:2856–2866
31. Scheinin NM, Aalto S, Koikkalainen J, Lötjönen J, Karrasch M, Kemppainen N, Vlitanen M, Någren K, Helin S, Scheinin M, Rinne JO: Follow-up of [11C]PIB uptake and brain volume in patients with Alzheimer disease and controls. Neurology 2009, 73:1186–1192
32. Jack CR Jr, Lowe VJ, Weigand SD, Wiste HJ, Senjem ML, Knopman DS, Shiung MM, Gunter JL, Boeve BF, Kemp BJ, Weiner M, Petersen

RC: Serial PIB and MRI in normal, mild cognitive impairment and Alzheimer's disease: implications for sequence of pathological events in Alzheimer's disease. Brain 2009, 132:1355–1365

33. Rinne JO, Brooks DJ, Rossor MN, Fox NC, Bullock R, Klunk WE, Mathis CA, Blennow K, Barakos J, Okello AA, Rodriguez Martinez de Liano S, Liu E, Koller M, Gregg KM, Schenk D, Black R, Grundman M: 11C-PiB PET assessment of change in fibrillar amyloid-beta load in patients with Alzheimer's disease treated with bapineuzumab: a phase 2, double-blind, placebo-controlled, ascending-dose study. Lancet Neurol 2010, 9:363–372

34. Jack CR Jr, Knopman DS, Jagust WJ, Shaw LM, Aisen PS, Weiner MW, Petersen RC, Trojanowski JQ: Hypothetical model of dynamic biomarkers of the Alzheimer's pathological cascade. Lancet Neurol 2010, 9:119–128

35. Cagnin A, Brooks DJ, Kennedy AM, Gunn RN, Myers R, Turkheimer FE, Jones T, Banati RB: In-vivo measurement of activated microglia in dementia. Lancet 2001, 358:461–467

36. Edison P, Archer HA, Gerhard A, Hinz R, Pavese N, Turkheimer FE, Hammers A, Tai YF, Fox N, Kennedy A, Rossor M, Brooks DJ: Microglia, amyloid, and cognition in Alzheimer's disease: an [11C](R)PK111595-PET and [11C]PIB-PET study. Neurobiol Dis 2008, 32:412–419

37. Wiley CA, Lopresti BJ, Venneti S, Price J, Klunk WE, DeKosky ST, Mathis CA: Carbon 11-labeled Pittsburgh Compound B and carbon 11-labeled (R)-PK11195 positron emission tomographic imaging in Alzheimer disease. Arch Neurol 2009, 66:60–67

38. Okello A, Edison P, Archer HA, Turkheimer FE, Kennedy J, Bullock R, Walker Z, Kennedy A, Fox N, Rossor M, Brooks DJ: Microglial activation and amyloid deposition in mild cognitive impairment: a PET study. Neurology 2009, 72:56–62

39. Maeda J, Zhang MR, Okauchi T, Ji B, Ono M, Hattori S, Kumata K, Iwata N, Saido TC, Trojanowski JQ, Lee VM-Y, Staufenbiel M, Tomiyama T, Mori H, Fukumura T, Suhara T, Higuchi M: In vivo positron emission tomographic imaging of glial responses to amyloid-β and tau pathologies in mouse models of Alzheimer's disease and related disorders. J Neurosci 2011, 31:4720–4730

40. Wilcock DM, DiCarlo G, Henderson D, Jackson J, Clarke K, Ugen KE, Gordon MN, Morgan D: Intracranially administered anti-Aβ antibodies reduce β-amyloid deposition by mechanisms both independent of and associated with microglial activation. J Neurosci 2003, 23:3745–3751

41. Koenigsknecht-Talboo J, Meyer-Luehmann M, Parsadanian M, García-Alloza M, Finn MB, Hyman BT, Bacskai BJ, Holtzman DM: Rapid microglial response around amyloid pathology after systemic anti-Aβ antibody administration in PDAPP mice. J Neurosci 2008, 28:14156–14164

42. Etminan M, Gill S, Samii A: Effect of non-steroidal anti-inflammatory drugs on risk of Alzheimer's disease: a systematic review and meta-analysis of observational studies. BMJ 2003, 327:128–132

43. Hayden KM, Zandi PP, Kachaturian AS, Szekely CA, Fotuhi M, Norton MC, Tschanz JT, Pieper CF, Corcoran C, Lyketsos CG, Breitner JC, Welsh-Bohmer KA; Cache County Investigators. Does NSAID use modify cognitive trajectories in the elderly? the Cache County Study. Neurology 2007, 69:275–282

44. Sastre M, Gentleman SM: NSAIDs: how they work and their prospects as therapeutics in Alzheimer's disease. Front Aging Neurosci 2010, 2:1–6

45. Arvanitakis Z, Grodstein F, Bienias JL, Schneider JA, Wilson RS, Kelly JF, Evans DA, Bennett DA: Relation of NSAIDs to incident AD, change in cognitive function, and AD pathology. Neurology 2008, 70:2219–2225

46. Breitner JC, Haneuse SJ, Walker R, Dublin S, Crane PK, Gray SL, Larson EB: Risk of dementia and AD with prior exposure to NSAIDs in an elderly community-based cohort. Neurology 2009, 72:1899–1905

47. Sonnen JA, Larson EB, Walker RL, Haneuse S, Crane PK, Gray SL, Breitner JC, Montine TJ: Nonsteroidal anti-inflammatory drugs are associated with increased neuritic plaques. Neurology 2010, 75: 1203–1210

48. Norris CM, Kadish I, Blalock EM, Chen KC, Thibault V, Porter NM, Landfield PW, Kraner SD: Calcineurin triggers reactive/inflammatory processes in astrocytes and is upregulated in aging and Alzheimer's models. J Neurosci 2005, 25:4649–4658

49. Nagamoto-Combs K, Combs CK: Microgial phenotype is regulated by activity of the transcription factor NFAT (nuclear factor of activated T cells). J Neurosci 2010, 30:9641–9646

50. Abdul HM, Sama MA, Furman JL, Mathis DM, Beckett TL, Weidner AM, Patel ES, Baig I, Murphy MP, LeVine H 3rd, Kraner SD, Norris CM: Cognitive decline in Alzheimer's disease is associated with selective changes in calcineurin/NFAT signaling. J Neurosci 2009, 29:12957–12969

51. Wu HY, Hudry E, Hashimoto T, Kuchibhotla K, Rozkalne A, Fan Z, Spires-Jones T, Xie H, Arbel-Ornath M, Grosskreutz CL, Bacskai BJ, Hyman BT: Amyloid-β induces the morphological neurodegenerative triad of spine loss, dendritic simplification, and neuritic dystrophies through calcineurin activation. J Neurosci 2010, 30:2636–2649

52. Dineley KT, Kayed R, Neugebauer V, Fu Y, Zhang W, Reese LC, Taglialatela G: Amyloid-beta oligomers impair fear conditioned memory in a calcineurin-dependent fashion in mice. J Neurosci Res 2010, 88:2923–2932

53. Rozkalne A, Hyman BT, Spires-Jones TL: Calcineurin inhibition with FK506 ameliorates dendritic spine density deficits in plaque-bearing Alzheimer model mice. Neurobiol Dis 2011, 41:650–654

Supplementary Table 1. The subsets of AD and control cases are representative of the corresponding entire cohorts in their demographic and neuropathological characteristics

	CTRL subset (n=6)	Remaining CTRL cases (n=9)	*P* value	AD subset (n=40)	Remaining AD cases (n=51)	*P* value
Age at death, *y* [*]	83.7 (14.0)	77.3 (13.0)	n.s.	77.6 (8.6)	80.2 (6.9)	n.s.
Gender, *n female (%)* †	4 (66.6)	6 (66.6)	n.s.	26 (65.0)	32 (62.7)	n.s.
Disease duration, *y* [*]	NA	NA	NA	9.9 (5.4-15.5)	9.5 (7.0-12.0)	n.s.
APOE **genotype: †**						
APOEε4 carriers, n (%)	2 (33.3)	2 (22.2)	n.s.	21 (52.5)	38 (74.5)	**0.0458**
APOEε4 alleles, n (%)	2 (16.6)	2 (11.1)	n.s.	25 (31.2)	47 (46.1)	**0.0480**
Postmortem interval, h [*]	21.0 (11.1)	23.3 (14.6)	n.s.	14.1 (6.2)	13.7 (10.8)	n.s.
Cortical thickness, μm ‡ '	2651 (97.7)	2730 (122.1)	n.s.	2351 (63.2)	2411 (49.2)	n.s.
Amyloid burden, % [*]	1.2 (0.3)	0.1 (0.1)	**0.0069**	3.8 (0.3)	3.8 (0.2)	n.s.
Total amyloid plaques [*]	566.6 (130.7)	67.5 (57.4)	**0.0099**	1651 (105.0)	1759 (87.7)	n.s.
Total NFTs [*]	21.8 (13.2)	4.7 (2.0)	n.s.	419.2 (43.3)	453.5 (38.4)	n.s.
Total astrocytes [*]	1687 (977.3)	665 (182.7)	n.s.	4092 (439.7)	3128 (346.0)	n.s.
Total microglia [*]	6996 (1349)	5568 (1004)	n.s.	10669 (672.8)	10179 (448.2)	n.s.

Age at death and postmortem interval are presented as Mean (SD), whereas the disease duration is reported as Median (interquartile range) and the neuropathological data are depicted as Mean (SEM). [*] Two-tailed Mann-Whitney test. † Two-tailed Chi-square with Fisher's exact test. ‡ Two-

tailed unpaired Student's *t* test. Statistically significant differences ($p<0.05$) are highlighted in bold fonts. NA = not applicable; n.s. = not significant. The criterion for selecting the subset of control cases (a high number of dense-core plaques) is reflected in the statistically significant difference in amyloid burden and total amyloid plaques respect to the remaining control cases. Compared to the remaining AD cases, the *APOEε4* genotype was less represented in the AD subset, although *APOE* genotype did not influence significantly the progression of glial responses (see Supplementary Figure S2 at http://ajp.amjpathol.org).

Supplemental Figure 1
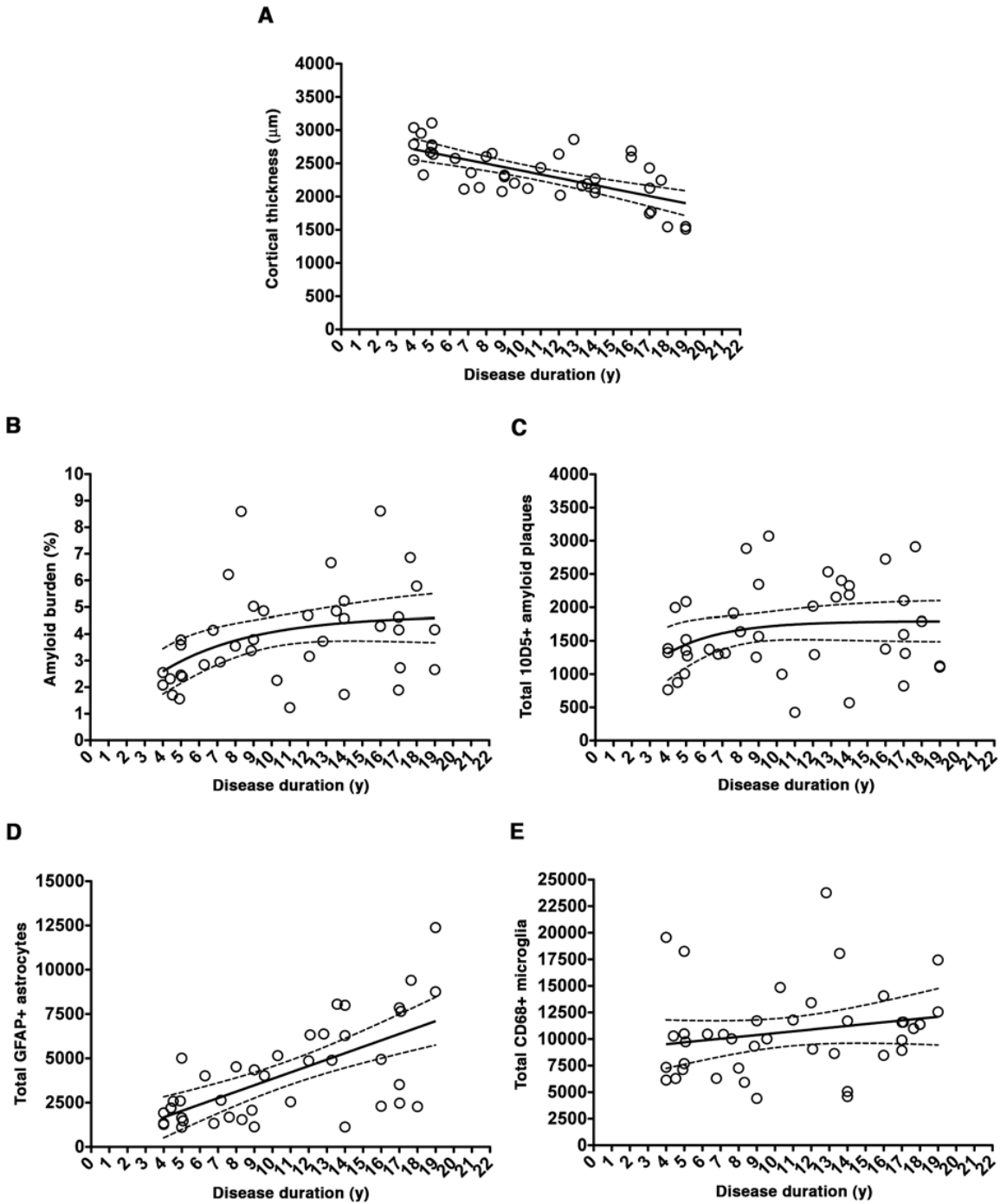
Supplemental Figure 2
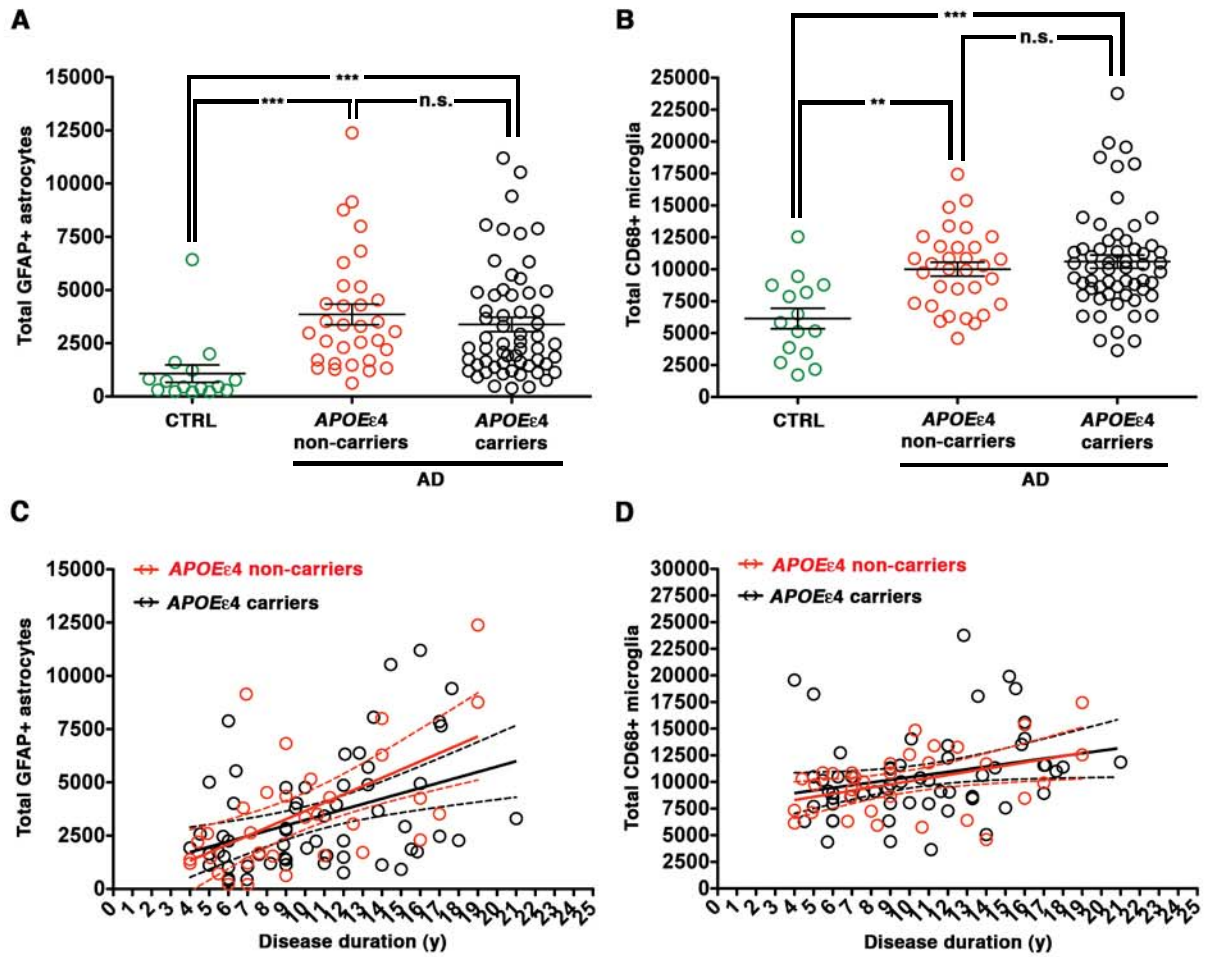
5.3. Original article#2:

Serrano-Pozo A, William CM, Ferrer I, Uro-Coste E, Delisle MB, Maurage CA, Hock C, Nitsch RM, Masliah E, Growdon JH, Frosch MP, Hyman BT. Beneficial effect of human anti-Aβ active immunization on neurite morphology and tau pathology. *Brain* 2010; 133(5): 1312-27.

BRAIN
A JOURNAL OF NEUROLOGY

Beneficial effect of human anti-amyloid-β active immunization on neurite morphology and tau pathology

Alberto Serrano-Pozo,[1,2] Christopher M. William,[1] Isidro Ferrer,[3] Emmanuelle Uro-Coste,[4] Marie-Bernadette Delisle,[4] Claude-Alain Maurage,[5] Christoph Hock,[6] Roger M. Nitsch,[6] Eliezer Masliah,[7] John H. Growdon,[1] Matthew P. Frosch[1,8] and Bradley T. Hyman[1]

1 MassGeneral Institute for Neurodegenerative Disease, Massachusetts General Hospital, Massachusetts Alzheimer Disease Research Center, Harvard Medical School, Building 114, 16th Street, 02129-4404, Charlestown, MA, USA
2 Servicio de Neurología, Instituto de Biomedicina de Sevilla (IBiS), Hospitales Universitarios Virgen del Rocío, Av. Manuel Siurot s/n 41013 Seville, Spain
3 Institut Neuropatologia-Servei Anatomia Patològica, IDIBELL-Hospital Universitari de Bellvitge, Hospitalet de Llobregat, 08907 Barcelona, Spain
4 Service d'Anatomie Pathologique et Histologie-Cytologie, CHU de Toulouse, Faculté de Médecine Rangueil, INSERM U858, 31432 Toulouse, France
5 Université Lille Nord de France, INSERM U837, F-59000 Lille, France
6 Division of Psychiatry Research, University of Zurich, 8008 Zurich, Switzerland
7 Department of Neuroscience and Department of Pathology, University of California-San Diego School of Medicine, La Jolla, 92093-0624 CA, USA
8 C. S. Kubik Laboratory for Neuropathology, Massachusetts General Hospital, 55 Fruit Street, 02114, Boston, MA, USA

Correspondence to: Bradley T. Hyman, MD, PhD,
Building 114,16th Street-2009,
Charlestown,
MA 02129-4404, USA
E-mail: bhyman@partners.org

Anti-amyloid-β immunization leads to amyloid clearance in patients with Alzheimer's disease, but the effect of vaccination on amyloid-β-induced neuronal pathology has not been quantitatively examined. The objectives of this study were to address the effects of anti-amyloid-β active immunization on neurite trajectories and the pathological hallmarks of Alzheimer's disease in the human hippocampus. Hippocampal sections from five patients with Alzheimer's disease enrolled in the AN1792 Phase 2a trial were compared with those from 13 non-immunized Braak-stage and age-matched patients with Alzheimer's disease, and eight age-matched non-demented controls. Analyses included neurite curvature ratio as a quantitative measure of neuritic abnormalities, amyloid and tau loads, and a quantitative characterization of plaque-associated neuritic dystrophy and astrocytosis. Amyloid load and density of dense-core plaques were decreased in the immunized group compared to non-immunized patients ($P < 0.01$ and $P < 0.001$, respectively). The curvature ratio in non-immunized patients with Alzheimer's disease was elevated compared to non-demented controls ($P < 0.0001$). In immunized patients, however, the curvature ratio was normalized when compared to non-immunized patients ($P < 0.0001$), and not different from non-demented controls. In the non-immunized patients, neurites close to dense-core plaques (within 50 μm) were more abnormal than those far from plaques (i.e. beyond 50 μm) ($P < 0.0001$). By contrast, in the immunized group neurites close to and far from the remaining dense-core plaques did not differ, and both were straighter compared to the non-immunized patients ($P < 0.0001$). Compared to non-immunized patients, dense-core plaques remaining after immunization had similar degree of astrocytosis ($P = 0.6060$), more embedded dystrophic neurites ($P < 0.0001$) and were more likely to have mitochondrial accumulation ($P < 0.001$). In addition, there was a significant decrease in the density of paired helical filament-1-positive neurons in the immunized group as compared to the non-immunized ($P < 0.05$), but not in the density of Alz50 or thioflavin-S positive tangles, suggesting a modest effect of

anti-amyloid-β immunization on tangle pathology. Clearance of amyloid plaques upon immunization with AN1792 effectively improves a morphological measure of neurite abnormality in the hippocampus. This improvement is not just attributable to the decrease in plaque load, but also occurs within the halo of the remaining dense-core plaques. However, these remaining plaques still retain some of their toxic potential. Anti-amyloid-β immunization might also ameliorate the hippocampal tau pathology through a decrease in tau phosphorylation. These data agree with preclinical animal studies and further demonstrate that human anti-amyloid-β immunization does not merely clear amyloid from the Alzheimer's disease brain, but reduces some of the neuronal alterations that characterize Alzheimer's disease.

Introduction

The major pathological hallmarks of Alzheimer's disease are neuronal loss, amyloid senile plaques and neurofibrillary tangles within the cerebral cortex (Braak and Braak, 1991). Senile plaques are extracellular deposits of amyloid-β (Aβ) peptide, a byproduct of the metabolism of the amyloid precursor protein after its sequential cleavage by the β- and γ-secretases. Neurofibrillary tangles are intraneuronal somatic aggregates comprised of the microtubule-stabilizing protein tau, which is abnormally hyperphosphorylated. Other pathological findings include synaptic loss in cortical areas, as well as astrogliosis and microgliosis surrounding senile plaques; cerebral amyloid angiopathy (i.e. Aβ deposits in the wall of cortical and leptomeningeal vessels) is a common concomitant pathological process. Clinicopathological studies have shown that neurofibrillary tangles, synaptic loss and neuronal loss correlate with dementia progression and severity better than amyloid deposits (DeKosky and Scheff, 1990; Terry *et al.*, 1991; Gómez-Isla *et al.*, 1996, 1997). However, substantial biochemical and genetic evidence points to Aβ as an essential trigger for the disease (Hardy and Selkoe, 2002). Aβ might directly trigger a cascade of pathogenic events that lead to synaptic and dendritic abnormalities, neurofibrillary tangles and neuronal death, but the course down these pathways to disease may remain dependent on Aβ or might become independent of Aβ once initiated. The latter proposal raises the possibility that therapies directed at reduction in brain levels of Aβ might not be capable of preventing the progression of dementia.

Immunotherapy against Aβ, either through active immunization with Aβ aggregates or by passive transfer of anti-Aβ antibodies, has proven to be effective in the prevention of Aβ deposition and the clearance of already existing Aβ plaques in a number of transgenic mouse models of Alzheimer's disease (Schenk *et al.*, 1999; Bard *et al.*, 2000; Bacskai *et al.*, 2001, 2002; DeMattos *et al.*, 2001; Lemere *et al.*, 2003; Wilcock *et al.*, 2004). Moreover, both active and passive immunization approaches prevented, improved or even reversed the memory deficits described in those mouse models (Janus *et al.*, 2000; Morgan *et al.*, 2000; Dodart *et al.*, 2002; Kotilinek *et al.*, 2002). Also, an amelioration of tau pathology has been reported after anti-Aβ immunization in several mouse models with both amyloid plaques and neuronal tau aggregates (Oddo *et al.*, 2004, 2008; Wilcock *et al.*, 2009).

The first immunotherapy clinical trial in patients with Alzheimer's disease was an active immunization trial with a pre-aggregated preparation of synthetic human Aβ42 (AN1792). The phase 2a of this trial was halted due to the occurrence of subacute meningoencephalitis among some patients in the treatment group, so that patients only received one to three injections out of the four doses initially planned (Orgogozo *et al.*, 2003). Despite the interruption of the trial, a modest but significant positive effect of immunization on some cognitive and functional outcome measures has been documented (Hock *et al.*, 2003; Gilman *et al.*, 2005). Recently, two long-term follow-up studies have yielded conflicting results, with no difference in the rates of survival to death and progression to severe dementia in subjects from an earlier phase 1 trial (Holmes *et al.*, 2008) and a reduced rate of functional decline in a subset of subjects from the phase 2a trial (Vellas *et al.*, 2009).

To date, the effects of AN1792 immunization on Alzheimer's disease neuropathology have been reported in five single case reports (Nicoll *et al.*, 2003; Ferrer *et al.*, 2004; Masliah *et al.*, 2005; Bombois *et al.*, 2007; Uro-Coste *et al.*, 2010) and one case series (Boche *et al.*, 2008; Holmes *et al.*, 2008). These neuropathological findings can be summarized as (i) significant reduction in amyloid load, with relative abundance of the collapsed or 'moth-eaten' morphology among the remaining plaques; (ii) increased extension and severity of cerebral amyloid angiopathy and increased frequency of cerebral amyloid angiopathy-related microhaemorrhages; (iii) decreased density of dystrophic neurite clusters; (iv) reduced density of reactive astrocytes clusters; (v) decreased density of activated microglia clusters, with some examples of microglial cells engulfing amyloid-β fibrils; and (vi) advanced neurofibrillary pathology (i.e. Braak stages V–VI). Interestingly, the amount of remaining amyloid load seems to correlate inversely with the anti-Aβ antibody titres in serum (Holmes *et al.*, 2008).

While there is evidence of the beneficial effects of active and passive anti-amyloid immunization on neurite morphology and synapses in Alzheimer's disease mouse models (Lombardo *et al.*, 2003; Buttini *et al.*, 2005; Brendza *et al.*, 2005; Spires-Jones *et al.*, 2009), little is known about the effects of AN1792 on neurites and neurons in the human Alzheimer's disease brain. Although there was a description of the appearance of collapsed 'moth-eaten' plaques, the characteristics of the amyloid plaques remaining after immunization have not been well described.

Additionally, the relationship between Aβ clearance and neurofibrillary tangles, tau phosphorylation and aggregation status has not been fully documented in AN1792-treated patients.

The present study was aimed at (i) addressing the effect of AN1792 on Aβ-related neurite abnormalities; (ii) characterizing the properties of amyloid plaques remaining after immunization; and (iii) characterizing the phosphorylation and aggregation status of neuronal tau after AN1792 immunization.

Materials and methods

Brain specimens

Formalin-fixed paraffin-embedded sections from the hippocampus of five patients who participated in the phase 2a active immunization trial with AN1792 (Elan-Wyeth Pharmaceuticals, Inc.) were compared with the hippocampal sections from non-demented controls ($n = 8$) and patients with Alzheimer's disease ($n = 13$) from the Massachusetts Alzheimer Disease Research Center Brain Bank. All the study subjects or their next-of-kin gave written informed consent for the brain donation at their respective institutions and the Massachusetts General Hospital Institutional Review Board approved the study protocol. Four of the immunized patients with Alzheimer's disease have been previously described as single reports (Ferrer *et al.*, 2004; Masliah *et al.*, 2005; Bombois *et al.*, 2007; Uro-Coste *et al.*, 2010). The three groups were matched by age and gender. Immunized patients and non-immunized Alzheimer's disease subjects were also matched by Braak stage (Table 1 and Supplementary Table 1).

Quantitative immunohistochemical studies

Eight-micrometre-thick sections were deparaffinized for immunohistochemistry by standard methods. Primary and secondary antibodies, pretreatments for antigen retrieval and developing strategies are listed in Supplementary Table 3. To minimize variability, all sections were stained in single batches. Negative controls lacking primary antibody were performed in parallel for all experiments. Immunohistochemical staining was performed with 3,3′-diaminobenzidine (Vector Lab, Burlingame, CA), counterstained with haematoxylin, dehydrated with increasing concentrations of ethanol, cleared with xylene and coverslipped with Permount® mounting media (Fisher Scientific, Fair Lawn, NJ). When fluorescently labelled secondary antibodies were used, sections were counterstained with Thioflavin S (Sigma, St. Louis, MO) 0.05% in 50% ethanol for 8 min and coverslipped with Vectashield® mounting media with 4′,6-diamidino-2-phenylindole (DAPI; Vector Lab., Burlingame, CA).

Amyloid load and amyloid plaque size distribution

Amyloid load was measured as the percent of total surface stained for Aβ by 10D5 antibody (Elan Pharmaceuticals, Inc.) in sections counterstained with haematoxylin and periodic acid–Schiff base method (for vascular basement membranes). Sections were imaged on an upright Leica DMRB microscope equipped with a motorized stage and a CCD camera (model DC330, DAGE-MTI, Inc. Michigan City, IN), and coupled with the BIOQUANT NOVA PRIME software (version 6.90.10, MBSR, Nashville, TN). Amyloid load was measured in three anatomical regions: the molecular layer of the dentate gyrus, CA1 and subiculum-presubiculum. Plaque and vascular amyloid loads were determined separately in order to detect a potential shift of the amyloid from plaques to blood vessel walls. The size distribution of the amyloid plaques was also measured.

Stereology-based studies

Stereological studies were performed using an Olympus BX51 upright microscope (Olympus, Tokyo, Japan) equipped with a motorized stage and an Olympus DP70 camera, and coupled with the CAST software (version 2.3.1.5). Densities of amyloid plaques and neurofibrillary tangles were quantified with the optical dissector technique as described previously (Hyman *et al.*, 1998) in sections stained with thioflavin-S and immunostained either with 3D6 anti-Aβ antibody (Elan Pharmaceuticals, Inc) or with the anti-tau antibodies paired helical filament (PHF)-1 or Alz50 (both kind gifts from Dr Peter Davies). Coefficient errors were calculated in preliminary studies to obtain appropriate sampling fractions. The regions of the hippocampus (granular layer of the dentate gyrus, molecular layer of the dentate gyrus, CA1 and subiculum-presubiculum) were outlined under the 4× objective and randomly sampled under the 20× objective, typically with a 10% sampling fraction. PHF1, Alz50 and thioflavin-S positive neurons were counted in the granular layer of the dentate gyrus, CA1 and subiculum-presubiculum with a counting frame of 5% (7130 μm^2). Amyloid plaques (3D6-immunoreactive and thioflavin-S positive) were counted in the molecular layer of the dentate gyrus, CA1 and subiculum-presubiculum with a counting frame of 10% (14 261 μm^2). Dense-core plaques immunoreactive for the mitochondrial marker

Table 1 Baseline characteristics of study subjects

	Non-demented controls ($n = 8$)	Non-immunized patients ($n = 13$)	AN1792-treated patients ($n = 5$)	*P* value
Age, years (mean ± SD)	82.7 ± 10.7	77.4 ± 7.3	78.6 ± 5.9	NS
Gender, *n* (% female)	4 (50)	8 (61.5)	2 (40)	NS
Duration of disease, years (mean ± SD)	NA	10.0 ± 4.5	8.4 ± 3.5	NS
Post-mortem interval, h (mean ± SD)	21.6 ± 13.8	12.7 ± 5.3	21.2 ± 29.9	NS
ApoE genotype:				
ApoE4 carriers, *n* (%)	2 (25)	10 (76.9)	3 (60)	0.0318[a]
ApoE4 alleles, *n* (%)	2 (12.5)	13 (50)	3 (30)	0.0203[a]

NA = not applicable; NS = non significant.
a Differences were significant only between non-demented controls and non-immunized patients (χ^2 with Fisher's exact test).

voltage-dependent anion-selective channel protein 1 (VDAC1) (porin, Abcam, ab15895) were counted in these same regions with a 20% sampling fraction and a counting frame of 10% (14 261 μm^2).

Curvature ratio analysis

Neurites were identified by immunohistochemistry directed against neurofilament heavy chain (Abcam, ab40796) and sections were counterstained with thioflavin-S and DAPI prior to imaging in the manner described above for stereologic measurements. The hippocampal regions were outlined with the CAST software under the 4× objective of the microscope, and randomly sampled under the 20× objective, with the following sampling fractions: 25% in the molecular layer of the dentate gyrus, 15% in the CA1 and 15% in the subiculum-presubiculum. Pictures were coded and stored in a blinded manner prior to analysis with ImageJ (http://rsbweb.nih.gov/ij/download .html). Neurite segments identified by the presence of neurofilament heavy chain were numbered, and their lengths measured by an observer blinded to the condition of the subject or the presence of dense-core plaques in the field under study. Curvature ratio of each neurite segment was calculated as the ratio of measured length to the end-to-end length of the same neurite; thus, increased neurite curvature results in a higher curvature ratio (Knowles et al., 1999). Only segments with a measured length longer than 20 μm were included in the analyses. The number of 20 × hippocampal fields analysed was not significantly different across groups [214 fields in 8 non-demented controls (mean ± SEM; 26.7 ± 2.6), 388 in 13 non-immunized patients with Alzheimer's disease (29.7 ± 2.1) and 122 in 4 immunized patients with Alzheimer's disease (30.5 ± 3.9)]. The neurofilament heavy chain immunohistochemistry was not feasible in one of the immunized cases.

To address the relationship between neurite curvature and their proximity to dense-core plaques, the curvature ratio analysis was focused on the CA1 subfield. 100% of CA1 was sampled and pictures of fields containing dense-core plaques were coded and stored in separate folders for neurofilament heavy chain and thioflavin-S images. Using ImageJ, dense-core plaques in the thioflavin-S pictures were outlined and transferred to the corresponding neurofilament heavy chain images. The curvature ratio of neurite segments within 50 μm from the dense-core plaques edge was compared with the curvature ratio of neurite segments located beyond this boundary (i.e. either in previous pictures containing dense-core plaques or in pictures lacking them). The distance of neurite segments to dense-core plaques edge was calculated as the average of three distances: distances from the nearest plaque edge to each end of the neurite segment as well as the distance from the plaque edge to the midpoint of the neurite segment.

Number of dystrophic neurites per plaque

To identify dystrophic neurites around dense-core plaques, immuno-histochemistry was performed with SMI312 antibody (Covance, SMI-312R), followed by thioflavin-S and DAPI counterstaining. Hippocampal regions were outlined with the CAST software under the 4 × objective as described previously. 100% of the molecular layer of the dentate gyrus, CA1, and subiculum-presubiculum was sampled under the 20× objective. Images of fields containing dense-core plaques were coded and stored in a blind fashion and analysed with ImageJ software. Dense-core plaques in the thioflavin-S pictures were outlined and transferred to the corresponding SMI312 pictures. Dystrophic neurites and varicosities/swellings either embedded or in contact with the thioflavin-S positive area were counted manually.

Number of reactive astrocytes per plaque

To visualize reactive astrocytes around dense-core plaques immunohistochemistry with a glial fibrillar acid protein antibody (Sigma, G9269) was done, followed by thioflavin-S and DAPI counterstaining. The same protocol as for SMI312-positive dystrophic neurites was followed, except that glial fibrillar acid protein and thioflavin-S pictures of the same fields were merged with the appropriate tool in ImageJ software. Reactive astrocytes with a visible nucleus by DAPI staining surrounding dense-core plaques as far as 50 μm from the plaques edge were manually counted. Reactive astrocytes located close to two or more dense-core plaques (i.e. within 50 μm) were 'split' among those plaques (i.e. 0.5 astrocytes for those close to two plaques, 0.33 for those close to three plaques and 0.25 for those close to four plaques). This conservative method was implemented to avoid double-counting of astrocytes per plaque in areas with high density of dense-core plaques, a situation that would be presumably more common in non-immunized Alzheimer's disease patients and might otherwise bias the results.

Statistical analysis

All statistical analyses were conducted with the statistical package PRISM Graph Pad for Mac (version 5.0). Normality of datasets was assessed with Kolmogorov–Smirnov and Schapiro–Wilk tests. Non-normal measures included the size of total amyloid plaques and dense-core plaques, neurite curvature ratio, number of dystrophic neurites per plaque and number of astrocytes per plaque. For these data, results are expressed as median (interquartile range). A non-parametric one-way ANOVA (Kruskal–Wallis) with Dunn's multiple comparison post-test was used for all-group comparisons and a non-parametric two-tailed t-test (Mann–Whitney, U) was run for pairwise comparisons. Normal data included amyloid load, densities of total amyloid plaques and dense-core plaques, and densities of PHF1, Alz50 and thioflavin-S positive neurons. For these, results are expressed as mean ± SEM. All-group comparisons were performed with a parametric one-way ANOVA with Bonferroni correction, and pairwise comparisons were done with a parametric two-tailed t-test with Welch's correction when variances were significantly different between groups. Pairwise comparisons between proportions were performed with χ^2 with Fisher's exact test. Correlations were carried out with the Pearson's statistic if both datasets were normally distributed or with the Spearman's rank test if one or both datasets were not normal. The level of significance was set at $P < 0.05$.

Results

Baseline characteristics

Baseline characteristics of the three groups are listed in Table 1 and Supplementary Table 1. Additional characteristics of the immunized patients with Alzheimer's disease can be found in Table 2 and Supplementary Table 2. Non-demented controls and non-immunized and immunized patients with Alzheimer's disease were matched by age and gender. These two latter groups

Table 2 Additional characteristics of AN1792-treated patients in this study

Subject	Number of doses	Antibody titres	Survival after first dose (months)	Reference
22	2	IgG+	15	Ferrer *et al*. 2004
23	3	1:2771	12	Masliah *et al*. 2005
24	2	Not detectable	40	Uro-Coste *et al*. 2010
25	2	TAPIR 1/4	46	Unpublished
26	2	IgM > 1:3500 IgG > 10 000	34	Bombois *et al*. 2007

TAPIR = tissue amyloid plaque immunoreactivity assay. A score of 1 (out of 4) denotes weak staining of amyloid plaques in immunohistochemical brain sections of APP^{swe} × PS1^{M146L} double transgenic mice with the patient's serum.

were also matched for Braak stage of neurofibrillary tangles and did not differ in terms of disease duration or *ApoE* genotype. Post-mortem interval was not significantly different across groups. The detailed results of each case for the main quantitative analyses are shown in Supplementary Table 4.

Amyloid load and density of amyloid plaques

Plaque and vascular amyloid loads were measured as the percent of total surface stained by 10D5 anti-Aβ antibody in the neuropil and vessels of hippocampal sections counterstained with haematoxylin and periodic acid-Schiff. Plaque amyloid load in the hippocampus was significantly different across the three groups (ANOVA, $F = 15.11$, $P < 0.0001$) (Fig. 1A, Supplementary Fig. 1). As expected, hippocampal plaque amyloid load was significantly higher in non-immunized Alzheimer's disease patients than in non-demented controls ($0.700 \pm 0.098\%$ versus $0.080 \pm 0.050\%$, $t = 5.588$, $df = 17$, $P < 0.0001$). Plaque amyloid load in the immunized Alzheimer's disease patients was significantly lower than that in the non-immunized patients ($0.146 \pm 0.069\%$ versus $0.700 \pm 0.098\%$, $t = 3.315$, $df = 16$, $P = 0.0044$); in fact, the load in these treated subjects was not different from age-matched non-demented controls ($0.146 \pm 0.069\%$ versus $0.080 \pm 0.050\%$, $t = 0.7781$, $df = 11$, $P = 0.4529$). No vascular amyloid was detected in non-demented controls. Hippocampal vascular amyloid load in immunized patients did not differ significantly from non-immunized patients ($0.013 \pm 0.005\%$ versus $0.026 \pm 0.008\%$, $t = 0.8895$, $df = 16$, $P = 0.3869$) (Fig. 1B).

Densities of total and dense-core plaques were quantified with an unbiased stereological approach in hippocampal sections double-stained with 3D6 anti-Aβ antibody and thioflavin-S (Fig. 1C–D). There were significant differences across groups in the densities of 3D6 (total) and of thioflavin-S positive (dense-core) plaques (ANOVA, $F = 34.68$ and 27.06, respectively, $P < 0.0001$ for both comparisons). As expected, non-immunized Alzheimer's disease patients had a density of both total and dense-core amyloid plaques significantly higher than non-demented controls (3D6: 22.07 ± 1.956 plaques/mm^2 versus 1.738 ± 0.970 plaques/mm^2, $t = 9.311$, $df = 16$, $P < 0.0001$; thioflavin-S: 16.17 ± 1.570 plaques/mm^2 versus 1.408 ± 0.788 plaques/mm^2, $t = 8.399$, $df = 16$, $P < 0.0001$). By contrast, AN1792-treated patients had a

density of total and dense-core amyloid plaques significantly lower than non-immunized patients (3D6: 4.566 ± 2.799 plaques/mm^2 versus 22.07 ± 1.956 plaques/mm^2, $t = 4.846$, $df = 16$, $P = 0.0002$; thioflavin-S: 4.102 ± 2.349 plaques/mm^2 versus 16.17 ± 1.570 plaques/mm^2, $t = 4.122$, $df = 16$, $P = 0.0008$) and not significantly different from non-demented controls (3D6: 4.566 ± 2.799 plaques/mm^2 versus 1.738 ± 0.970 plaques/mm^2, $t = 1.137$, $df = 11$, $P = 0.2796$; thioflavin-S: 4.102 ± 2.349 plaques/mm^2 versus 1.408 ± 0.788 plaques/mm^2, $t = 1.087$, $df = 4$, $P = 0.3381$). A sub-regional analysis revealed significant differences between both Alzheimer's disease groups in all the hippocampal regions analysed (data not shown).

We also calculated the proportion of dense-core plaques among the total amyloid plaques in each group using the same sections double-stained with 3D6 and thioflavin-S and the raw data obtained with the quantification above (Fig. 1E). This proportion was significantly different across groups ($\chi^2 = 22.30$, $df = 2$, $P < 0.0001$; χ^2 for trend $= 8.499$, $df = 1$, $P = 0.0036$). Pairwise comparisons revealed that the immunized group had a significantly higher proportion of dense-core plaques than the non-immunized Alzheimer's disease cases (89.09% versus 72.89%, Fisher's exact test, $P < 0.0001$). Non-demented controls had a proportion of dense-core plaques intermediate between non-immunized and immunized patients, but not significantly different from them (82.26% versus 72.89%, Fisher's exact test, $P = 0.1082$ and 82.26% versus 89.09%, Fisher's exact test, $P = 0.1840$, respectively). A comparison of the correlation between density of total and dense-core amyloid plaques in both Alzheimer's disease groups also revealed the overwhelming predominance of the dense-core type of amyloid plaques in the immunized group ($r = 0.9990$, $P < 0.0001$ in the immunized group versus $r = 0.6624$, $P = 0.0136$ in the non-immunized group; Pearson's correlation test) (Fig. 1F).

The size of total amyloid plaques was measured in 10D5-immunostained sections and that of dense-core plaques was measured in thioflavin-S stained sections. Both total and dense-core amyloid plaques were significantly smaller in immunized patients with respect to non-immunized patients (Fig. 1G–H, Supplementary Fig. 2A–B) [total amyloid plaques: 197.1 $(98.88–404.7)$ μm^2 versus 261.1 $(126.6–638.3)$ μm^2, $U = 1039\,000$, $P < 0.0001$; dense-core plaques: 930.7 $(555.2–1565)$ μm^2 versus 1181 $(753.4–1974)$ μm^2, $U = 119\,700$, $P < 0.0001$]. No significant differences were found in the size of both total and dense-core amyloid plaques between the
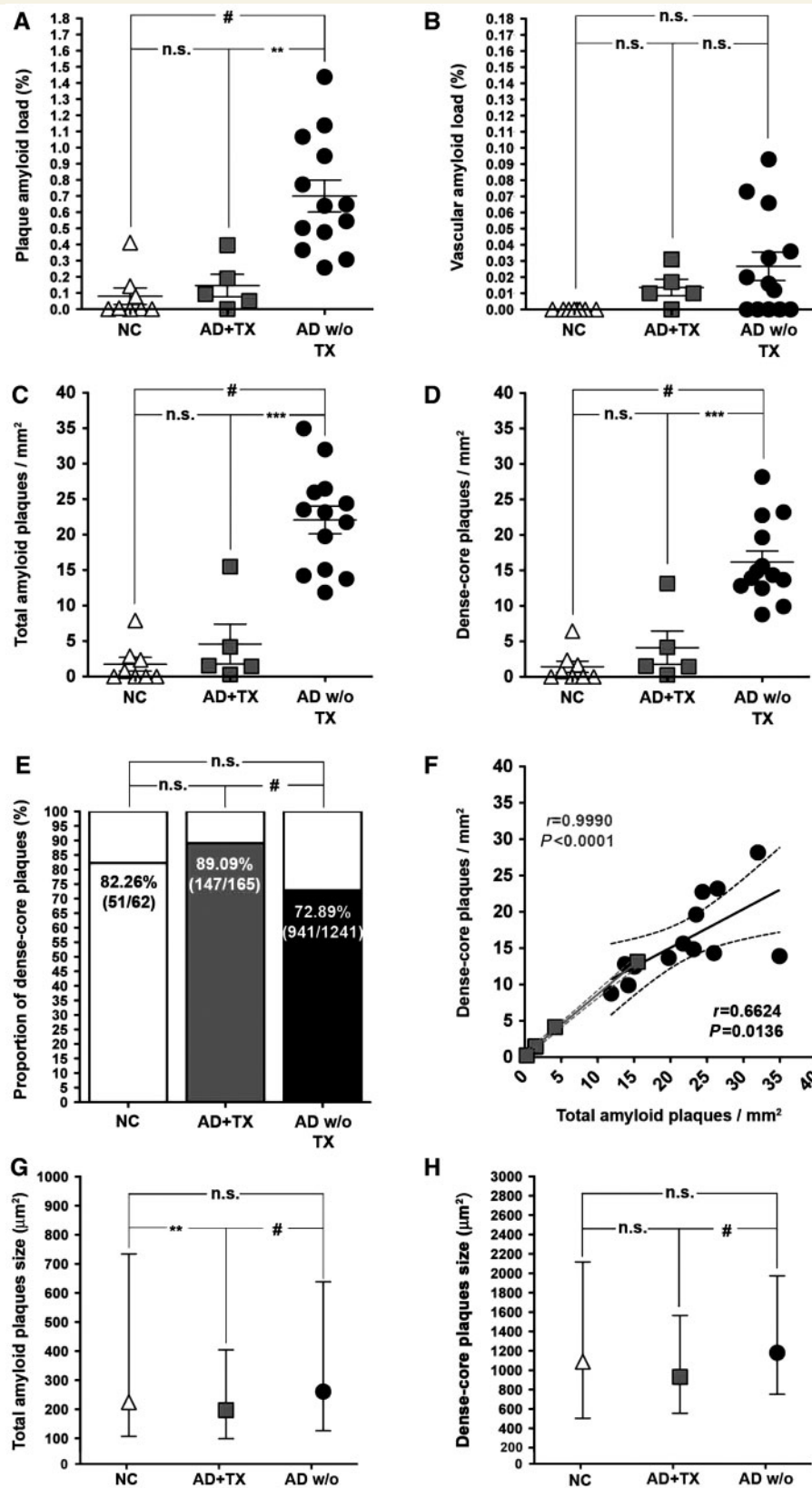
Figure 1 Decreased hippocampal amyloid deposition after anti-Aβ immunization. Plaque amyloid load in AN1792-treated Alzheimer's disease patients is reduced down to the levels of non-demented controls (NC) (**A**), without significant increase of vascular amyloid load (**B**). Density of both total amyloid plaques (**C**) and dense-core plaques (**D**) is significantly decreased in the immunized group. Bars in scatter-dot plots **A–D** denote mean ± SEM. Two-tailed unpaired t-tests were run for these pairwise comparisons (n.s. = non-significant; **$P < 0.01$; ***$P < 0.001$; #$P < 0.0001$). (**E, F**) The proportion of dense-core plaques is significantly increased after immunization. In **E**, the

non-immunized Alzheimer's disease group and the non-demented group [total amyloid plaques: 261.1 (126.6–638.3) μm^2 versus 224.5 (107–734.3) μm^2, $U = 437\,100$, $P = 0.5765$; dense-core plaques: 1181 (753.4–1974) μm^2 versus 1089 (503.9–2117) μm^2, $U = 27\,460$, $P = 0.6599$]. Lastly, total amyloid plaques were also significantly smaller in the immunized group compared to non-demented controls, but this difference did not reach statistical significance for dense-core plaques [total amyloid plaques: 197.1 (98.88–404.7) μm^2 versus 224.5 (107–734.3) μm^2, $U = 61\,760$, $P = 0.0062$; dense-core plaques: 930.7 (555.2–1565) μm^2 versus 1089 (503.9–2117) μm^2, $U = 6894$, $P = 0.1575$].

Analysis of neurite curvature ratio

Neurite curvature ratio was measured in sections immunostained with an anti-neurofilament heavy chain antibody and counterstained with thioflavin-S and DAPI.

When considering neuritic curvature independent of the distance to dense-core plaques, there was a significant positive correlation between the median curvature ratio and density of both total amyloid plaques and dense-core plaques in the non-immunized Alzheimer's disease group (total amyloid plaques: $r = 0.7692$, $P = 0.0021$; for dense-core plaques: $r = 0.5714$, $P = 0.0413$, Spearman's rank test) (Fig. 2A–B). There were statistically significant differences in the curvature ratio across the three groups of subjects (Kruskal–Wallis ANOVA $= 84.73$, $P < 0.0001$). As expected, the curvature ratio was abnormally higher in non-immunized Alzheimer's disease patients compared to non-demented controls [1.027 (1.014–1.047) versus 1.020 (1.010–1.037), $U = 1\,129\,000$, $P < 0.0001$]. Importantly, the curvature ratio was significantly lower in immunized compared to non-immunized patients [1.021 (1.010–1.041) versus 1.027 (1.014–1.047), $U = 567\,400$, $P < 0.0001$], reaching a value not different from non-demented controls [1.021 (1.010–1.041) versus 1.020 (1.010–1.037), $U = 339\,700$, $P = 0.0960$] (Fig. 2C, Supplementary Fig. 2C).

We then examined the influence of the proximity to dense-core plaques on the curvature ratio, performing the analysis in a plaque-based rather than in a random fashion, focusing on the CA1 subfield (Fig. 2D). As expected, in the non-immunized Alzheimer's disease group, the curvature ratio was significantly higher close to the plaques ($<50\,\mu m$) than far away from them ($\geq 50\,\mu m$) [1.043 (1.023–1.075) close versus 1.028 (1.015–1.049) far, $U = 453\,600$, $P < 0.0001$]. Conversely, in the immunized group

both curvature ratio values close to and far from the dense-core plaques were almost identical [1.022 (1.009–1.038) close versus 1.020 (1.010–1.036) far, $U = 40\,570$, $P = 0.5641$]. Moreover, both curvature ratio values in the immunized group were significantly lower than the corresponding curvature ratio values in the non-immunized group (close: $U = 117\,200$, $P < 0.0001$; far: $U = 100\,800$, $P < 0.0001$). Importantly, in neither of the Alzheimer's disease groups was the curvature ratio of neurites close to plaques influenced by the size of the plaques (Kruskal–Wallis ANOVA with Dunn's multiple comparison post-test: $P > 0.05$), whereas the significant difference observed in the curvature ratio close to plaques between both Alzheimer's disease groups was preserved across different plaque size intervals (Kruskal–Wallis ANOVA with Dunn's multiple comparison post-test: $P \leq 0.001$, except for the plaque size interval 1500–2000 μm^2, which did not reach significance, probably due to the small number of neurites measured close to plaques of this size in the immunized group, $n = 18$) (Fig. 2E).

Dystrophic neurites/varicosities per dense-core plaque

Dystrophic neurites and axonal swellings or spheroids per dense-core plaque were counted within the thioflavin-S positive area in sections stained with SMI312 antibody and counterstained with thioflavin-S. Dense-core plaques in non-immunized Alzheimer's disease patients had significantly more dystrophic neurites compared to plaques in non-demented controls [2 (1–4) dystrophies/plaque versus 1 (0–3) dystrophy/plaque, $U = 20\,790$, $P = 0.0007$]. Unexpectedly, there was a significant increase in the number of dystrophic neurites per dense-core plaque in the immunized patients compared to non-immunized patients [4 (2–6) dystrophies/plaque versus 2 (1–4) dystrophies/plaque, $U = 116\,800$, $P < 0.0001$] (Fig. 3A, Supplementary Fig. 2D).

Proportion of VDAC1-immunoreactive dense-core plaques

Accumulation of mitochondria in dystrophic neurites of dense-core plaques was examined by immunohistochemistry for the outer mitochondrial membrane marker VDAC1 with thioflavin-S counterstaining. The proportion of dense-core plaques immunoreactive for VDAC1 in non-immunized Alzheimer's disease patients was higher than that in non-demented controls, although this

Figure 1 Continued
bar graph shows total amyloid plaques counted on sections immunostained for 3D6 anti-Aβ antibody normalized to 100%. Filled bars represent the percent of amyloid plaques co-stained with thioflavin-S (dense-core plaques). Raw fractions are presented in parenthesis within the filled bars, with the number of total amyloid plaques counted in the denominator and the number of dense-core plaques in the numerator. In **F**, the correlation between total amyloid plaques and dense-core plaques in both Alzheimer's disease groups is shown. Pairwise comparisons in **E** were done with χ^2 with Fisher's exact test ([#]$P < 0.0001$), whereas correlations in **F** were performed with Pearson's test. (**G**, **H**) Remaining total amyloid plaques and dense-core plaques in immunized patients are significantly smaller compared to plaques in non-immunized patients, whereas their size does not differ between non-immunized patients and non-demented controls. Single-symbol plots in **G** and **H** represent median values, whereas bars denote interquartile ranges. These pairwise comparisons were performed with a Mann–Whitney test ([**]$P < 0.01$, [#]$P < 0.0001$). Automatic measurement of total amyloid plaques size included 225 plaques from non-demented controls (NC), 626 plaques from immunized patients (AD + TX) and 3973 plaques from non-immunized patients (AD w/o TX). Manual measurement of dense-core plaques size was performed on 55 plaques from non-demented controls, 285 plaques from immunized patients and 1035 plaques from non-immunized patients.
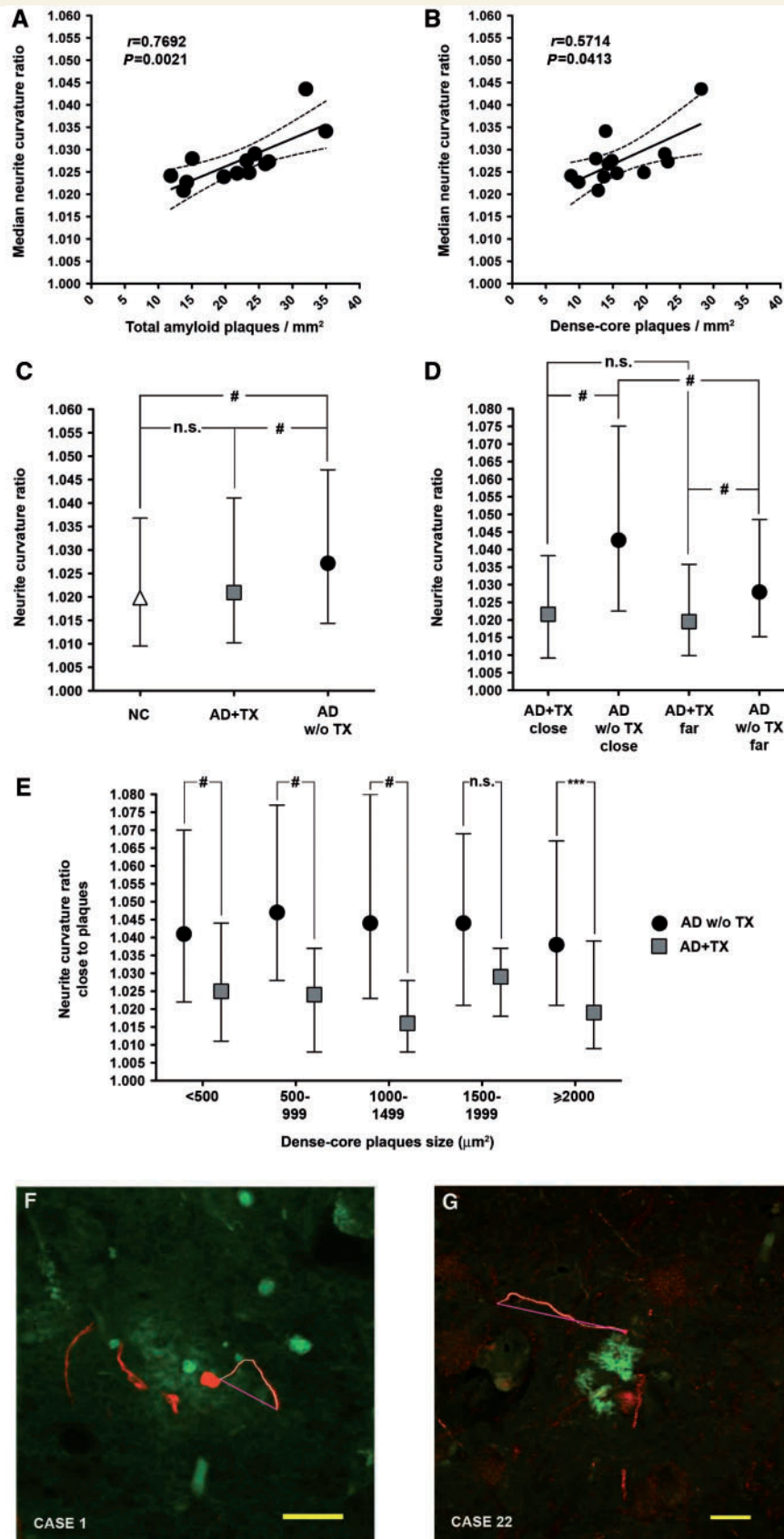
Figure 2 Improvement of neurite trajectories in immunized patients with Alzheimer's disease. (**A**, **B**) Neurite curvature ratio correlates significantly with the density of total and dense-core amyloid plaques in non-immunized patients with Alzheimer's disease. Correlations were performed with Spearman's rank test. Dotted lines represent the 95% confidence intervals. (**C**) Neurite trajectories in the

Continued

difference did not reach statistical significance (38.96% versus 31.43%, respectively, Fisher's exact test, $P = 0.4771$). Remarkably, more than half (56.25%) of the dense-core plaques in the AN1792-treated patients were VDAC1-positive, a proportion significantly higher compared to the other two groups ($P = 0.0009$ versus non-immunized group; $P = 0.0121$ versus non-demented group, Fisher's exact test) (Fig. 3B).

Reactive astrocytes per dense-core plaque

We counted the number of glial fibrillar acid protein-positive reactive astrocytes per dense core-plaque (up to 50 μm from the edge of the plaque) in sections counterstained with thioflavin-S. Dense-core plaques had a more severe astrocytosis in non-immunized Alzheimer's disease patients than that in non-demented controls [1.5 (0.4575–3) astrocytes/plaque versus 0.33 (0–1.040) astrocytes/plaque, $U = 22\,070$, $P < 0.0001$]. The extent of astrocytosis surrounding dense-core plaques remaining after immunization was slightly but not significantly decreased, when compared to plaques from non-immunized patients with Alzheimer's disease [1 (0–3) astrocyte/plaque versus 1.5 (0.4575–3) astrocytes/plaque, $U = 73\,110$, $P = 0.6060$], but still more severe than that around dense-core plaques from non-demented controls ($U = 3548$, $P = 0.0006$) (Fig. 3C, Supplementary Fig. 2E).

Alterations in neuronal tau

To analyse the amount of abnormal neuronal tau quantitatively, we performed immunohistochemical studies with two different anti-tau antibodies: the phosphorylation-dependent antibody PHF1 to assess the phosphorylation status of tau and the conformation-dependent antibody Alz50 to evaluate the misfolding status of tau (Fig. 4A–B). The density of thioflavin-S positive neurofibrillary tangles (i.e. tau fibrillar aggregates with a β-sheet conformation) was also quantitated in a stereological fashion (Fig. 4C).

As expected, densities of Alz50-positive and PHF1-positive neurons and thioflavin-S positive neurofibrillary tangles were significantly higher in non-immunized Alzheimer's disease patients (Braak stages IV–VI) than in non-demented controls (Braak stages I–III) (Alz50: 16.08 ± 2.534 neurons/mm^2 versus 6.948 ± 2.915 neurons/mm^2, $t = 2.305$, $df = 19$, $P = 0.0326$; PHF1: 47.44 ± 6.138 neurons/mm^2 versus 5.464 ± 2.042 neurons/mm^2, $t = 6.489$, $df = 14$, $P < 0.0001$; thioflavin-S: 34.12 ± 6.990 neurofibrillary tangles/mm^2 versus 4.468 ± 1.885 neurofibrillary tangles/mm^2, $t = 4.096$, $df = 13$, $P = 0.0013$). Of note, immunized patients showed a significant reduction in the density of PHF1-positive neurons compared to non-immunized patients, despite being matched for the Braak stage (18.53 ± 10.49 neurons/mm^2 versus 47.44 ± 6.138 neurons/mm^2, $t = 2.445$, $df = 16$, $P = 0.0264$) (Figs 4A and 4E–L). No difference was found in the densities of Alz50-positive neurons and thioflavin-S positive neurofibrillary tangles between the Alzheimer's disease groups (Alz50: 17.42 ± 9.152 neurons/mm^2 in AN1792-treated versus 16.08 ± 2.534 neurons/mm^2 in non-treated, $t = 0.1407$, $df = 4$, $P = 0.8949$; thioflavin-S: 18.56 ± 7.690 neurofibrillary tangles/mm^2 in AN1792-treated versus 34.12 ± 6.990 neurofibrillary tangles/mm^2 in non-treated, $t = 1.261$, $df = 16$, $P = 0.2255$). A correlation between densities of PHF1-positive and Alz50-positive neurons for both Alzheimer's disease groups revealed a predominance of PHF1-positive over Alz50-positive neurons in non-immunized patients with Alzheimer's disease whereas both densities were similar in the immunized group ($r = 0.3899$, $P = 0.1878$, in the non-immunized group, versus $r = 0.9755$, $P = 0.0046$, in the immunized group, Pearson's correlation test) (Fig. 4D).

Discussion

Successful removal of hippocampal amyloid

Both active and passive immunotherapy against Aβ peptide have been shown to clear amyloid plaques or prevent Aβ deposition in

Figure 2 Continued

hippocampus of immunized patients are significantly straighter compared to non-immunized patients and similar to non-demented controls. Curvature ratio was analysed in 1231 neurites from 8 normal controls, 580 neurites from 4 immunized patients and 2243 neurites from 13 non-immunized patients. In one of the immunized cases an appropriate neurofilament heavy chain immunostaining was not feasible, probably due to differences in fixation protocols. (**D**) Improvement of curvature ratio in immunized patients is not only attributable to a lower plaque load but also occurs within the vicinity (<50 μm) of remaining dense-core plaques. Curvature ratio was determined in 321 neurites close to and 260 neurites far from plaques in the immunized group, and in 1256 neurites close to and 972 neurites far from plaques in the non-immunized group. Pairwise comparisons in **C** and **D** were performed with Mann–Whitney test (#$P < 0.0001$). (**E**) Curvature ratio of neurites close to plaques is not simply due to a 'mass effect' caused by the plaques because plaque size does not affect the curvature ratio of surrounding neurites (within-group comparisons were not significant but are not illustrated for clarity purposes). Moreover, the improvement of the curvature ratio close to plaques in the immunized subjects is not explained by the smaller size of their plaques because between-group significant difference is preserved across different plaque size intervals. This analysis included 143, 281, 202, 171 and 276 neurites close to plaques of increasing size intervals from the non-immunized Alzheimer's disease subjects, and 112, 59, 41, 18 and 50 neurites close to plaques of the same size intervals from the AN1792-treated Alzheimer's disease subjects. A Kruskal–Wallis ANOVA with Dunn's multiple comparison post-test was run (***$P < 0.001$, #$P < 0.0001$, n.s. = non significant). (**F, G**) Representative pictures of neurite segments within the vicinity of a dense-core plaque in the CA1 region of a non-immunized patient with Alzheimer's disease (**F**, Case 1), and an AN1792-treated patient with Alzheimer's disease (**G**, Case 22). Neurites were immunostained with a neurofilament heavy chain antibody (in red) and plaques were stained with thioflavin-S (in green). Neurite curvature ratio was calculated as the ratio of the measured length (white line) to the end-to-end length (pink line). Compare the abnormally curve trajectory of neurites in **F** with the straighter trajectory of neurites in **G**. Scale bars = 20 μm. NC = non-demented controls; AD + TX = plaques from immunized patients; AD w/o TX = non-immunized patients.
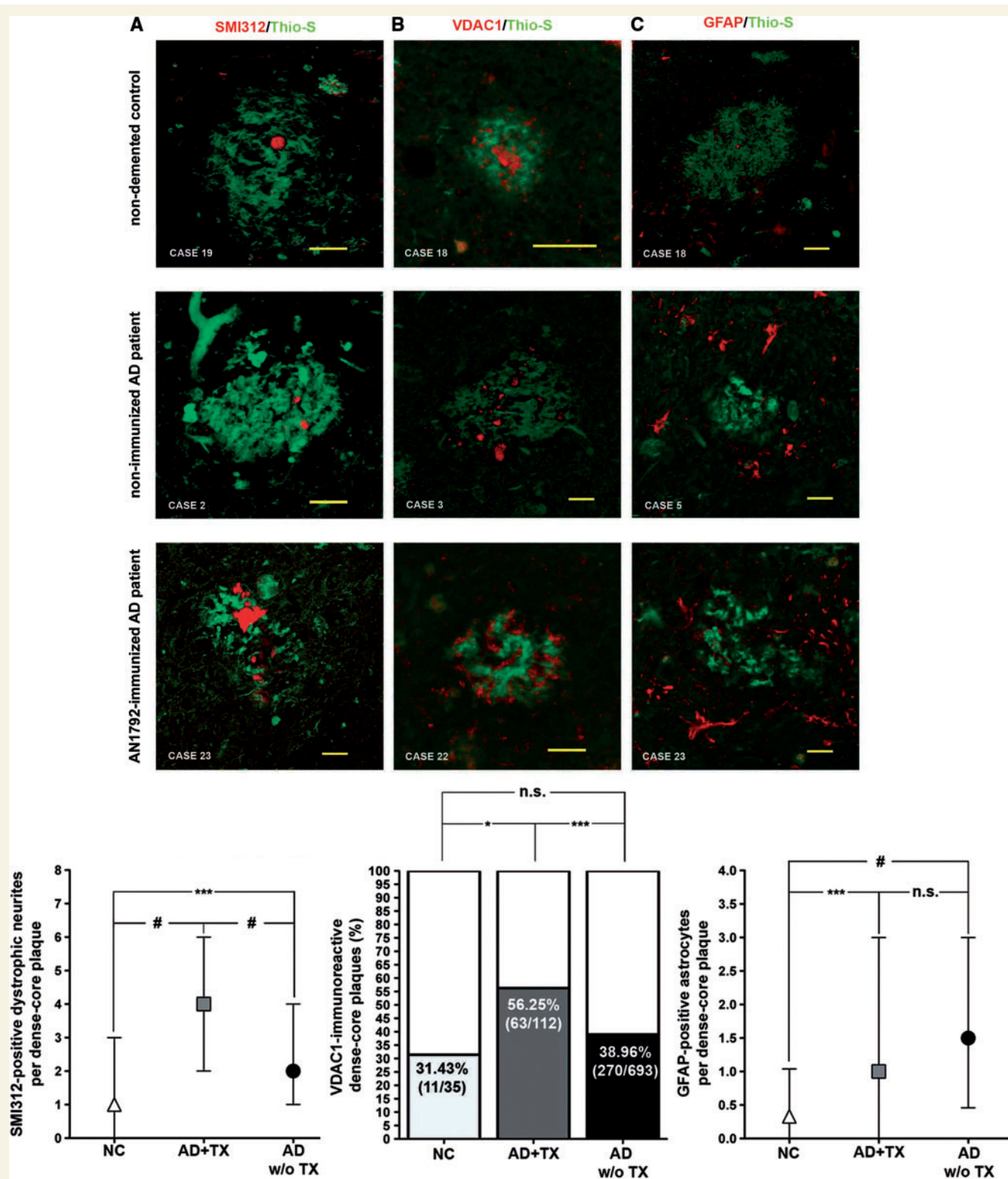
Figure 3 Dense-core plaques remaining after immunization retain some of their toxic properties. (**A**) Representative images of dense-core plaques (in green) from a non-demented control (Case 19), a non-immunized patient (Case 2) and an AN1792-treated patient (Case 23), with the neurofilament antibody SMI312 depicting associated dystrophic neurites and axonal varicosities or swellings (in red). Quantification of the number of dystrophic neurites and varicosities per plaque yielded a significant increase in the amount of neuritic dystrophy in the remaining plaques of immunized patients, as compared to non-immunized patients. Pairwise comparisons were done with the Mann–Whitney test [***P < 0.001, #P < 0.0001; n = 55, 285 and 1035 plaques in normal controls (NC), immunized patients (AD + TX) and non-immunized patients (AD w/o TX), respectively]. (**B**) Representative images of mitochondria accumulation in dense-core plaques associated-dystrophic neurites from a non-demented control (Case 19), a non-immunized patient (Case 3) and an

Continued

several mouse models of Alzheimer's disease (Schenk *et al.*, 1999; Bard *et al.*, 2000; Morgan *et al.*, 2000; Janus *et al.*, 2000; Bacskai *et al.*, 2001, 2002; DeMattos *et al.*, 2001; Lemere *et al.*, 2003; Wilcock *et al.*, 2004). Post-mortem studies of brain specimens from participants in the Phase 2a active immunization trial also revealed a significant decrease in amyloid pathology, as measured with either amyloid load or density of amyloid plaques per field (Nicoll *et al.*, 2003; Ferrer *et al.*, 2004; Masliah *et al.*, 2005; Bombois *et al.*, 2007; Holmes *et al.*, 2008).

Our results are in agreement with these previous autopsy reports. Compared to the hippocampus of non-immunized patients from our brain bank, the hippocampus of this subset of immunized Alzheimer's disease patients had a significantly lower amount of amyloid deposits, as measured in sections stained with the 10D5 antibody, an antibody that recognizes the N-terminus of the Aβ peptide. Indeed, active immunization reduced the hippocampal plaque amyloid load in the treatment group down to the levels existing in age-matched non-demented controls. The same result was achieved after the stereological quantification of density of amyloid plaques in sections stained with the 3D6 antibody, which also binds to the N-terminus of the Aβ peptide. Since anti-Aβ antibodies generated after AN1792 immunization are mainly directed against the N-terminus of the Aβ peptide (Lee *et al.*, 2005), the results herein could be explained by a competition between 10D5 and 3D6 antibodies and *de novo* endogenous anti-Aβ antibodies to bind amyloid plaques. However, stereological quantification of plaques in thioflavin-S stained sections also yielded similarly lower density of dense-core plaques in immunized patients, ruling out this possibility.

Interestingly, our quantitative analysis revealed a significantly higher proportion of dense-core plaques among the remaining amyloid plaques in the immunized cases, as compared to non-immunized Alzheimer's disease cases. A sub-regional analysis showed that this difference was mainly driven by the stereological quantification in the subiculum-presubiculum (data not shown). Indeed, the hippocampal sections from four out of the five immunized Alzheimer's disease patients were virtually devoid of the confluent, diffuse, 'cloud-like' amyloid deposits, typically seen in the parvopyramidal layer of the presubiculum (see Supplementary Fig. 1) (Kalus *et al.*, 1989; Akiyama *et al.*, 1990; Wisniewski *et al.*, 1998). Thus, these data indicate that AN1792 immunization was comparatively more effective at clearing diffuse amyloid deposits than dense-core plaques.

We compared the size distribution of amyloid plaques in hippocampal sections from the three groups of subjects and found that both total amyloid plaques and dense-core plaques were significantly smaller in immunized patients, with respect to non-immunized patients and non-demented controls. Despite the static nature of any post-mortem study, this result is consistent with the *in vivo* observation of a reduction in dense-core plaques size after topical administration of anti-Aβ antibodies in an Alzheimer's disease mouse model (Bacskai *et al.*, 2002). This observation, together with the relative abundance of collapsed 'moth-eaten' plaques remaining after AN1792 immunization already noted in previous post-mortem reports (Nicoll *et al.*, 2003; Ferrer *et al.*, 2004), also points towards a sequential pattern of amyloid removal: plaques halo, containing more soluble amyloid species, would be removed more readily, whereas insoluble amyloid fibrils compactly packed within the plaque core would be harder to solubilize.

According to previous reports, amyloid removal seems to be proportional to the immunological response to AN1792 as measured with antibody titres in plasma or CSF (Holmes *et al.*, 2008). Of note, in our study, both an antibody responder patient who developed a subacute meningoencephalitis and a patient with undetectable antibody titres by enzyme-linked immunosorbent assay had the highest amyloid loads and densities of dense-core plaques among the immunized patients.

A recent post-mortem study of eight other AN1792-immunized patients showed an overall increase in the extension and severity of cerebral amyloid angiopathy, suggesting that amyloid peptide is cleared through the vessels wall and efflux to the circulation (Boche *et al.*, 2008). Unlike this study, the clearance of amyloid plaques in the hippocampus of our subset of immunized patients was not translated into an increase of their vascular amyloid load, which was not significantly different from non-immunized patients. However, since cerebral amyloid angiopathy is usually more prominent in neocortical areas and our analysis was restricted to the hippocampus, we cannot rule out an overall increase of cerebral amyloid angiopathy in our immunized group.

Removal of amyloid plaques leads to recovery of neurite abnormal trajectories

We previously showed that the neurites within the dense-core amyloid plaques in the human Alzheimer's disease brain have a more abnormal trajectory compared to the neurites outside the

Figure 3 Continued
AN1792-treated patient (Case 22), as revealed by the mitochondrial marker VDAC1 (in red). Quantification of dense-core plaques immunoreactive for VDAC1 in the three study groups revealed an increase of the proportion of plaques VDAC1-positive in the immunized group, as compared to the non-immunized group. Dense-core plaques were normalized to 100% and filled bars represent the proportion of dense-core plaques immunoreactive for VDAC1. Raw fractions are shown in parenthesis within the filled bars, with the number of dense-core plaques counted in the denominator and the number of VDAC1-positive plaques in the numerator. Pairwise comparisons were done with χ^2 with Fisher's exact test (*$P<0.05$, ***$P<0.001$). (**C**) Representative images of reactive astrocytosis surrounding dense-core plaques (in green) from a non-demented control (Case 18), a non-immunized patient (Case 5) and a patient treated with AN1792 (Case 23), as shown with a glial fibrillar acid protein immunostaining (in red). Quantification of the number of astrocytes per plaque resulted in a non-significant decrease of plaque-associated astrocytosis in the immunized group compared to the non-immunized patients. However, plaques from immunized patients still have more severe astrocytosis than plaques from non-demented controls. Pairwise comparisons were done with the Mann–Whitney test (***$P<0.001$, #$P<0.0001$; $n=66$, 151 and 994 dense-core plaques, in the non-demented, immunized and non-immunized groups, respectively). Scale bars in **A–C** = 20 μm.
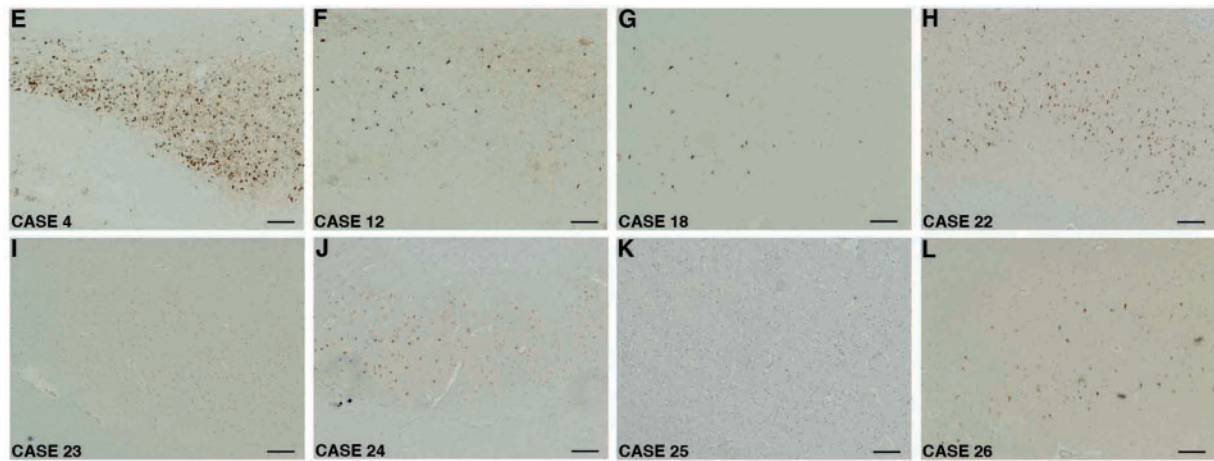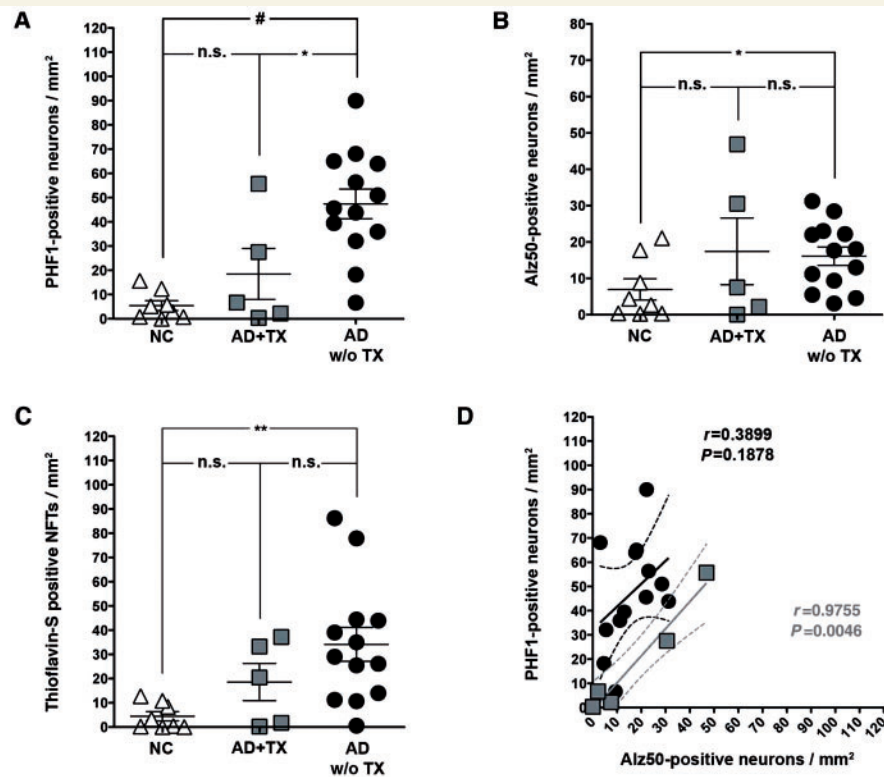
Figure 4 Decreased tau phosphorylation in neurofibrillary tangles after anti-Aβ immunization. (**A**) Hippocampal density of PHF1-positive neurons is significantly decreased in the immunized Alzheimer's disease patients compared to the patients with non-immunized Alzheimer's disease, despite both groups being matched for Braak stage. (**B**, **C**) No significant difference is observed in the densities of Alz50-positive neurons and thioflavin-S positive neurofibrillary tangles (NFT) between both Alzheimer's disease groups. Pairwise comparisons in **A–C** were done with a two-tailed t-test and bars represent mean ± SEM (*$P < 0.05$, **$P < 0.01$, #$P < 0.0001$). (**D**) Correlations between densities of PHF1-positive neurons and Alz50-positive neurons in both Alzheimer's disease groups reveal a predominance of the late-stage phospho-tau species (PHF1) over the early-stage misfolded tau species (Alz50) in the non-immunized group. By contrast, neither of both tau epitopes is predominant in the Braak-matched immunized Alzheimer's disease group. Black circles represent each of non-immunized patients and grey squares represent immunized patients. Correlations were done with Pearson's test and dotted lines indicate the 95% confidence interval. For clarity purposes, non-demented controls are not represented. (**E–L**) Pictures show some of the PHF1-immunostained hippocampal sections used in the above analysis. The transition from the CA1 region to the subiculum (left-to-right in each picture) is illustrated for two representative non-immunized Alzheimer's disease patients (**E**, Case 4, Braak VI; and **F**, Case 12, Braak IV), one representative non-demented control (**G**, Case 18, Braak II) and the five AN1792-treated Alzheimer's disease patients (**H–L**, Cases 22–26). Scale bars = 200 μm.

plaques, and also compared to the neurites in the brain of non-demented controls (Knowles *et al.*, 1999). We also showed in Alzheimer's disease transgenic mouse models that the curvature ratio in neurites within 50 μm from the edge of the dense-core plaques is abnormally higher than the curvature ratio far away from this boundary (D'Amore *et al.*, 2003; Lombardo *et al.*, 2003; Spires-Jones *et al.*, 2009). In addition, *in vivo* imaging of the brain in one of these models revealed that changes in neurite trajectories follow the appearance of new plaques, arguing that this morphologic change is secondary to Aβ deposition (Meyer-Luehmann *et al.*, 2008). Lastly, passive immunotherapy in these Alzheimer's disease mouse models was able to normalize the curvature ratio of the neurites upon removal of amyloid plaques (Lombardo *et al.*, 2003; Spires-Jones *et al.*, 2009).

Based on this previous work in transgenic models of Aβ deposition, we analysed the curvature ratio of the neurites (dendrites and axons) in the hippocampus of the three groups of subjects and studied the influence of their proximity to dense-core plaques. The presence of a curvature ratio significantly higher in non-immunized Alzheimer's disease patients compared to non-demented controls confirmed the reproducibility and validity of this measure of neurite morphological abnormality. A subsequent analysis in the CA1 subfield with a plaque-based approach yielded a significantly higher curvature ratio of neurites located close to dense-core plaques (<50 μm), as compared to neurites far from them (≥50 μm), in non-immunized patients with Alzheimer's disease. This higher curvature ratio close to plaques was not influenced by the plaque size, supporting a local toxic effect of dense-core plaques on the trajectories of surrounding neurites rather than a 'mass effect', and further reinforcing the usefulness of this morphological measure. Examination of double-labelled hippocampal sections revealed that the 50 μm boundary around the edge of the thioflavin-S positive area was far away from the thin halo of more diffuse 3D6-positive but thioflavin-S-negative amyloid, also arguing against this 'mass effect' (results not shown).

Importantly, in the first of the two analyses, the neurite curvature ratio was significantly lower in AN1792-immunized patients than in non-immunized patients. Indeed, we observed an apparent normalization of this parameter of neuronal degeneration, since there was no significant difference between immunized patients and non-demented controls. This result is not merely due the existence of fewer plaques in the immunized Alzheimer's disease group, because in the plaque-based analysis performed subsequently, curvature ratios of both neurites located close to and far from dense-core plaques also were significantly lower in AN1792-treated patients, compared to the non-immunized patients. In fact, unlike these results in the non-immunized group, in the immunized patients both curvature ratios were almost identical. In addition, the significant difference observed in the curvature ratio close to plaques between both Alzheimer's disease groups is not merely due to the plaques from the immunized group being smaller and exerting less 'mass effect' on surrounding neurites; first, as mentioned above, the plaque size did not influence the curvature ratio of surrounding neurites, and second, the difference was preserved across different plaque size intervals. Thus, the significantly lower curvature ratio in the proximity of

the remaining plaques in the AN1792 group unequivocally points to the reduction of an abnormal neurite morphology otherwise existing around the dense-core plaques.

Taken together, these results indicate that AN1792 immunization reproduces the beneficial effects on neurite trajectories observed with anti-Aβ passive immunization in preclinical studies (Lombardo *et al.*, 2003; Spires-Jones *et al.*, 2009) and further extend previous evidence of anti-Aβ immunization-induced improvement in markers of neuronal degeneration in the human Alzheimer's disease brain (Nicoll *et al.*, 2003; Ferrer *et al.*, 2004; Masliah *et al.*, 2005). While we have previously shown that plaque-induced neuritic curvature can potentially contribute to the cognitive deficits seen in Alzheimer's disease by disrupting the cortical synaptic integration (Knowles *et al.*, 1999; Stern *et al.*, 2004), the restoration of neurite trajectories observed in the hippocampus of this subset of immunized patients may not be sufficient to slow their cognitive decline (Supplementary Table 2) (Ferrer *et al.*, 2004; Masliah *et al.*, 2005; Bombois *et al.*, 2007; Uro-Coste *et al.*, 2010).

Toxic potential of amyloid plaques remaining after immunization

Passive anti-Aβ immunotherapy can promote a rapid recovery of amyloid-associated neuritic dystrophy in mouse models of Alzheimer's disease (Brendza *et al.*, 2005), and also previous autopsy reports of AN1792-treated patients have described a decrease in the density of clusters of dystrophic neurites upon amyloid removal (Nicoll *et al.*, 2003; Ferrer *et al.*, 2004; Masliah *et al.*, 2005). We sought to compare the amount and characteristics of plaque-associated neuritic dystrophy in hippocampal sections from the three groups of subjects. First, we counted the number of SMI312-positive dystrophic neurites and axonal swellings or spheroids within the boundaries of dense-core plaques and observed an unexpected increase in dystrophic neurites associated with the remaining plaques of AN1792-treated patients, as compared to non-immunized patients. Next, we wondered whether this resistance of dystrophic neurites to anti-Aβ immunotherapy might be due to their end-stage properties. Electron microscopy studies have described the accumulation of degenerating mitochondria in the dystrophic processes of dense-core amyloid plaques (Kidd, 1964; Fiala *et al.*, 2007). Indeed, a staging of mitochondrial degeneration has been proposed, starting with the accumulation of smaller but otherwise normal-looking mitochondria, followed by the swelling of mitochondrial cristae and the formation of lamellar bodies, and lastly clustering into multivesicular, presumably autophagic, bodies (Fiala *et al.*, 2007). We sought to depict this pathological feature with immunostaining for VDAC1 (porin, voltage-dependent anion channel type 1), a channel protein present in the outer mitochondrial membrane. As expected by these previous ultrastructural descriptions, VDAC1 decorated dystrophic processes of some dense-core plaques, intermingled with the fibrillar amyloid. Surprisingly, we found a significantly increased proportion of VDAC1-immunoreactive dense-core plaques in the immunized group. Thus, the results of this characterization of plaque-associated

neuritic dystrophy suggest that anti-Aβ active immunization might be ineffective in ameliorating amyloid-embedded end-stage dystrophic neurites unless compact amyloid is completely removed. By contrast, we postulate that the restoration of the trajectory of surrounding neurites would occur as soon as the process of plaque removal begins. Alternatively, new dystrophic neurites and axonal swellings and further mitochondrial degeneration might occur within the remaining dense-core plaques as a result of the ongoing solubilization of amyloid fibrils, perhaps due to an increase in the local concentration of toxic Aβ oligomers (Cruz et al., 1997; Carulla et al., 2005; Patton et al., 2006; Martins et al., 2008).

Previous autopsy studies of AN1792-treated patients have reported a lower density of reactive astrocyte clusters upon amyloid clearance but have not assessed the amount of astrocytosis surrounding the remaining plaques (Nicoll et al., 2003; Masliah et al., 2005). We measured the number of reactive astrocytes per dense core-plaque up to 50 μm from the edge of the plaques in the three study groups, and found no significant difference between plaques remaining after immunization and those from non-immunized patients, further suggesting that the former still retain toxic properties.

Notably, despite being similar in size, dense-core plaques were substantially less toxic in non-demented controls than in non-treated Alzheimer's disease patients, as judged by these measures of neuritic dystrophy and astrocytosis.

Active immunization also ameliorates the hippocampal tau pathology

In the triple transgenic mouse (3×Tg), which sequentially develops both amyloid plaques and neuronal tau aggregates, anti-Aβ immunization not only removed amyloid but also improved early tau pathology in the same sequential fashion. Yet success was not complete because late hyperphosphorylated tau aggregates remained intact after treatment (Oddo et al., 2004). However, the same authors have shown that, when initiated at an earlier stage, before the mice develop plaques and tau aggregates, anti-Aβ immunization is able to prevent the development of both amyloid and tau pathologies in this mouse model (Oddo et al., 2008). Recently, anti-Aβ active immunization has been shown to decrease tau hyperphosphorylation in two other mouse models that sequentially develop amyloid plaques and neuronal aggregates of hyperphosphorylated native murine tau, thus adding further evidence for its potential beneficial effect on tau pathology (Wilcock et al., 2009). By contrast, previous autopsy studies of AN1792-treated patients have reported a density of neurofibrillary tangles and neuropil threads similar to non-treated patients with Alzheimer's disease and a pattern of neurofibrillary tangles distribution consistent with Braak V–VI stages. However, in a subset of 11 antibody responders with baseline and follow-up CSF samples tau levels were significantly reduced, as compared with 10 placebo recipients (Gilman et al., 2005).

To analyse tau neuronal pathology, we used two different well-characterized antibodies, PHF1 and Alz50. While PHF1 binds tau protein phosphorylated at serine residues 396 and 404

(Otvos Jr. et al., 1994), Alz50 is a phosphorylation-independent but conformation-dependent anti-tau antibody, with an epitope consisting of the N-terminus and one of the microtubule-binding domains of the tau molecule (Carmel et al., 1996). Although both antibodies are highly specific for tau species in the Alzheimer's disease brain, Alz50 has been shown to label early misfolded tau (Carmel et al., 1996), whereas PHF1 binds to later-stage hyperphosphorylated tau (Augustinack et al., 2002).

Surprisingly, stereological quantification of the density of PHF1-positive neurons yielded a significant reduction in immunized patients, as compared to non-immunized patients. However, no difference was found in the quantification of Alz50 positive cells between both Alzheimer's disease groups. Furthermore, there was no significant difference between the groups in the density of late-stage thioflavin-S positive neurofibrillary tangles.

Taken together, these results suggest that anti-Aβ active immunization is able to decrease tau hyperphosphorylation but is less effective in ameliorating the misfolding and aggregation of the tau molecules. Further, they are in line with a previous autopsy study of one of these immunized patients describing a reduced immunoreactivity of phospho-tau and the stress kinases stress-activated protein kinase/c-Jun N-terminal kinase and p38 within the dystrophic neurites surrounding collapsed plaques (Ferrer et al., 2004). Remarkably, among the immunized patients, both the subject who developed an autoimmune meningoencephalitis and the subject who did not generate an enzyme-linked immunosorbent assay-detectable anti-AN1792 antibody response had the highest densities of Alz50, PHF1 and thioflavin-S positive neurons. Therefore, it is possible that immunization at an earlier stage of the disease (i.e. in patients with mild cognitive impairment) would have reverted or even prevented the development of neurofibrillary tangles to a greater extent. These findings suggest a link between Aβ and tau, and provide strong support for the amyloid cascade hypothesis, which postulates that Aβ accumulation triggers the onset of Alzheimer's disease and that tau hyperphosphorylation, subsequent neurofibrillary tangles formation and neuronal death are downstream consequences of the Aβ aggregation (Hardy and Selkoe, 2002). To our knowledge, this is the first evidence of improvement of neuronal tangle pathology upon anti-Aβ immunization in patients with Alzheimer's disease. Differences with previous reports might be due to the different tau epitopes depicted in the immunohistochemical studies and to the different quantification approaches (sterology-based versus non-stereology based).

In summary, we show that clearance of amyloid plaques by anti-Aβ active immunization within the hippocampus promotes potentially beneficial structural changes of neurites and decreases the hyperphosphorylation of tau. However, dense-core plaques that remain after immunization retain at least some of their toxic properties. The morphological improvements are relatively subtle and may not be sufficient to alter the clinical course of these patients. Nonetheless, they extend previous evidence that an Aβ-directed therapy can modify the neuropathology of the human disease beyond the effects on amyloid plaques and support the idea that Aβ toxicity directly mediates at least some of the neurodegenerative phenomena associated with neural system

collapse in Alzheimer's disease. Immunization of patients at an earlier stage of the disease might enhance these positive changes and render a more robust improvement of cognitive functions. Larger clinicopathological studies on patients enrolled in ongoing active and passive immunization clinical trials are needed to confirm these results. Also, whether plaque removal by immunization leads to an increase of synaptic density or prevents further synaptic loss—the main pathological correlate of cognitive function in Alzheimer's disease—remains to be investigated.

Acknowledgements

# Funding
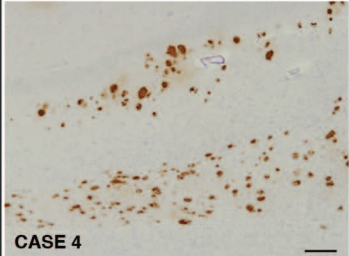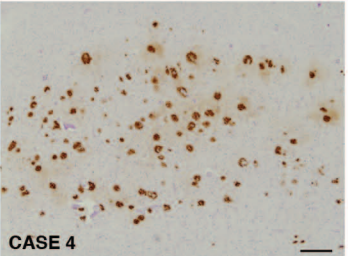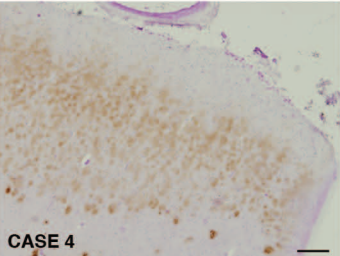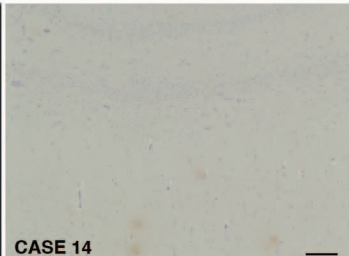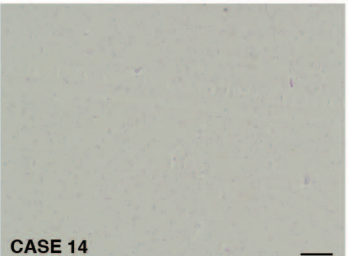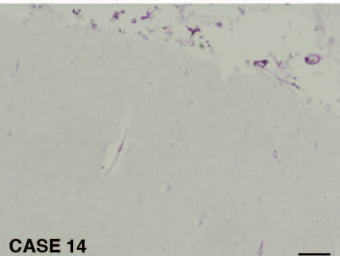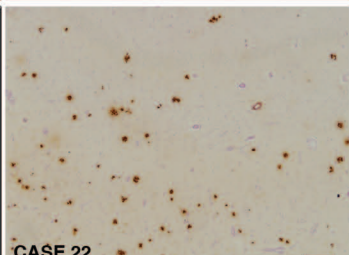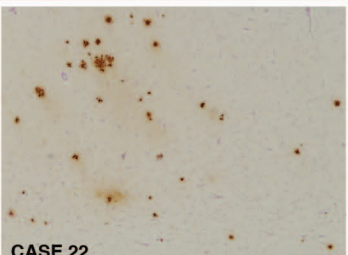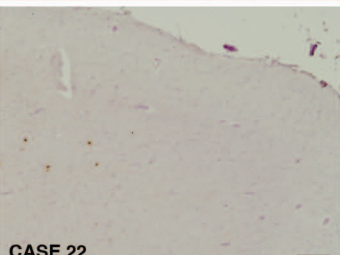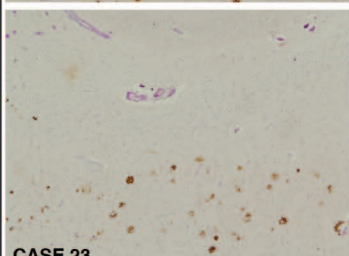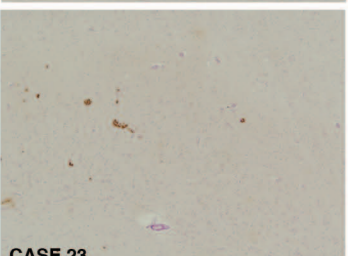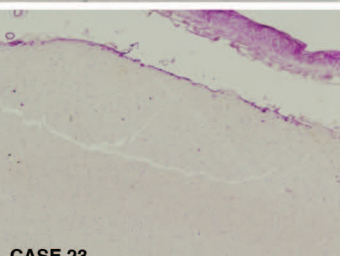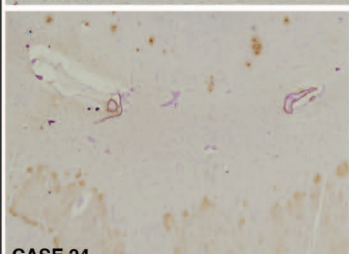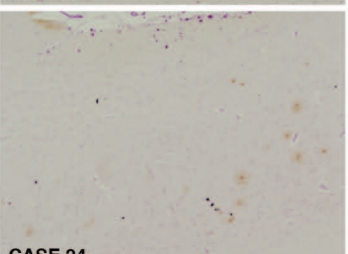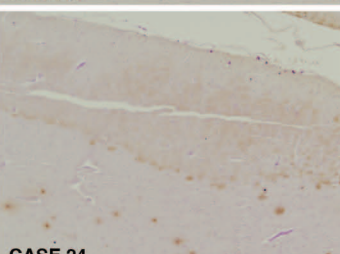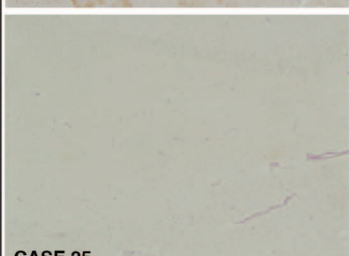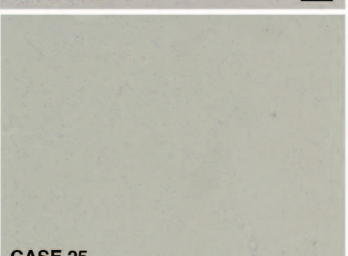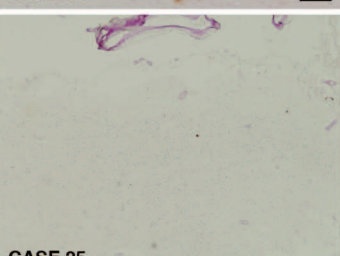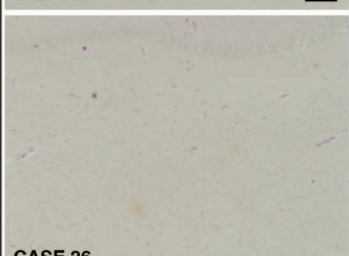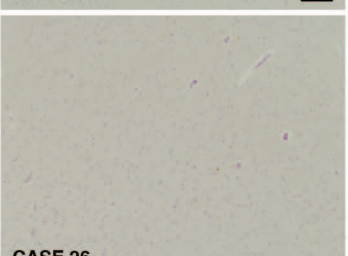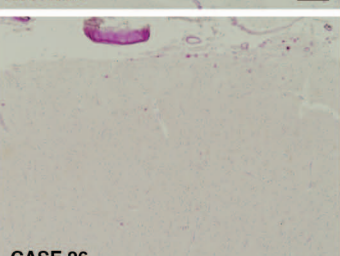
Supplementary material

Supplementary material is available at *Brain* online.

References

Akiyama H, Tago H, Itagaki S, McGeer PL. Occurrence of diffuse amyloid deposits in the presubicular parvopyramidal layer in Alzheimer's disease. Acta Neuropathol 1990; 79: 537–44.

Augustinack JC, Schneider A, Mandelkow EM, Hyman BT. Specific tau phosphorylation sites correlate with severity of neuronal cytopathology in Alzheimer's disease. Acta Neuropathol 2002; 103: 26–35.

Bacskai BJ, Kajdasz ST, Christie RH, Carter C, Games D, Seubert P, et al. Imaging of amyloid-β deposits in brains of living mice permits direct observation of clearance of plaques with immunotherapy. Nat Med 2001; 7: 369–72.

Bacskai BJ, Kajdasz ST, McLellan ME, Games D, Seubert P, Schenk D, et al. Non-Fc-mediated mechanisms are involved in clearance of amyloid-β in vivo by immunotheraphy. J Neurosci 2002; 22: 7873–8.

Bard F, Cannon C, Barbour R, Burke RL, Games D, Grajeda H, et al. Peripherally administered antibodies against amyloid β-peptide enter the central nervous system and reduce pathology in a mouse model of Alzheimer disease. Nat Med 2000; 6: 916–9.

Boche D, Zotova E, Weller RO, Love S, Neal JW, Pickering RM, et al. Consequence of Aβ immunization on the vasculature of human Alzheimer's disease brain. Brain 2008; 131: 3299–310.

Bombois S, Maurage CA, Gompel M, Deramecourt V, Mackowiak-Cordoliani MA, Black RS, et al. Absence of β-amyloid deposits after immunization in Alzheimer disease with Lewy body dementia. Arch Neurol 2007; 64: 583–7.

Braak H, Braak E. Neuropathological stageing of Alzheimer-related changes. Acta Neuropathol 1991; 82: 239–59.

Brendza RP, Bacskai BJ, Cirrito JR, Simmons KA, Skoch JM, Klunk WE, et al. Anti-Aβ antibody treatment promotes the rapid recovery of amyloid-associated neuritic dystrophy in PDAPP transgenic mice. J Clin Invest 2005; 115: 428–33.

Buttini M, Masliah E, Barbour R, Grajeda H, Motter R, Johnson-Wood K, et al. β-amyloid immunotherapy prevents synaptic degeneration in a mouse model of Alzheimer's disease. J Neurosci 2005; 25: 9096–101.

Carmel G, Mager EM, Binder LI, Kuret J. The structural basis of monoclonal antibody Alz50's selectivity for Alzheimer's disease pathology. J Biol Chem 1996; 51: 32789–95.

Carulla N, Caddy GL, Hall DR, Zurdo J, Gairi M, Feliz M, et al. Molecular recycling within amyloid fibrils. Nature 2005; 436: 554–8.

Cruz L, Urbanc B, Buldyrev SV, Christie R, Gómez-Isla T, Havlin S, et al. Aggregation and disaggregation of senile plaques in Alzheimer disease. Proc Natl Acad Sci 1997; 94: 7612–6.

D'Amore JD, Kajdasz ST, McLellan ME, Bacskai BJ, Stern EA, Hyman BT. In vivo multiphoton imaging of a transgenic mouse model of Alzheimer disease reveals marked thioflavin-S-associated alterations in neurite trajectories. J Neuropathol Exp Neurol 2003; 62: 137–45.

DeKosky ST, Scheff SW. Synapse loss in frontal cortex biopsies in Alzheimer's disease: Correlation with cognitive severity. Ann Neurol 1990; 27: 457–64.

DeMattos RB, Bales KR, Cummins DJ, Dodart JC, Paul SM, Holtzman DM. Peripheral anti-Aβ antibody alters CNS and plasma Aβ clearance and decreases brain Aβ burden in a mouse model of Alzheimer's disease. Proc Natl Acad Sci 2001; 98: 8850–5.

Dodart JC, Bales KR, Gannon KS, Greene SJ, DeMattos RB, Mathis C, et al. Immunization reverses memory deficits without reducing brain Aβ burden in Alzheimer's disease model. Nat Neurosci 2002; 5: 452–7.

Ferrer I, Boada-Rovira M, Sánchez-Guerra ML, Rey MJ, Costa-Jussá F. Neuropathology and pathogenesis of encephalitis following amyloid-β immunization in Alzheimer's disease. Brain Pathol 2004; 14: 11–20.

Fiala JC, Feinberg M, Peters A, Barbas H. Mitochondrial degeneration in dystrophic neurites of senile plaques may lead to extracellular deposition of fine filaments. Brain Struct Funct 2007; 212: 195–207.

Gilman S, Koller M, Black RS, Jenkins L, Griffith SG, Fox NC, et al. Clinical effects of Aβ immunization (AN1792) in patients with AD in an interrupted trial. Neurology 2005; 64: 1553–62.

Gómez-Isla T, Price JL, McKeel DW Jr, Morris JC, Growdon JH, Hyman BT. Profound loss of layer II entorhinal cortex neurons occurs in very mild Alzheimer's disease. J Neurosci 1996; 16: 4491–500.

Gómez-Isla T, Hollister R, West H, Mui S, Growdon JH, Petersen RC, et al. Neuronal loss correlates with but exceeds neurofibrillary tangles in Alzheimer's disease. Ann Neurol 1997; 41: 17–24.

Hardy J, Selkoe DJ. The amyloid hypothesis of Alzheimer's disease: progress and problems on the road to therapeutics. Science 2002; 297: 353–6.

Hock C, Konietzko U, Streffer JR, Tracy J, Signorell A, Müller-Tillmanns B, et al. Antibodies against β-amyloid slow cognitive decline in Alzheimer's disease. Neuron 2003; 38: 547–54.

Holmes C, Boche D, Wilkinson D, Yadegarfar G, Hopkins V, Bayer A, et al. Long-term effects of Aβ42 immunisation in Alzheimer's disease: follow-up of a randomised, placebo-controlled phase I trial. Lancet 2008; 372: 216–23.

Hyman BT, Gómez-Isla T, Irizarry MC. Stereology: a practical primer for neuropathology. J Neuropathol Exp Neurol 1998; 57: 305–10.

Janus C, Pearson J, McLaurin J, Mathews PM, Jiang Y, Schmidt SD, et al. Aβ immunization reduces behavioural mathewsimpairment and plaques in a model of Alzheimer's disease. Nature 2000; 408: 979–82.

Kalus P, Braak H, Braak E, Bohl J. The presubicular region in Alzheimer's disease: topography of amyloid deposits and neurofibrillary changes. Brain Res 1989; 494: 198–203.

Kidd M. Alzheimer's disease. An electron microscopical study. Brain 1964; 87: 307–20.

Knowles RB, Wyart C, Buldyrev SV, Cruz L, Urbanc B, Hasselmo ME, et al. Plaque-induced neurite abnormalities: implications for disruption

of neural networks in Alzheimer's disease. Proc Natl Acad Sci 1999; 96: 5274–9.

Kotilinek LA, Bacskai B, Westerman M, Kawarabayashi T, Younkin L, Hyman BT, et al. Reversible memory loss in a mouse transgenic model of Alzheimer's disease. J Neurosci 2002; 22: 6331–5.

Lee M, Bard F, Johnson-Wood K, Lee C, Hu K, Griffith SG, et al. Aβ42 immunization in Alzheimer's disease generates Aβ N-terminal antibodies. Ann Neurol 2005; 58: 430–5.

Lemere CA, Spooner ET, LaFrancois J, Malester B, Mori C, Leverone JF, et al. Evidence for peripheral clearance of cerebral Aβ protein following chronic, active Aβ immunization in PSAPP mice. Neurobiol Dis 2003; 14: 10–8.

Lombardo JA, Stern ES, McLellan ME, Kajdasz ST, Hickey GA, Bacskai BJ, et al. Amyloid-β antibody treatment leads to rapid normalization of plaque-induced neuritic alterations. J Neurosci 2003; 23: 10879–83.

Martins IC, Kupperstein I, Wilkinson H, Maes E, Vanbrabant M, Jonckheere W, et al. Lipids revert inert Aβ amyloid fibrils to neurotoxic protofibrils that affect learning in mice. Embo J 2008; 27: 224–33.

Masliah E, Hansen L, Adame A, Crews L, Bard F, Lee C, et al. Aβ vaccination effects on plaque pathology in the absence of encephalitis in Alzheimer disease. Neurology 2005; 64: 129–31.

Meyer-Luehmann M, Spires-Jones TL, Prada C, García-Alloza M, de Calignon A, Rozkalne A, et al. Rapid appearance and local toxicity of amyloid-β plaques in a mouse model of Alzheimer's disease. Nature 2008; 451: 720–5.

Morgan D, Diamond DM, Gottschall PE, Ugen KE, Dickey C, Hardy J, et al. Aβ peptide vaccination prevents memory loss in an animal model of Alzheimer's disease. Nature 2000; 408: 982–5.

Nicoll JAR, Wilkinson D, Holmes C, Steart P, Markham H, Weller RO. Neuropathology of human Alzheimer disease after immunization with amyloid-β peptide: a case report. Nat Med 2003; 9: 448–52.

Oddo S, Billings L, Kesslak JP, Cribbs DH, LaFerla FM. Aβ immunotherapy leads to clearance of early, but not late, hyperphosphorylated tau aggregates via the proteasome. Neuron 2004; 43: 321–32.

Oddo S, Caccamo A, Tseng B, Cheng D, Vasilevko V, Cribbs DH, et al. Blocking Aβ42 accumulation delays the onset and progression of tau pathology via the C terminus of Heat Shock Protein70-Interacting Protein: a mechanistic link between Aβ and tau pathology. J Neurosci 2008; 28: 12163–75.

Orgogozo JM, Gilman S, Dartigues JF, Laurent B, Puel M, Kirby LC, et al. Subacute meningoencephalitis in a subset of patients with AD after Aβ42 immunization. Neurology 2003; 61: 46–54.

Otvos L Jr, Feiner L, Lang E, Szendrei GI, Goedert M, Lee VMY. Monoclonal antibody PHF-1 recognizes tau protein phosphorylated at serine residues 396 and 404. J Neurosci Res 1994; 39: 669–73.

Patton RL, Kalback WM, Esh CL, Kokjohn TA, Van Vickle GD, Luehrs DC, et al. Amyloid-β peptide remnants in AN-1792-immunized Alzheimer's disease patients. A biochemical analysis. Am J Pathol 2006; 169: 1048–63.

Schenk D, Barbour R, Whitney D, Gordon G, Grajeda H, Guido T, et al. Immunization with amyloid-β attenuates Alzheimer-disease-like pathology in the PDAPP mouse. Nature 1999; 400: 173–7.

Spires-Jones TL, Mielke ML, Rozkalne A, Meyer-Luehmann M, de Calignon A, Bacskai BJ, et al. Passive immunotheraphy rapidly increases structural plasticity in a mouse model of Alzheimer disease. Neurobiol Dis 2009; 33: 213–20.

Stern EA, Bacskai BJ, Hickey GA, Attenello FJ, Lombardo JA, Hyman BT. Cortical synaptic integration in vivo is disrupted by amyloid-β plaques. J Neurosci 2004; 24: 4535–40.

Terry RD, Masliah E, Salmon DP, Butters N, DeTeresa R, Hill R, et al. Physical basis of cognitive alterations in Alzheimer's disease: synapse loss is the major correlate of cognitive impairment. Ann Neurol 1991; 30: 572–80.

Uro-Coste E, Russano de Paiva G, Guilbeau-Frugier C, Sastre N, Ousset PJ, Adolfo da Silva N, et al. Cerebral amyloid angiopathy and microhaemorrhages after amyloid β vaccination: case report and brief review. Clin Neuropathol 2010 in press.

Vellas B, Black R, Thal LJ, Fox NC, Daniels M, McLennan G, et al. Long-term follow-up of patients immunized with AN1792: reduced functional decline in antibody responders. Curr Alzheimer Res 2009; 6: 144–51.

Wilcock DM, Rojiani A, Rosenthal A, Levkowitz G, Subbarao S, Alamed J, et al. Passive amyloid immunotherapy clears amyloid and transiently activates microglia in a transgenic mouse model of amyloid deposition. J Neurosci 2004; 24: 6144–51.

Wilcock DM, Gharkholonarche N, Van Nostrand WE, Davis J, Vitek MP, Colton CA. Amyloid reduction by amyloid-β vaccination also reduces mouse tau pathology and protects from neuron loss in two mouse models of Alzheimer's disease. J Neurosci 2009; 29: 7957–65.

Wisniewski HM, Sadowski M, Jakubowska-Sadowska K, Tarnawski M, Wegiel J. Diffuse, lake-like amyloid-β deposits in the parvopyramidal layer of the presubiculum in Alzheimer disease. J Neuropathol Exp Neurol 1998; 57: 674–83.

	MOLECULAR LAYER OF DENTATE GYRUS / CA1	SUBICULUM	PRESUBICULUM
NON-IMMUNIZED AD PATIENT	CASE 4	CASE 4	CASE 4
NON-DEMENTED CONTROL	CASE 14	CASE 14	CASE 14
AN1792-IMMUNIZED AD PATIENTS	CASE 22	CASE 22	CASE 22
	CASE 23	CASE 23	CASE 23
	CASE 24	CASE 24	CASE 24
	CASE 25	CASE 25	CASE 25
	CASE 26	CASE 26	CASE 26
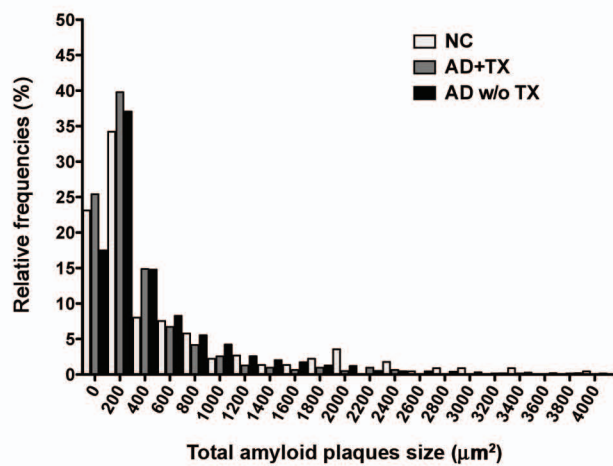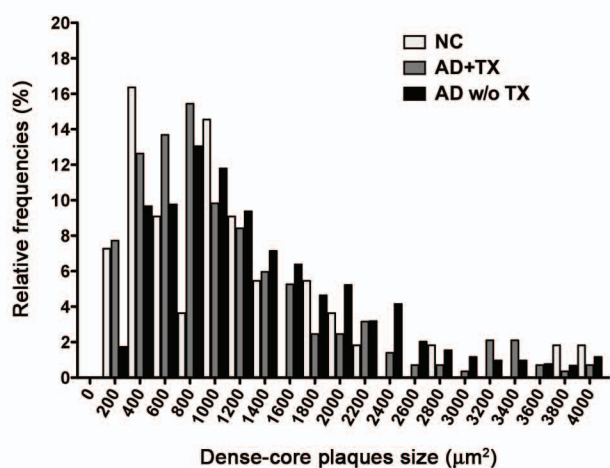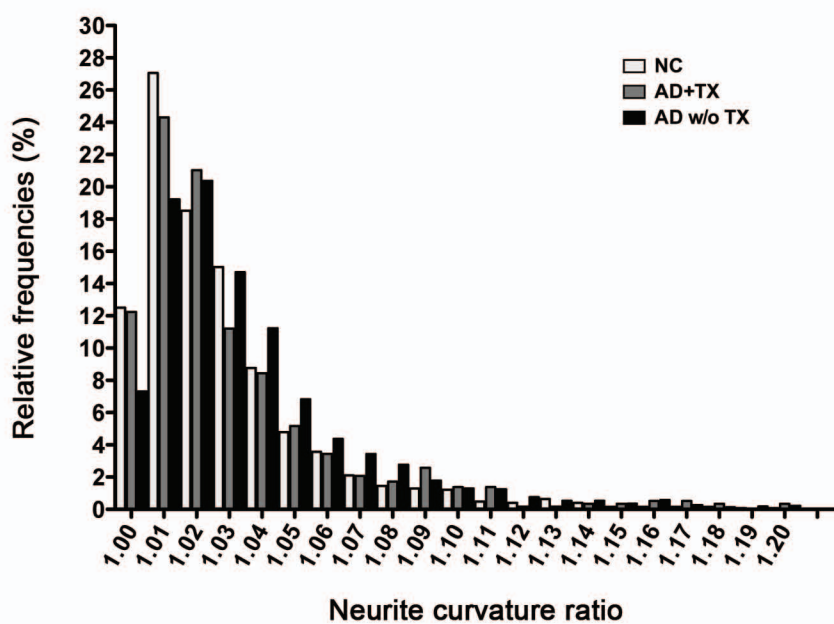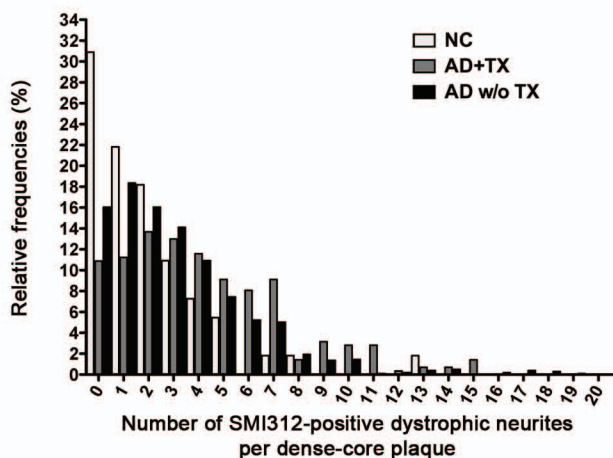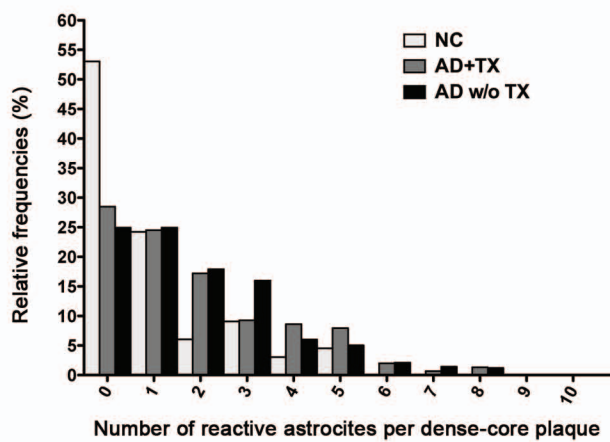
LEGENDS OF SUPPLEMENTARY FIGURES

Supplementary Figure 1: Decreased hippocampal amyloid deposition after anti-Aβ immunization.

Pictures show some of the 10D5-immunostained hippocampal sections used in the analysis of amyloid load. Vessels were counterstained with PAS (in *magenta*). The typical distribution of amyloid deposition within the hippocampus is illustrated in a subject with advanced AD (case 4): one row of conspicuous plaques in the molecular layer of the dentate gyrus (*upper row* in the picture); a parallel row of plaques in the pyramidal layer of the CA1 region (*lower row* in the picture), which becomes wider as it enters the subiculum, and diffuse cloud-like amyloid deposits in the parvopyramidal layer of the presubiculum. Note the overall reduced amyloid load in the AN1792-treated AD group, which at least in cases 25 and 26 is comparable to the amyloid load of the non-demented control (case 14). Scale bars, 200 μm.

Supplementary Figure 2: Frequency distribution histograms of neuropathological quantitative measures.

Frequency distribution histogram of total amyloid plaques size (A) and of dense-core plaques size (B) reveals a shift of the immunized group to the left, compared to the non-immunized group (i.e. smaller size). (C) Frequency distribution histogram of neurite curvature ratio also shows a shift of the immunized group to the left, compared to the non-immunized group (i.e. lower curvature ratio, straighter neurites), paralleling the non-demented group. (D) Frequency distribution histogram of the number of SMI312-positive dystrophic neurites per dense-core plaque shows a shift of the immunized group to the

right, compared to the non-immunized group (i.e. more dystrophic neurites per plaque), due to an apparent bimodal distribution. By contrast, non-demented group is shifted to the left (i.e. less dystrophic neurites per plaque). (E) Frequency distribution histogram of the number of GFAP-positive reactive astrocytes per dense-core plaque reveals a similar distribution in both AD groups. Conversely, non-demented group is shifted to the left (i.e. less astrocytes per plaque).

Supplementary Table 1. Demographic characteristics, pathological diagnosis and APOE genotype of study subjects.

Subject	Age	Gender	Diagnosis	Duration of disease (y)	Braak	*APOE* alleles	PMI (h)
1	72	F	AD	13	VI	3,4	14
2	79	M	AD	9	VI	3,4	14
3	79	F	AD	5	VI	3,4	11
4	71	F	AD	10	VI	4,4	5
5	71	F	AD	17	VI	4,4	14
6	78	F	AD	9.9	VI	3,4	22
7	78	F	AD	17	VI	3,4	20
8	78	M	AD	4.9	VI	3,3	14
9	87	F	AD	10	V	3,3	15
10	89	F	AD	14	V	3,3	12
11	88	M	AD	9.5	V	4,4	10
12	66	M	AD	1.5	IV	3,4	12
13	70	M	AD+DLB	10	IV	3,4	2
14	63	M	CTRL	N.A.	III	3,3	3
15	88	F	CTRL	N.A.	II	3,3	16
16	92	F	CTRL	N.A.	II	2,3	24
17	85	M	CTRL	N.A.	II	3,3	24
18	85	F	CTRL	N.A.	II	3,4	27
19	97	M	CTRL	N.A.	II	3,3	7
20	76	F	CTRL	N.A.	I	3,3	24
21	76	M	CTRL	N.A.	I	3,4	48
22	76	M	AD	4.2	VI	3,4	4
23	72	M	AD	11	VI	3,4	6
24	88	F	AD	13	V-VI	3,4	?
25	79	M	AD	7	V-VI	3,3	66
26	78	F	AD+DLB	7	IV	3,3	7

M = male; F = female; AD = Alzheimer's disease; DLB = Dementia with Lewy Bodies; CTRL = non-demented control (white rows). N.A. = not applicable. PMI = postmortem interval. ? = missing data. Dark-grey rows depict non-immunized cases, whereas light-grey rows show AN1792-treated patients.

Supplementary Table 2. Additional clinical and pathological characteristics of AN1792-treated patients in this study.

Subject	Baseline MMSE	MMSE at death	Survival after first dose (mo)	Other clinical and/or pathological features	Reference
22	18	0	15	Severe CAA with microbleeds, T-cell mediated autoimmune meningoencephalitis	Ferrer *et al.*, 2004
23	?	12	12	Severe CAA, low amyloid load in the frontal cortex	Masliah *et al.*, 2005
24	21	4	40	Severe CAA with microbleeds, low amyloid load in the frontal cortex	Uro-Coste *et al.*, 2010
25	26	12	46	Clinical course typical of AD, with behavioral disturbances and parkinsonism at the late phase	Unpublished
26	15	19	34	AD-DLB patient with cognitive fluctuations and delirium episodes but globally stable cognition and function	Bombois *et al.*, 2007

MMSE = MiniMental State Examination; CAA = Cerebral amyloid angiopathy; AD = Alzheimer's disease; DLB = Dementia with Lewy bodies; ? missing data (note that an inclusion criteria in this clinical trial was a baseline MMSE score of 15 to 26)

Supplementary Table 3. Antibodies, antigen retrieval protocols and developing strategies used in the immunohistochemical studies.

PRIMARY Ab	HOST	BLOCKING SOLUTION	SECONDARY Ab	ANTIGEN RETRIEVAL	DEVELOPING STRATEGY
10D5 (1:50, Elan Pharmaceuticals, Inc.)	Ms	5% fat-free milk in TBS	HRP anti-ms IgG (1:200)	-Citrate buffer 0.01M pH 6 with Tween20 in MW 95ºC 20 min. -Formic acid 90% 5 min	DAB (Vector Lab.)
3D6 (1:1000, Elan Pharmaceuticals, Inc.)	Ms	10% NGS in TBS	Cy3 anti-ms IgG (1:200)	-Citrate buffer 0.01M pH 6 with Tween20 in MW 95ºC 20 min.	None
PHF1 (1:200, Dr. Peter Davies' kind gift)	Ms	5% fat-free milk in TBS	Biotin anti-ms IgG (1:200)	-Citrate buffer 0.01M pH 6 with Tween20 in MW 95ºC 20 min.	-ABC kit (Vector Lab.) -Streptavidin-AlexaFluor546 (1:200)
Alz50 (1:50, Dr. Peter Davies' kind gift)	Ms	5% fat-free milk in TBS	Biotin anti-ms IgM (1:200)	-Citrate buffer 0.01M pH 6 with Tween20 in MW 95ºC 20 min	-ABC kit (Vector Lab.) -Streptavidin-AlexaFluor546 (1:200)
NF-H (1:100, Abcam, ab40796)	Rb	10% NGS in TBS	Biotin anti-rb IgG (1:200)	-Citrate buffer 0.01M pH 6 with Tween20 in MW 95ºC 20 min.	-ABC kit (Vector Lab.) -TSA-AlexaFluor594

				-Formic acid 70% 10 min.	(1:100, Invitrogen)
SMI-312 (1:1000, Covance, SMI-312R)	Ms	10% NGS in TBS	Cy3 anti-ms IgG (1:200)	None	None
VDAC1 (1:500, Abcam, ab15895)	Rb	10% NGS in TBS	Cy3 anti-rb IgG (1:200)	-Citrate buffer 0.1M pH 6 with Tween20 in MW 95ºC 20 min	None
GFAP (1:1000, Sigma, G9269)	Rb	5% fat-free milk in TBS	Cy3 anti-rb IgG (1:200)	-Citrate buffer 0.1M pH 6 with Tween20 in MW 95ºC 20 min	None

Abbreviations: NF-H = Neurofilament-Heavy Chain; VDAC1 = Voltage-Dependent Anion Channel type 1; GFAP = Glial Fibrillar Acid Protein; TBS = Tris-Buffered Saline; NGS = Normal Goat Serum; HRP = Horseradish Peroxidase; ms = mouse; rb = rabbit; MW = Microwave oven; DAB = 3,3'-diaminobenzidine; ABC = Avidin-Biotin Complex; TSA = Tyramide Signal Amplification. All secondary antibodies were from Jackson ImmunoResearch Labs.

Supplementary Table 4. Pathological quantitative measures obtained in the study subjects.

Subject	Plaque amyloid load (%)	Vascular amyloid load (%)	Total amyloid plaques (n/mm^2)	Dense-core plaques (n/mm^2)	Median neurite CR	Alz50+ neurons (n/mm^2)	PHF1+ neurons (n/mm^2)	Thioflavin-S+ NFTs (n/mm^2)
1	1.138	0.016	21.74	15.64	1.024	3.07	68.11	44.39
2	0.308	0.093	14.23	9.91	1.022	28.46	51.00	39.02
3	0.948	0.000	13.76	12.82	1.020	31.20	43.89	26.14
4	1.438	0.000	31.99	28.18	1.043	18.01	65.10	43.93
5	0.640	0.012	26.45	23.21	1.027	22.17	90.02	86.22
6	0.648	0.000	15.06	12.47	1.027	12.97	39.55	34.97
7	1.068	0.000	23.53	19.64	1.024	17.64	64.00	77.88
8	0.772	0.032	24.40	22.76	1.029	5.48	32.13	11.23
9	0.477	0.066	19.75	13.67	1.023	21.98	45.62	29.05
10	0.545	0.036	23.18	14.86	1.027	11.19	35.98	14.03
11	0.503	0.073	34.95	13.93	1.034	23.01	56.38	25.47
12	0.258	0.020	11.86	8.77	1.024	4.55	18.26	10.69
13	0.366	0.000	25.95	14.34	1.026	9.34	6.67	0.56

14	0.003	0.000	0.00	0.00	1.020	2.65	2.87	0.45
15	0.079	0.000	2.36	2.36	1.024	0.26	0.77	0.00
16	0.001	0.000	0.00	0.00	1.019	8.82	5.81	8.33
17	0.006	0.000	0.00	0.00	1.014	17.74	15.73	10.80
18	0.412	0.000	7.90	6.46	1.011	4.35	5.21	3.24
19	0.143	0.000	2.88	1.68	1.022	21.05	12.42	12.72
20	0.001	0.000	0.00	0.00	1.029	0.33	0.00	0.00
21	0.000	0.000	0.76	0.76	1.026	0.38	0.90	0.20
22	0.191	0.031	4.15	4.15	1.023	46.89	55.72	37.15
23	0.093	0.010	1.43	1.43	-	7.53	2.22	20.47
24	0.396	0.010	15.47	13.15	1.015	30.53	27.59	33.21
25	0.051	0.017	1.50	1.50	1.033	0.00	0.39	0.24
26	0.001	0.000	0.28	0.28	1.016	2.14	6.71	1.73

CR = curvature ratio. NFTs = neurofibrillary tangles. Dark-grey rows depict non-immunized patients; white rows, non-demented controls, and light-grey rows, AN1792-treated patients. Median CR is not available for one immunized patient because of the poor quality, likely fixation-dependent, of NF-H immunohistochemical study in that case.

5.4. Summary of results.

Original article#1

1. Amyloid burden plateaus early after onset of symptoms in AD;

2. Despite this stabilization of amyloid deposition, cerebral cortex suffers a progressive atrophy over the clinical course of the disease (due to loss of synapses, neuritis and neurons);

3. Despite the stabilization of amyloid burden, glial responses —reactive astrocytes and activated microglia traditionally associated with plaques– increase linearly through the clinical course of the disease;

4. Glial responses correlate positively with the number of NFTs but not with the amyloid burden; the astrocytic response also correlates with the severity of cortical atrophy;

5. The linear increase of both astroglial and microglial responses observed over the clinical course of the disease occurs in the proximity of dense-core amyloid plaques but also in the vicinity of NFTs.

Original article#2

1. Anti-Aβ active immunotherapy is effective at clearing and reducing the burden of amyloid plaques at the hippocampus of AD patients;

2. Anti-Aβ active immunotherapy is more effective at clearing diffuse amyloid deposits (i.e. "lake-like" deposits at the presubiculum), whereas dense-core amyloid plaques are more resistance to clearance;

3. Both diffuse and dense-core plaques remaining after immunization are smaller than those plaques from non-immunized AD patients;

4. Anti-Aβ active immunotherapy improves the abnormal trajectory of neurites observed in the vicinity of dense-core plaques in AD; this correction of neurite abnormal trajectories is not only due to the overall reduction of the number of amyloid plaques, but also occur in the vicinity of dense-core plaques remaining after immunization;

5. However, dense-core plaques remaining after immunization retain some of their toxic features, as indicated by the number of embedded neuritic dystrophies, the mitochondrial accumulation in those dystrophic neurites, and the magnitude of their surrounding astrocytic response;

6. Anti-Aβ active immunotherapy is associated with a reduction of tau hyperphosphorylation in the hippocampal NFTs, as revealed by immunohistochemistry with the PHF1 antibody (pTau$^{Ser396/401}$), but does not affect the aberrant misfolding and aggregation, as indicated by immunohistochemistry with the Alz50 antibody and by staining with Thioflavin-S.

6 *CONCLUDING REMARKS*

The results of the present work support the two-stage hypothesis of the pathophysiology and progression of Alzheimer disease:

1. The progression of the pathological hallmarks of AD was quantitatively assessed in the temporal association cortex using unbiased stereology-based techniques and clinical disease duration as a proxy of dementia severity. The results of these quantitative analyses provide evidence that amyloid deposition in the temporal cortex occurs primarily before symptom onset and reaches a plateau either before or early on during the symptomatic stage of the disease. By contrast, neurofibrillary degeneration, glial responses and cortical atrophy continue to increase during this symptomatic phase, becoming progressively more independent from amyloid plaques. The results from this cross-sectional postmortem study are largely in agreement with the evidence obtained from longitudinal imaging studies using volumetric MRI and amyloid PET in cognitively intact elderly individuals, and patients with MCI and AD dementia, which have enabled the study of the pathophysiology of AD *in vivo*. Although some controversy remains about whether amyloid continues to accumulate during clinically full-blown dementia, these

studies have helped to establish a sequential order of pathological events in AD, with amyloid deposition largely predating cortical atrophy (reviewed in Jack et al., 2010).

2. The results of our quantitative neuropathological study on the hippocampus of AD patients that were treated with anti-Aβ active immunotherapy in the mild-to-moderate phase of the disease also support this model. The anti-Aβ active immunization was effective at clearing amyloid plaques and also caused some potentially beneficial effects on neurite morphology and tau hyperphosphorylation. The latter observation is not attributable to a different stage of neurofibrillary degeneration since both AD groups were matched by disease duration and Braak stage of NFTs. This finding is in agreement with the original postulate of the amyloid cascade hypothesis that NFTs are a downstream consequence of Aβ accumulation. However, despite these promising results, it should be recognized that the observed effects were overall subtle and likely had little impact on the progression of cognitive decline and survival in these patients (Holmes et al., 2008). Thus, they support the idea that the pathological processes downstream of Aβ become independent of Aβ and progress on their own, so that anti-Aβ directed therapies may only be effective if administered at the initial stage of the disease. In fact, ongoing and future clinical trials are aiming at enrolling patients at earlier stages of the disease, including patients with MCI and positive biomarkers of AD (i.e. CSF and/or amyloid PET) or even FAD mutation carriers at pre-symptomatic stages (Dominantly Inherited Alzheimer Network, DIAN initiative).

Of note, the efforts of two international consensus panels have recently made possible important advances in the clinical and pathological diagnostic framework of AD, which will have direct consequences on the design of clinical trials with disease-modifying drugs and in the clinical management of AD patients. The clinical diagnostic criteria of mild-cognitive impairment due to AD and of AD dementia have been updated to implement for the first time the use of CSF and imaging biomarkers of amyloid deposition and neuronal injury in order to classify the natural history of the patient's disease in one of these two distinct pathophysiological stages (Albert et al, 2011; McKahn et al., 2011). Moreover, based on these biomarkers, a new diagnostic category termed "preclinical AD" has been devised to anticipate the diagnosis of AD at the pre-symptomatic stage, that is, when there is no evidence of cognitive decline or only subjective complaints that are not corroborated by neuropsychological testing (Sperling et al.,

2011). On the other hand, the criteria for the neuropathological diagnosis of AD have also been updated after 15 years to recognize that AD is a pathological continuum between normal aging and dementia, so that for the first time the presence of dementia is not required to make a definite diagnosis of AD. Instead, neuropathologists will report the severity of "AD pathological changes" using descriptors of the amount and distribution of amyloid plaques (CERAD grades and Thal stages) and NFTs (Braak stages) (Montine et al., 2011; Hyman et al., 2011).

7 REFERENCES

1.   Albert MS, DeKosky ST, Dickson D, Dubois B, Feldman HH, Fox NC, et al. The diagnosis of mild cognitive impairment due to Alzheimer's disease: recommendations from the National Institute on Aging-Alzheimer's Association workgroups on diagnostic guidelines for Alzheimer's disease. *Alzheimers Dement* **2011**; 7: 270-279.

2.   Alzheimer's Association, Thies W, Bleiler L. 2011 Alzheimer's disease facts and figures. *Alzheimers Dement* **2011**; 7: 208-244.

3.   Arriagada PV, Growdon JH, Hedley-White ET, Hyman BT. Neurofibrillary tangles but not senile plaques parallel duration and severity of Alzheimer's disease. *Neurology* **1992**; 42: 631-639.

4.   Arriagada PV, Marzloff K, Hyman BT. Distribution of Alzheimer-type pathologic changes in nondemented elderly individuals matches the pattern in Alzheimer's disease. *Neurology* **1992**; 42: 1681-1688.

5.   Bacskai BJ, Kajdasz ST, Christie RH, Carter C, Games D, Seubert P, et al. Imaging of amyloid-β deposits in brains of living mice permits direct observation of clearance of plaques with immunotherapy. *Nat Med* **2001**; 7: 369-372.

6.   Bard F, Cannon C, Barbour R, Burke RL, Games D, Grajeda H, et al. Peripherally administered antibodies against amyloid β-peptide enter the central nervous system and reduce pathology in a mouse model of Alzheimer disease. *Nat Med* **2000**; 6: 916-919.

7.   Benilova I, Karran E, De Strooper B. The toxic Aβ oligomer and Alzheimer's disease: an emperor in need of clothes. *Nat Neurosci* **2012**; 15: 349-357.

8.   Bierer LM, Hof PR, Purohit DP, Carlin L, Schmeidler J, Davis K, et al. Neocortical neurofibrillary tangles correlate with dementia severity in Alzheimer's disease. *Arch Neurol* **1995**; 52: 81-88.

9.   Boche D, Zotova E, Weller RO, Love S, Neal JW, Pickering RM, et al. Consequence of Aβ immunization on the vasculature of human Alzheimer's disease brain. *Brain* **2008**; 131: 3299-3310.

10.   Bombois S, Maurage CA, Gompel M, Deramecourt V, Mackowiak-Cordoliani MA, Black RS, et al. Absence of β-amyloid deposits after immunization in Alzheimer disease with Lewy body dementia. *Arch Neurol* **2007**; 64: 583-587.

11.   Braak H, Braak E. Neuropathological stageing of Alzheimer-related changes. Acta *Neuropathol* **1991**; 82: 239-259.

12.   Brendza RP, Bacskai BJ, Cirrito JR, Simmons KA, Skoch JM, Klunk WE, et al. Anti-Aβ antibody treatment promotes the rapid recovery of amyloid-associated neuritic dystrophy in PDAPP transgenic mice. *J Clin Invest* **2005**; 115: 428-433.

13.   Buttini M, Masliah E, Barbour R, Grajeda H, Motter R, Johnson-Wood K, et al. β-amyloid immunotherapy prevents synaptic degeneration in a mouse model of Alzheimer's disease. *J Neurosci* **2005**; 25: 9096-101.

14.   Castano EM, Prelli F, Wisniewski T, Golabek A, Kumar RA, Soto C, et al. Fibrillogenesis in Alzheimer's disease of amyloid beta peptides and apolipoprotein E. *Biochem J* **1995**; 306: 599–604.

15.   Castellano JM, Kim J, Stewart FR, Jiang H, DeMattos RB, Patterson BW, et al. Human apoE isoforms differentially regulate brain amyloid-β peptide clearance. *Sci Transl Med* **2011**; 3: 89ra57.

16.   Cleary JP, Walsh DM, Hofmeister JJ, Shankar GM, Kuskowski MA, Selkoe DJ, et al. Natural oligomers of the amyloid-β protein specifically disrupt cognitive function. *Nat Neurosci* **2005**; 8: 79-84.

17.   D'Amore JD, Kajdasz ST, McLellan ME, Bacskai BJ, Stern EA, Hyman BT. In vivo multiphoton imaging of a transgenic mouse model of Alzheimer disease reveals marked thioflavine-S-associated alterations in neurite trajectories. *J Neuropathol Exp Neurol* **2003**; 62: 137-145.

18.   Deane R, Sagare A, Hamm K, Parisi M, Lane S, Finn MB, et al. apoE isoform-specific disruption of amyloid beta peptide clearance from mouse brain. *J Clin Invest* **2008**; 118: 4002-4013.

19.   DeKosky ST, Scheff SW. Synapse loss in frontal cortex biopsies in Alzheimer's disease: correlation with cognitive severity. *Ann Neurol* **1990**; 27: 457-464.

20.   DeMattos RB, Bales KR, Cummins DJ, Dodart JC, Paul SM, Holtzman DM. Peripheral anti-Aβ antibody alters CNS and plasma Aβ clearance and decreases brain Aβ burden in a mouse model of Alzheimer's disease. *Proc Natl Acad Sci USA* **2001**; 98: 8850-8855.

21.   Dodart JC, Bales KR, Gannon KS, Greene SJ, DeMattos RB, Mathis C, et al. Immunization reverses memory deficits without reducing brain Aβ burden in Alzheimer's disease model. *Nat Neurosci* **2002**; 5: 452-457.

22.   El Khoury J, Toft M, Hickman SE, Means TK, Terada K, Geula C, et al. Ccr2 deficiency impairs microglial accumulation and accelerates progression of Alzheimer-like disease. *Nat Med* **2007**; 13: 432-438.

23.   Ferrer I, Boada-Rovira M, Sánchez-Guerra ML, Rey MJ, Costa-Jussá F. Neuropathology and pathogenesis of encephalitis following amyloid-β immunization in Alzheimer's disease. *Brain Pathol* **2004**; 14: 11-20.

24.   Fuhrmann M, Bittner T, Jung CK, Burgold S, Page RM, Mitteregger G, et al. Microglial Cx3cr1 knockout prevents neuron loss in a mouse model of Alzheimer's disease. *Nat Neurosci* **2010**; 13: 411-413.

25.   Grathwohl SA, Kälin RE, Bolmont T, Prokop S, Winkelmann G, Kaeser SA, et al. Formation and manteinance of Alzheimer's disease beta-amyloid plaques in the absence of microglia. *Nat Neurosci* **2009**; 12: 1361-1363.

26.   Hickman SE, Allison EK, El-Khoury J. Microglial dysfunction and defective beta-amyloid clearance pathways in aging Alzheimer's disease mice. *J Neurosci* **2008**; 28: 8354-8360.

27.   Gómez-Isla T, Price JL, McKeel Jr. DW, Morris JC, Growdon JH, Hyman BT. Profound loss of layer II entorhinal cortex neurons occurs in very mild Alzheimer's disease. *J Neurosci* **1996**; 16: 4491-4500.

28.   Gómez-Isla T, Hollister R, West H, Mui S, Growdon JH, Petersen RC, et al. Neuronal loss correlates with but exceeds neurofibrillary tangles in Alzheimer's disease. *Ann Neurol* **1997**; 41: 17-24.

29.   Haas C. Strategies, development, and pitfalls of therapeutic options in Alzheimer's disease. *J Alzheimers Dis* **2012**; 28: 241-281.

30.   Hardy JA, Higgins GA. Alzheimer's disease: the amyloid cascade hypothesis. *Science* **1992**; 256: 184-185.

31.   Hardy J, Selkoe DJ. The amyloid hypothesis of Alzheimer's disease: progress and problems on the road to therapeutics. *Science* **2002**; 297: 353-356.

32.   Heneka MT, Nadrigny F, Regen T, Martinez-Hernandez A, Dumitrescu-Ozimek L, Terwel D, et al. Locus ceruleus controls Alzheimer's disease pathology by modulating microglial functions through norepinephrine. *Proc Natl Acad Sci USA* **2010**; 107: 6058-6063.

33.   Hirtz D, Thurman DJ, Gwinn-Hardy K, Mohamed M, Chaudhuri AR, Zalutsky R. How common are the "common" neurologic disorders? *Neurology* **2007**; 68: 326-337.

34.   Holmes C, Boche D, Wilkinson D, Yadegarfar G, Hopkins V, Bayer A, et al. Long-term effects of Abeta42 immunisation in Alzheimer's disease: follow-up of a randomised, placebo-controlled phase I trial. *Lancet* **2008**; 372: 216-223.

35.   Hsia AY, Masliah E, McConlogue L, Yu GQ, Tatsuno G, Hu K, et al. Plaque-independent disruption of neural circuits in Alzheimer's disease mouse models. *Proc Natl Acad Sci USA* **1999**; 96: 3228-3233.

36.   Hyman BT, Gómez-Isla T, Irizarry MC. Stereology: a practical primer for neuropathology. *J Neuropathol Exp Neurol* **1998**; 57: 305-310.

37.   Hyman BT. Amyloid-dependent and amyloid-independent stages of Alzheimer disease. *Arch Neurol* **2011**; 68: 1062-1064.

38.   Hyman BT, Phelps CH, Beach TG, Bigio EH, Cairns NJ, Carrillo MC, et al. National Institute of Aging-Alzheimer's Association guidelines for the neuropathologic assessment of Alzheimer's disease. *Alzheimer Dement* **2012**; 8: 1-13.

39.   Ingelsson M, Fukumoto H, Newell KL, Growdon JH, Hedley-Whyte ET, Frosch MP, et al. Early Aβ accumulation and progressive synaptic loss, gliosis and tangle formation in AD brain. *Neurology* **2004**; 62: 925-931.

40.   Itagaki S, McGeer PL, Akiyama H, Zhu S, Selkoe D. Relationship of microglia and astrocytes to amyloid deposits of Alzheimer disease. *J Neuroimmunol* **1989**; 24: 173-182.

41.   Jack CR Jr, Knopman DS, Jagust WJ, Shaw LM, Aisen PS, Weiner MW, et al. Hypothetical model of dynamic biomarkers of the Alzheimer's pathological cascade. *Lancet Neurol* **2010**; 9: 119-128.

42.   Janus C, Pearson J, McLaurin J, Mathews PM, Jiang Y, Schmidt SD, et al. Aβ immunization reduces behavioural impairment and plaques in a model of Alzheimer's disease. *Nature* **2000**; 408: 979-982.

43.   Jaturapatporn D, Isaac MG, McCleery J, Tabet N. Aspirin, steroidal and non-steroidal anti-inflammatory drugs for the treatment of Alzheimer's disease. *Cochrane Database Syst Rev* **2012** Feb 15;2:CD006378.

44.   Jiang Q, Lee CY, Mandrekar S, Wilkinson B, Cramer P, Zelcer N, et al. ApoE promotes the proteolytic degradation of Abeta. *Neuron* **2008**; 58: 681–693.

45.   Jin M, Shepardson N, Yang T, Chen G, Walsh D, Selkoe DJ. Soluble amyloid beta-protein dimers isolated from Alzheimer cortex directly induce Tau hyperphosphorylation and neuritic degeneration. *Proc Natl Acad Sci USA* **2011**; 108: 5819-5824.

46.   Knowles RB, Wyart C, Buldyrev SV, Cruz L, Urbanc B, Hasselmo ME, et al. Plaque-induced neurite abnormalities: implication for disruption of neural networks in Alzheimer's disease. *Proc Natl Acad Sci USA* **1999**; 96: 5274-5279.

47.   Koffie RM, Meyer-Luehmann M, Hashimoto T, Adams KW, Mielke ML, García-Alloza M, et al. Oligomeric amyloid β associates with postsynaptic densities and correlates with excitatory synapse loss near senile plaques. *Proc Natl Acad Sci USA* **2009**; 106: 4012-4017.

48.   Lacor PN, Buniel MC, Chang L, Fernandez SJ, Gong Y, Viola KL, et al. Synaptic targeting by Alzheimer's-related amyloid β oligomers. *J Neurosci* **2004**; 24: 10191-10200.

49.   Lambert MP, Barlow AK, Chromy BA, Edwards C, Freed R, Liosatos M, et al. Diffusible, nonfibrillar ligands derived from Aβ1-42 are potent central nervous system neurotoxins. *Proc Natl Acad Sci USA* **1998**; 95: 6448-6453.

50.   Lesné S, Koh MT, Kotilinek L, Kayed R, Glabe CG, Yang A, et al. A specific amyloid-β protein assembly in the brain impairs memory. *Nature* **2006**; 440: 352-357.

51.   Li S, Hong S, Shepardson DM, Walsh DM, Shankar GM, Selkoe D. Soluble oligomers of amyloid β protein facilitate hippocampal long-term depression by disrupting neuronal glutamate uptake. *Neuron* **2009**; 62: 788-801.

52.   Loane DJ, Pocivavsek A, Moussa CEH, Thompson R, Matsuoka Y, Faden AI, et al. Amyloid precursor protein secretases as therapeutic targets for traumatic brain injury. *Nat Med* **2009**; 15: 377-379.

53.   Lue LF, Kuo YM, Roher AE, Brachova L, Shen Y, Sue L, et al. Soluble amyloid beta peptide concentration as a predictor of synaptic change in Alzheimer's disease. *Am J Pathol* **1999**; 155: 853-862.

54.   Ma J, Yee A, Brewer HB Jr., Das S, Potter H. Amyloid-associated proteins alpha 1-antichymotrypsin and apolipoprotein E promote assembly of Alzheimer beta-protein into filaments. *Nature* **1994**; 372: 92–94.

55.   Masliah E, Hansen L, Adame A, Crews L, Bard F, Lee C, et al. Aβ vaccination effects on plaque pathology in the absence of encephalitis in Alzheimer disease. *Neurology* **2005**; 64: 129-131.

56.   McGuiness B, O'Hare J, Craig D, Bullock R, Malouf R, Passmore P. Statins in the treatment of dementia. *Cochrane Database Syst Rev* **2010** Aug 4;(8):CD007514.

57.   McKahn GM, Knopman DS, Chertkow H, Hyman BT, Jack CR Jr, Kawas CH, et al. The diagnosis of dementia due to Alzheimer's disease: recommendations from the National Institute on Aging-Alzheimer's Association workgroups on diagnostic guidelines for Alzheimer's disease. *Alzheimers Dement* **2011**; 7: 263-269.

58.   McLean CA, Cherny RA, Fraser FW, Fuller SJ, Smith MJ, Beyreuther K, et al. Soluble pool of Aβ amyloid as a determinant of severity of neurodegeneration in Alzheimer's disease. *Ann Neurol* 1999; 46: 860-866.

59.   Mirra SS, Heyman, A, McKeel D, Sumi SM, Crain BJ, Brownlee LM, et al. The Consortium to Establish a Registry for Alzheimer's Disease (CERAD). Part II. Standardization of the neuropathological assessment of Alzheimer's disease. *Neurology* **1991**; 41: 479-486.

60.   Montine TJ, Phelps CH, Beach TG, Bigio EH, Cairns NJ, Dickson DW, et al. *Acta Neuropathol* **2012**; 123: 1-11.

61.   Morgan D, Diamond DM, Gottschall PE, Ugen KE, Dickey C, Hardy J, et al. Aβ peptide vaccination prevents memory loss in an animal model of Alzheimer's disease. *Nature* **2000**; 408: 982-985.

62.   Näslund J, Haroutunian V, Mohs R, Davis KL, Davies P, Greengard P, et al. Correlation between elevated levels of amyloid β-peptide in the brain and cognitive decline. *JAMA* **2000**; 283: 1571-1577.

63.   Nicoll JAR, Wilkinson D, Holmes C, Steart P, Markham H, Weller RO. Neuropathology of human Alzheimer disease after immunization with amyloid-β peptide: a case report. *Nat Med* **2003**; 9: 448-452.

64.   Orgogozo JM, Gilman S, Dartigues JF, Laurent B, Puel M, Kirby LC, et al. Subacute meningoencephalitis in a subset of patients with AD after Aβ42 immunization. *Neurology* **2003**; 61: 46-54.

65.   Paolicelli RC, Bolasco G, Pagani F, Maggi L, Scianni M, Panzanelli P, et al. Synaptic pruning by microglia is necessary for normal brain development. *Science* **2011**; 333: 1456-1458.

66.   Perea G, Navarrete M, Araque A. Tripartite synapses: astrocytes process and control synaptic information. *Trends Neurosci* **2009**; 32: 421-431.

67.   Pike CJ, Cummings BJ, Cotman CW. Early association of reactive astrocytes with senile plaques in Alzheimer's disease. *Exp Neurol* **1995**; 132: 172-179.

68.   Rozkalne A, Spires Jones TL, Stern EA Hyman BT. A single dose of passive immunotherapy has extended benefits on synapses and neurites in an Alzheimer's disease mouse model. *Brain Res* **2009**; 1280: 178-185.

69.   Schafer DP, Lehrman EK, Kautzman AG, Koyama R, Mardinly AR, Yamasaki R, et al. Microglia sculpts postnatal neural circuits in an activity and complement-dependent manner. *Neuron* **2012**; 74: 691-705.

70.   Schenk D, Barbour R, Whitney D, Gordon G, Grajeda H, Guido T, et al. Immunization with amyloid-β attenuates Alzheimer-disease-like pathology in the PDAPP mouse. *Nature* **1999**; 400: 173-177.

71.   Selkoe DJ. Alzheimer's disease is a synaptic failure. *Science* **2002**; 298: 789-791.

72.   Selkoe DJ. Resolving controversies on the path to Alzheimer's therapeutics. *Nat Med* **2011**; 17: 1060-1065.

73.   Shepardson NE, Shankar GM, Selkoe DJ. Cholesterol level and statin use in Alzheimer disease. I. Review of epidemiological and preclinical studies. *Arch Neurol* **2011**; 68: 1239-1244.

74.   Shepardson NE, Shankar GM, Selkoe DJ. Cholesterol level and statin use in Alzheimer disease. II. Review of human trials and recommendations. *Arch Neurol* **2011**; 68: 1385-1392.

75.   Small SA, Duff K. Linking Aβ and Tau in late-onset Alzheimer's disease: a dual pathway hypothesis. *Neuron* **2008**; 60: 534-542.

76.   Sperling RA, Aisen PS, Beckett LA, Bennett DA, Craft S, Fagan AM et al. Towards defining the preclinical stages of Alzheimer's disease: Recommendations from the National Institute of Aging and the Alzheimer Association Workgroup. *Alzheimers Dement* **2011**; 7: 280-292.

77.   Spires-Jones TL, Mielke ML, Rozkalne A, Meyer-Luehmann M, de Calignon A, Bacskai BJ, et al. Passive immunotherapy rapidly increases structural plasticity in a mouse model of Alzheimer disease. *Neurobiol Dis* **2009**; 33: 213-220.

78.   Sun X, He G, Qing H, Zhou W, Dobie F, Cai F, et al. Hypoxia facilitates Alzheimer's disease pathogenesis by up-regulating BACE1 gene expression. *Proc Natl Acad Sci USA* **2006**; 103: 18727-18732.

79.   Tesco G, Koh YH, Kang EL, Cameron AN, Das S, Sena-Esteves M et al. Depletion of GGA3 stabilizes BACE and enhances β-secretase activity. *Neuron* **2007**; 54: 721-737.

80.   Uro-Coste E, Russano de Paiva G, Guilbeau-Frugier C, Sastre N, Ousset PJ, da Silva NA, et al. Cerebral amyloid angiopathy and microhaemorrhages after amyloid β vaccination: case report and brief review. *Clin Neuropathol* **2010**; 29: 209-216.

81.   Velliquette RA, O'Connor T, Vassar R. Energy inhibition elevates β-secretase levels and activity and is potentially amyloidogenic in APP transgenic mice: posible early events in Alzheimer's disease pathogenesis. *J Neurosci* **2005**; 25: 10874-10883.

82.   Wisniewski T, Castaño EM, Golabek A, Vogel T, Frangione B. Acceleration of Alzheimer's fibril formation by apolipoprotein E in vitro. *Am J Pathol* **1994**; 145: 1030–1035.

83.   Wyss-Coray T. Inflammation in Alzheimer disease: driving force, bystander or beneficial response? *Nat Med* **2006**; 12: 1005-1015.

84.   Zempel H, Thies E, Mandelkow E, Mandelkow EM. Abeta oligomers cause localized Ca(2+) elevation, missorting of endogenous Tau into dendrites, Tau phosphorylation, and destruction of microtubules and spines. *J Neurosci* **2010**; 30: 11938-11950.

8 *ACKNOWLEDGEMENTS*

I would like to thank my co-advisors. Besides their role as co-advisors of this research, each of them has been a reference for me at some point during my short career as a neurologist, and of my incipient career as a scientist.

Dr. Enrique Calderón-Sandubete was the first attending physician I worked with and learned from when I started my residency at the Hospital Universitario Virgen del Rocío (HUVR) in Seville, Spain. I believe he quickly understood my natural curiosity about the causes of disease and that is why he advised me to publish my first paper ever. It was just a short case report in a Spanish journal with no impact factor, but at that time I felt that it was a great accomplishment for me and hoped that it would be the first of many. He is an example of how to do clinical research in a "hostile" environment without burning out in the attempt, or I should say, as a way not to get completely burnt out, and I will always appreciate his knowledgeable recommendations on this regard.

Dr. Eulogio Gil-Néciga has taught me everything I know about the clinical management of dementias, or at least that is how I feel. My gratitude to him is and always will be unlimited. This thesis work would lack meaning for me, and as a result for its readers too, without the clinical background he has passed on me over the years. He has taught me to appreciate the subtlest changes of each of the cognitive functions through the clinical interview with the patient and his/her caregiver, how to use and interpret the neuropsychological tests and the neuroimaging modalities available in our beloved HUVR, and more importantly, how to combine clinical interview, neuropsychology and neuroimaging to make the most accurate diagnosis possible. I learned from him that one of our main responsibilities as clinicians who care patients with dementia is to do our best to accurately classify our patients from a diagnostic standpoint, even if there are no effective therapies for their condition at the moment, because this is the only way our patients will be ready to benefit from curative therapies when better therapies become available (hopefully soon). I also learned from him the need of offering our patients the possibility to participate in multicenter multinational clinical trials with potentially disease-modifying drugs. Indeed, perhaps his most valuable teaching has been to fight the natural tendency towards a diagnostic and therapeutic "nihilism" that, in a scenario without cure, can contaminate the care of patients with dementia.

Dr. Bradley T. Hyman is my current and future reference. I am convinced that I have found in him the model of clinician scientist that I want to be. Unfortunately, this is still a very rare species in Spain. I am not so pretentious to think I will get that far, but looking at his career I do feel that he has shown me the way to go from now on. I must thank him for accepting me in his lab, for not only guiding me through the main unanswered questions in the pathophysiology of Alzheimer disease but also letting me formulate my own questions, for his kindness with me, unconditional trust, and close mentorship, … and also for understanding that some Spaniards' blood is naturally warmer than 36.5ºC and, therefore, easier to boil under certain circumstances. It is a well-known saying in his lab that "nobody ever leaves the lab forever" and I really hope that this saying applies to me too and I can some day come back and work together with him.

I also feel that this work would have been also impossible without the people who have contributed to my clinical and experimental training over the years, both in Seville and in Boston:

On the clinical side in Seville, I would like to acknowledge **Dr. Román Alberca** for creating an authentic school of Neurology at HUVR by transmitting his encyclopedic neurological knowledge and clinical reasoning to all the attending neurologists who trained me as a neurologist. Among these attending neurologists, special thanks to **Drs. José Ramón González-Marcos**, **Fernando Gómez-Aranda**, **Juan Bautista**, **Antonio Uclés**, and **Emilio Franco**, and very special thanks to the great **Alberto Gil-Peralta**, a.k.a. Rober, who at that time was my reference to follow and imitate, both professionally and personally. Finally, thanks to Lola Jiménez for helping me to decide my future. On the clinical side in Boston, I would like to thank **Dr. John Growdon** for accepting me in the MGH Memory Disorders Unit, and **Dr. Teresa Gómez-Isla** for pioneering and sponsoring the advent of Spaniards to MGH and for her wise career advises.

On the lab side in Seville, I would like to thank **Prof. José López-Barneo** for accepting me in his lab at HUVR, supporting me at the beginning of my incipient scientific career, and understanding that I truly love Science, **Alberto Pascual** and **José Ignacio Piruat** for their help and friendship during my 2 years at the Laboratorio de Investigaciones Biomédicas (LIB), and everybody else belonging to the LIB between July 2006 and June 2008 for accepting an MD like me among them without making me feel like an animal in extinction danger. Finally, I would like to thank the input and friendship from the all the members of the Alzheimer Research Unit at the MassGeneral Institute for Neurodegenerative Disease (MIND), including principal investigators, postdocs, PhD students and technicians, with a special mention to my Japanese colleagues and "tomodachis" **Tadafumi Hashimoto** and **Kengo Uemura**.

Finally, I would like to thank my fantastic family, especially my parents **Francisco** and **Milagros**, my brother **Ignacio**, my two sisters **Beatriz** and **Ángela**, and my wife **Paloma** for their encouragement and support.

Alberto Serrano Pozo
Seville (Spain), July 2012